INVESTIGATION OF MALIGNANT MELANOMA CANCER AND CANCER STEM CELLS USING OPTICAL SPECTROSCOPY TECHNIQUES

A Thesis Submitted to
the Graduate School of
İzmir Institute of Technology
in Partial Fulfillment of the Requirements for the Degree of

MASTER OF SCIENCE

in Physics

by
Bensu Rüya USLU

July 2024
İZMİR

We approve the thesis of **Bensu Rüya USLU**

Examining Committee Members:

Asst. Prof. Dr. Günnur GÜLER
Department of Physics, İzmir Institute of Technology

Prof. Dr. Lütfi ÖZYÜZER
Department of Physics, İzmir Institute of Technology

Prof. Dr. Hüseyin AKTUĞ
Department of Histology and Embryology, Ege University

11 July 2024

Asst. Prof. Dr. Günnur GÜLER
Supervisor, Department of Physics
İzmir Institute of Technology

Prof. Dr. Lütfi ÖZYÜZER
Head of the Department of
Physics

Prof. Dr. Mehtap EANES
Dean of the Graduate School

ACKNOWLEDGEMENTS

I would like to thank my supervisor Asst. Prof. Dr. Günnur Güler for her guidance, encouragement, patience, and contribution to this thesis.

I would like to thank the committee members Prof. Dr. Lütfi Özyüzer and Prof. Dr. Hüseyin Aktuğ for their participation and feedback. I am also thankful to Prof. Dr. Hüseyin Aktuğ for providing the samples.

I am thankful to Dr. Berrin Özdil for her sample preparation and helps throughout my thesis.

I would like to thank all the Biophysics Laboratory members. I am also thankful to Berken Hamarat and Esra Koçak for their technical supports.

I would like to thank Assoc. Prof. Dr. Enver Tarhan, Dr. Adem Yavuz, and Dr. Yasemin Demirhan for Raman measurements.

I would like to express my sincere gratitude to my family for their support, love, and understanding.

This work was funded by the IZTECH Research Universities Support Program Scientific Research Projects (AUDP BAP) program as project 2022İYTE-2-0017 to Günnur GÜLER.

ABSTRACT

INVESTIGATION OF MALIGNANT MELANOMA CANCER AND CANCER STEM CELLS USING OPTICAL SPECTROSCOPY TECHNIQUES

Cancer stem cells arising from accumulated mutations in stem cells and progenitor cells are highly responsible for recurrence, resistance to therapy, and metastasis of cancer though they are a small percentage of cancer cells. Malignant melanoma is a common type of cancer and its incidence rate, mortality, and morbidity have increase alarmingly. The goal of this study is to investigate cancer stem cells in malignant melanoma model using vibrational spectroscopy. Vibrational spectroscopy confers both qualitative and quantitative information regarding the molecules which means both biochemical composition of cells and concentrations of biomolecules can be determined with vibrational spectroscopy. Moreover, relationships between the experimental groups and statistical importance of spectral data can be evaluated by applying multivariate analysis methods to collected spectra. Vibrational spectroscopy i.e. infrared and Raman spectroscopy has been widely used in many cellular and other biological studies, obtaining successful results. In this work, cancer stem cells, non-stem cancer cells, and bulk population of cancer cells were analysed with infrared and Raman spectroscopy and recorded data were analysed with multivariate methods at 11^{th}, 24^{th}, 48^{th}, and 72^{nd} hours of cell cycle. As a result, biochemical and biophysical differences between three groups at different hours were determined, and information related to cell cycle of cells were obtained. This study supports that vibrational spectroscopy can be used in the characterization of cells and combined with multivariate analyses information gathered from spectra can be enhanced significantly.

Keywords: Cancer stem cells, Malignant melanoma, Infrared spectroscopy, Raman spectroscopy

ÖZET

OPTİK SPEKTROSKOPİ TEKNİKLER KULLANILARAK MALİGN MELANOM KANSER VE KANSER KÖK HÜCRELERİNİN ARAŞTIRILMASI

Kanser kök hücreleri, kök hücre ve progenitör hücrelerdeki akümüle mutasyonlardan kaynaklanan kanser hücrelerinin düşük bir yüzdesini oluşturmalarına rağmen kanserin tekrarından, tedaviye direnç göstermesinden ve metastazından büyük ölçüde sorumludurlar. Malign melanom yaygın bir kanserdir, ve insidansı, mortatalitesi ve morbitesi alarm verici seviyede artmaktadır. Bu çalışmanın amacı kanser kök hücrelerinin malign melanom modeli üzerinde titreşimsel spektroskopi ile incelenmesidir. Titreşimsel spektroskopi moleküllere dair hem nitel hem nicel bilgi verir. Yani hücrelerin biyokimyasal içeriği ve moleküllerin miktarı titreşimsel spektroskopi ile belirlenebilir. Dahası, deney grupları arasındaki ilişkiler ve spektral verinin istatistiksel önemi kaydedilen spektrumlara çok-değişkenli Analiz yöntemleri uygulanarak değerlendirilebilir. Titreşimsel spektroskopi, infrared ve Raman spektroskopileri, hücresel ve diğer biyolojik çalışmalarda yaygın olarak kullanılmaktadır ve başarılı sonuçlar elde edilmektedir. Bu çalışmada, kanser kök hücreleri, kök hücre olmayan kanser hücreleri ve bulk hücre popülasyonu hücreleri infrared ve Raman spektroskopileri ile incelenmiştir ve elde edilen veriler hücre döngüsünün 11, 24, 48 ve 72. saatlerinde çok-değişkenli yöntemlerle analiz edilmiştir. Sonuç olarak, üç grup arasındaki biyokimyasal ve biyofiziksel farklar farklı saatler için belirlenmiş ve hücrelerin hüçre döngüsüne ilişkin bilgiler elde edilmiştir. Bu çalışma titreşimsel spektroskopinin hücre karakterizasyonunda kullanılabileceğini ve çok-değişkenli analizlerle birleştirildiğinde spektrumlardan elde edilen bilginin ciddi ölçüde geliştirilebileceğini desteklemektedir.

Anahtar Kelimeler: Kanser kök hücreleri, Malign melanom, İnfrared spektroskopisi, Raman spektroskopisi

TABLE OF CONTENTS

LIST OF FIGURES

Figure **Page**

Figure **Page**

Figure **Page**

Figure **Page**

Figure **Page**

LIST OF TABLES

Table **Page**

LIST OF ABBREVIATIONS

IR: infrared

FT: Fourier transform

FT-IR: Fourier transform-IR

ATR: attenuated total reflectance

CCD: charge-coupled device

MM: malignant melanoma

UV: ultraviolet

CDK: cyclin-dependent kinase

EMT: epithelial to mesenchymal transition

CSCs: cancer stem cells

SCs: stem cells

CKIs: CDK inhibitors

PC: principal component

PCA: principal component analysis

HCA: hierarchical clustering analysis

A: adenine

C: cytosine

G: guanine

T: thymine

trp: tryptophan

tyr: tyrosine

phe: phenylalanine

CHAPTER 1

INTRODUCTION

1.1. Dual Nature of Light

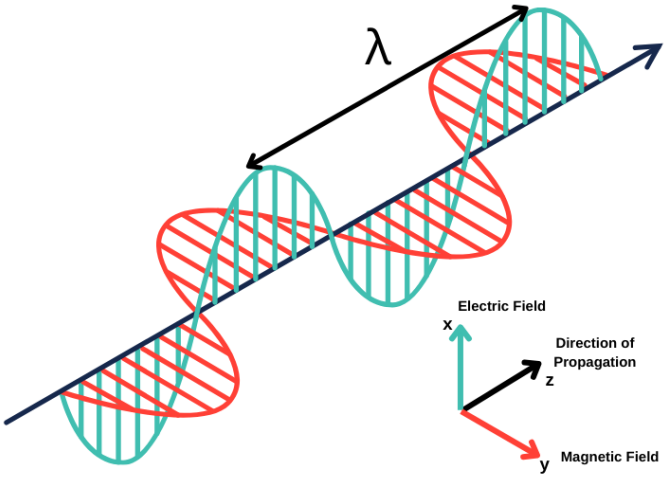

Figure 1.1. Electromagnetic wave (Recreated from[1])

Electromagnetic radiation, the term covers not only visible light but all frequencies of light, that radiates through perpendicularly conjoined electric and magnetic fields. Monochromatic light propagates mutually perpendicular to both fields and propagates periodically with a constant wavelength (λ) and at the speed of light (c) (in vacuum $c=c_0=3x10^8$ m/s) as can be seen in the Figure 1.1. Oscillation frequency (ν) corresponds to c/λ. In the case of the propagation of light is in the z direction, then electric field is directed towards to x direction and can be represented by following equation:[1]

$$E(z,t) = E_0 sin(kz - wt) \tag{1.1}$$

where E_0 is the amplitude of the field, t is the time in seconds, k is the wavenumber and can be expressed as $k=2\pi/\lambda$, and w is the angular frequency and can be expressed as $w=2\pi\nu=ck$.

In this case, magnetic field is in the y direction and can be represented by following equation:

$$B(z,t) = B_0 sin(kz - wt) \tag{1.2}$$

where B_0 is the amplitude of the field.

Light exhibits not only wave properties but also particle properties, which is called wave-particle duality. An electromagnetic radiation with frequency ν, propagates with discrete energy units called "photons". Photons have zero rest mass, polarization and energy proportional with their frequency which can be described by the following equation:[1]

$$E = h\nu \tag{1.3}$$

where h is Planck's constant (h= 6.63 x 10^{-34} J.s).

Photons have wavelength,

$$\lambda = \frac{c}{\nu} \tag{1.4}$$

then energy equation becomes,

$$E = \frac{hc}{\lambda} \tag{1.5}$$

In general, inverse of wavelength which is called wavenumber expressed in cm^{-1} is used in spectroscopy, $\bar{\upsilon}$ is[1]

$$\bar{\upsilon} = \frac{1}{\lambda} \tag{1.6}$$

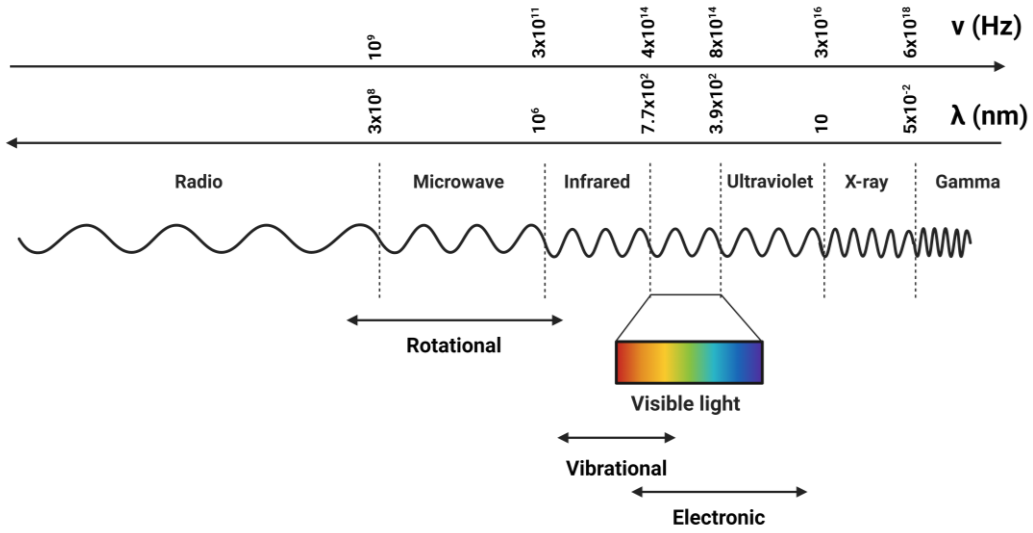

Figure 1.2. Electromagnetic Spectrum[1,2] (Created with BioRender.com)

Electromagnetic spectrum covers radio waves, microwaves, infrared radiation, visible light, ultraviolet radiation, X-rays, and gamma rays with ascending energy levels as can be seen in Figure 2.2. A molecule exposed to electromagnetic radiation may experience electronic, vibrational, and rotational changes, the frequency ranges that cause changes in rotational, vibrational, and electronic energy levels are roughly indicated in the Figure 2.2.[1,2]

1.2. Vibrational Spectroscopy

1.2.1. Fundamental Vibrational Modes

Theoretically, a linear molecule containing n atoms can have 3n-5 vibrational modes, while a nonlinear molecule can have 3n-6 vibrational modes. However, all modes cannot be detected with IR spectroscopy because of factors such as weak or degenerate absorptions, absorptions outside the range of the spectrum, and vibrations causing no dipole moment change in the bonds. The latter one is a prerequisite for IR spectroscopy as the intensity of the absorption band is strongly correlated with the dipole moment

changes. Vibrations without dipole moment change are IR inactive and is common in molecules that have symmetry.[3]

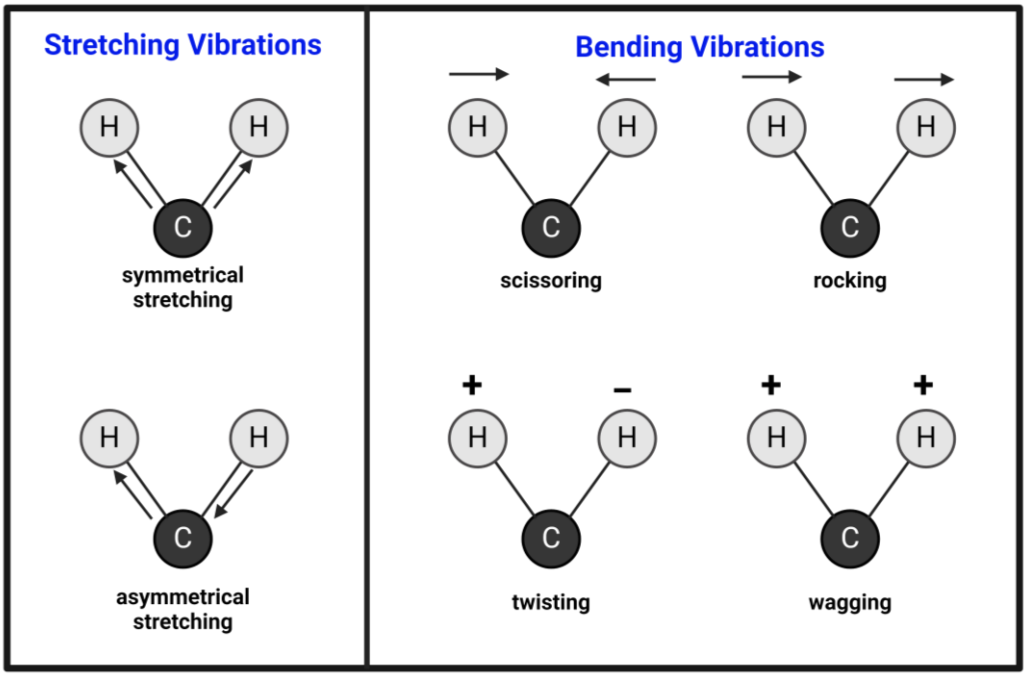

Figure 1.3. Molecular vibrations of CH_2 molecule (+: above the plane of paper, -: behind the plane of paper)[3] (Recreated with Biorender)

Figure 1.3 depicts the molecular vibrations observed in molecules. Bonds in a molecule can make various vibrations. Stretching and bending vibrations are fundamental ones of these vibrations. In the first one, atoms move in the same direction with bonds, while in the latter one also referred as deformations, movements of atoms cause bond angles to change. Stretching vibrations can be symmetrical or asymmetrical. Bonds moving away and toward to a common atom simultaneously is considered as symmetrical stretching, while in the same situation except bonds moving oppositely is considered as asymmetrical stretching. Bending vibrations involve scissoring, rocking, twisting, and wagging. In scissoring, also referred as in plane bending, atoms are in the same plane, whereas bond angle experiences deformations and the atoms move towards to and away from each other. In bending, atoms also remain in the same plane, and swing back and forth simultaneously. In twisting, as the name suggests bonds twist out of plane around a central atom, and atoms move opposite directions. Wagging involves out of plane swinging of bonds to back and forth simultaneously.[3]

1.2.2. Harmonic Oscillator Model

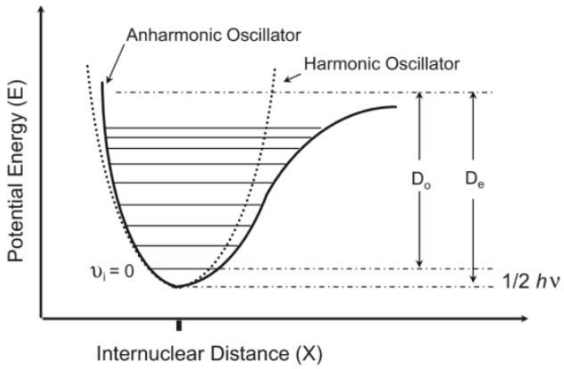

Figure 1.4. Energy (E) versus internuclear distance (X) diagrams for harmonic and anharmonic oscillators (Source[4])

In the case of two masses m_1 and m_2 are connected to each other with a massless spring. X_1 and X_2 are the displacement from equilibrium points for m_1 and m_2, respectively. x_1 and x_2 are periodic functions of time, as in classical harmonic oscillator, with different amplitudes but the same frequency. There is an inverse relationship between masses and displacements as:[4]

$$-\frac{X_1}{X_2} = \frac{m_2}{m_1} \tag{1.7}$$

Vibrational frequency and wavenumber of masses can be expressed as:

$$\nu = \frac{1}{2\pi}\sqrt{\frac{k}{\mu}} \tag{1.8}$$

$$\bar{\upsilon} = \frac{1}{2\pi c}\sqrt{\frac{k}{\mu}} \tag{1.9}$$

where k is force constant and μ is reduced mass:

$$\mu = \frac{m_1 m_2}{m_1 + m_2} \tag{1.10}$$

As can be seen from equation 1.8 vibrational frequency depends only on masses and force constant.

The potential energy of classical harmonic oscillator is given by:

$$U = \frac{1}{2}kx^2 \tag{1.11}$$

However, energy can take only discrete values in quantum mechanics and a molecule make transition to different energy states with condition of:

$$\Delta n = \pm 1 \tag{1.12}$$

In quantum mechanical harmonic oscillator energy levels of vibrational states are equidistant and given by:

$$E_n = \left(n + \tfrac{1}{2}\right) hv \tag{1.13}$$

where n=0, 1, 2, …

The quantum number n can only take integer values. Energy cannot be zero for since when n=0 energy becomes,

$$E_0 = \frac{hv}{2} \tag{1.14}$$

However, in the case of existence of a nonlinear relationship between dipole moment change and nuclear displacement, anharmonicity is observed. Figure 1.4 depicts the harmonic and anharmonic potentials with respect to internuclear distance, X. D_0 and D_e represent the energy amounts required to break the bond. In anharmonic oscillator, energy levels are unevenly spaced because of mechanical anharmonicity; while bands are overtoned i.e. Δn = ± 2, 3 and combined as consequences of electrical anharmonicity. Anharmonic oscillator deviates more from harmonic oscillator as the quantum number, n, increases due to the smaller energy differences between adjoining energy levels. Moreover, in this model vibrations can interact with each other. Energy can be corrected by adding an anharmonicity correction term:[4]

$$E_n = \left(n + \tfrac{1}{2}\right) hv - hXv\left(n + \tfrac{1}{2}\right)^2 \tag{1.15}$$

where Xv depicts the level of anharmonicity.[4]

1.2.3. FT-IR (Fourier Transform-Infrared) Spectroscopy

IR region can be divided into subregions as near-IR, mid-IR, and far-IR which contains 14000-4000, 4000-400, and 400-10 cm^{-1}, respectively. Energy of IR radiation leads vibrations in the bonds that connect atoms in a molecule. Since the energy differences between vibrational energy levels are quantized as the electronic ones vibrational transitions occur with discrete energies i.e. absorption of IR photons by molecules occurs only at specific frequencies that match with the vibrational energy of the bonds. Different functional groups have different frequencies and when they subjected to IR radiation their IR spectrum enables to characterization of them. IR spectroscopy first gives an interferogram of the signals and then the interferogram is converted to spectrum that gives absorption intensity for all frequencies by Fourier Transformation (FT). This process is implemented by computers.[5]

1.2.3.1. Instrumentation of FT-IR Spectroscopy

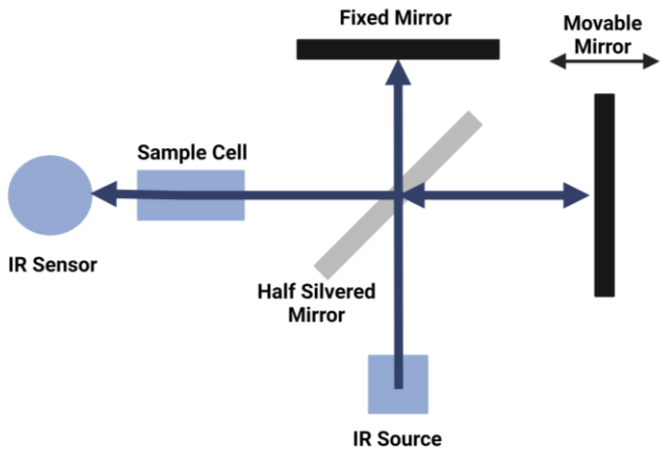

Figure 1.5. Set-up for an FT-IR spectrometer (Recreated from[5])

Set-up of the FT-IR spectroscopy simply designed with Michelson interferometer which contains a beam splitter, a movable mirror and a fixed mirror. Mirrors are perpendicularly placed to each other, and beam splitter reflects half of the incoming light.

An IR spectrometer contains an IR radiation source, a Michelson interferometer, and an IR sensor as detector. Beam splitter in the interferometer causes path difference between IR beams and interfered signals are detected by the IR detector. Interference signals give information about the composition of the sample. Figure 1.5 shows the sample diagram for IR spectrometer. IR source can be chosen according to targeted spectral range as different sources radiate with different frequencies. For example, globar and Nerst glower correspond to mid-IR range, while Hg arc lamp radiates at far-IR range. Detectors are also designed for various properties and different spectral ranges. For example, photoconducting detectors made up from materials such as CdS are rapid and have high sensitivity in the near-IR range. Pyroelectric detectors made up from triglycine sulphate materials that have piezoelectric properties, they are rapid and highly sensitive in the mid-IR range. Although thermocouple detectors work with the thermoelectric effect are cheap, they are not sensitive or rapid.[5]

1.2.3.2. Quantification of IR Spectra

IR spectra can be analysed quantitatively by Beer-Lambert law which states that for a homogeneous sample absorbance can be expressed as:[6]

$$A = \varepsilon C l \tag{1.16}$$

where A is absorbance, ε is absorptivity, C is the concentration of the sample, and l is the path length of incoming beam through the sample. According to the Beer-Lambert law intensities of absorption signals are correlated linearly with the concentration of components of the sample.[6]

1.2.3.3. ATR (Attenuated Total Reflectance) FT-IR Spectroscopy

Attenuated Total Reflectance (ATR) FT-IR spectroscopy relies on internal reflectance of IR beam. Materials with high refractive indices are used as ATR crystals such as diamond, silicon, and zinc selenide. IR beams pass through ATR crystal with a

high refractive index and meets a lower refractive index sample at the boundary. The angle of incidence with the surface normal can be represented with θ_i. In the case where θ_i is small a part of beam will be reflected from the internal surface of the crystal and left of them will be refracted outward from ATR unit to the sample with the angle of refraction, θ_r. If the incident light comes with critical angle or greater than it, θ_c, θ_r will be 90° and total internal reflection occur i.e. all the IR beam will remain in the crystal. Critical angle can be determined by the following formula:[6]

$$\Theta_c = sin^{-1}\left(\frac{n_s}{n_c}\right) \tag{1.17}$$

where n_s and n_c are refractive indices of sample and crystal, respectively.

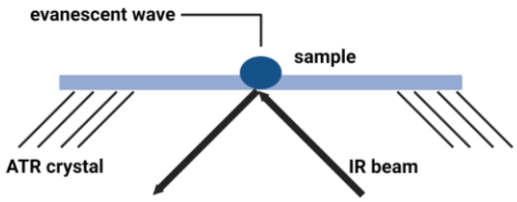

Figure 1.6. Working principle of ATR (Recreated from[6])

Incoming and outgoing IR radiation constructively interfere at the point that total internal reflectance occurs. Then IR radiation is confined to in the scale of microns above the ATR crystal and referred as evanescent waves or hot spots as can be seen in the Figure 1.6. At that point sample can absorb some of the IR radiation and absorbed radiation reaches to the IR detector. This is referred as attenuated total reflectance as the intensity of reflected IR radiation i.e. evanescent wave attenuates due to the absorption by the sample. Pathlength is correlated with depth of penetration of IR radiation in ATR-FTIR spectroscopy.[6]

ATR-FTIR technique has many advantages. It can be used to analyse various kinds and forms of samples including powders, polymers, biological samples, liquid samples, and semi-solid samples. It is an easy, fast, non-destructive technique and needs low labour. However, it is expensive, has limited frequency range and ATR crystal is vulnerable.[6]

1.2.4. IR Spectroscopy of Cells

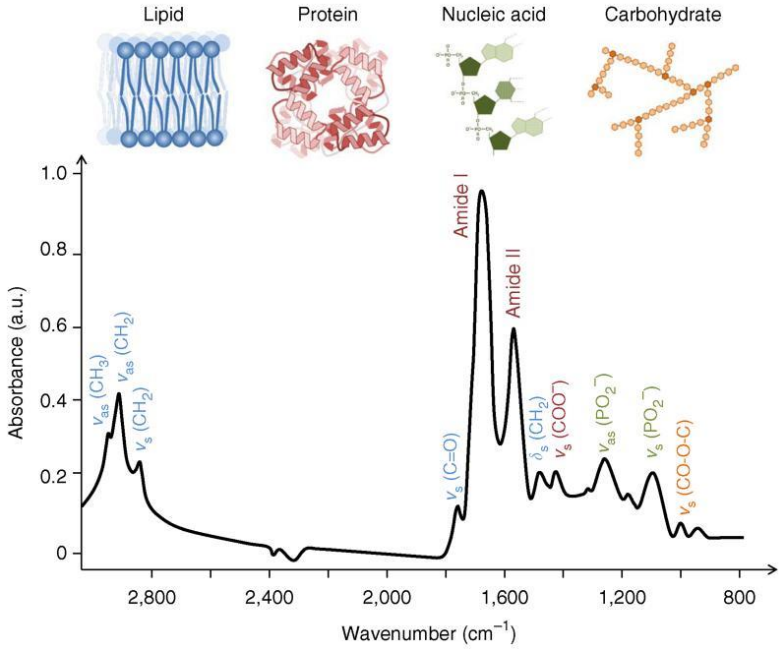

Figure 1.7. Typical IR spectrum of biological samples (Source[7])

FT-IR spectroscopy is an advantageous technique commonly used in biological studies[8–12] that enables analysis of biological samples in a non-destructive, label-free, and practical manner. It quantizes vibrational bonds and offers a unique spectrum for samples that enable characterization of sample in terms of composition of it in molecular level as well as it gives information about the dynamics of the sample. The typical IR spectrum of biological samples can be seen in the Figure 1.7. The fingerprint region of cells includes the region between 600 and 1450 cm^{-1}, the region between 1500 and 1700 cm^{-1} contains amide I and amide II signals of proteins (amide I/II region), and the high wavenumber region i.e. between 2550 and 3500 cm^{-1} contains stretching vibrations of C-H, O-H, S-H etc.[7]

1.2.5. The Raman Effect

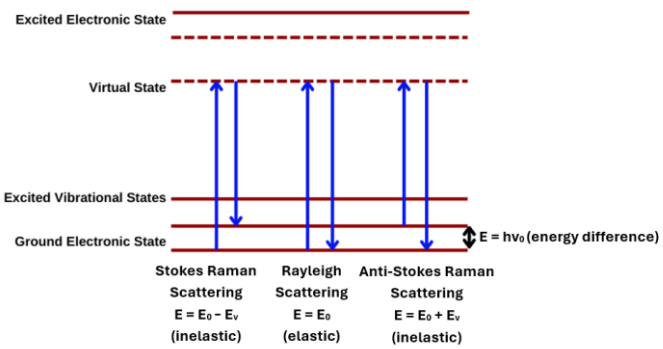

Figure 1.8. Raman Scattering (Recreated from[13])

Raman effect, discovered by Chandrashekhara Venkata Raman in 1928. When the light from a monochromatic source directed to a molecule light can scatter either elastic or inelastic. Figure 1.8 shows possible scenarios for scattering light after molecular interactions. The first one is called Rayleigh scattering, in that case incoming light interact with the matter but this causes no net energy change and frequency of the photon do not change. The latter one is called Raman effect. In that case incoming photon gain or lose some of its energy after the interaction with the molecule and its frequency will change. If the incident photon gains vibrational energy resulted from interaction with the molecule, then frequency of scattered photon will increase by the amount of energy difference between vibrational states, that case is referred as anti-Stokes Raman scattering. If the photon transfers some of its energy to the molecule, then its frequency will be lower, and this is called Stokes Raman scattering. Raman phenomena provides both quantitative and qualitative information about the molecules by using light-matter interactions.[13]

1.2.6. Raman Spectroscopy

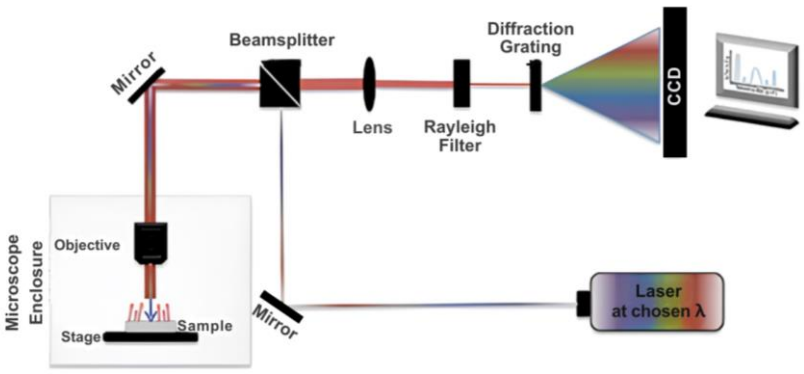

Figure 1.9. Dispersive Raman spectrometer set-up (Source[14])

Figure 1.9 depicts the typical set up for a confocal Raman micro-spectroscopy system. Dispersive Raman spectrometer set up basically contains a laser source, detector, microscope compartment, mirrors, lens, beamsplitter, Rayleigh filter, and diffraction grating. Different wavelengths of monochromator lasers can be used as an excitation source depending on the experimental conditions. Wavelength of the source affects sensitivity of the scattering, as the wavelength decreases sensitivity increases and mathematically scattering sensitivity equals to λ^{-4}. Spatial resolution can be calculated by using the following formula:[14]

$$spatial\ res. = \frac{1.22\lambda}{Numerical\ aperture\ of\ objective\ focusing\ laser\ beam} \quad (1.18)$$

Mirrors, slits, beam splitter, and lenses are aligned in a way that laser beams are directed on the sample and then scattered light from the sample reaches to the detector. Raman intensity is weak compared to the intensity of Rayleigh scattering. Hence, Rayleigh filter is an important component of the Raman system, which blocks most of the Rayleigh scattering. Diffraction grating strongly affects spectral resolution. It contains evenly separated lines on its surface and disperse incoming filtered Raman beams. It diffracts each wavelength with different angles, by this way it separates multiwavelength light as monochromatic parts. To obtain higher spectral resolution grating should include higher number of lines. Multi-channel CCD (charge-coupled device) detectors are mostly used detectors in Raman systems. It contains pixels i.e. a 1D or 2D array of light-sensitive components and charge resulted because of interactions of pixels and light. Signals

become enhanced as the charge increases. Resulting spectra is obtained as Raman intensity versus wavenumber plots and relationship between the wavenumber ($\bar{\upsilon}$) and wavelength (λ) can be expressed as[14]

$$\bar{\upsilon} = \frac{10^7}{\lambda} \tag{1.19}$$

where $\bar{\upsilon}$ in cm^{-1}. Confocal Raman microscope provides 3D resolution, which is especially useful for analysis of biological samples.[14]

1.2.7. Raman Spectroscopy of Cells

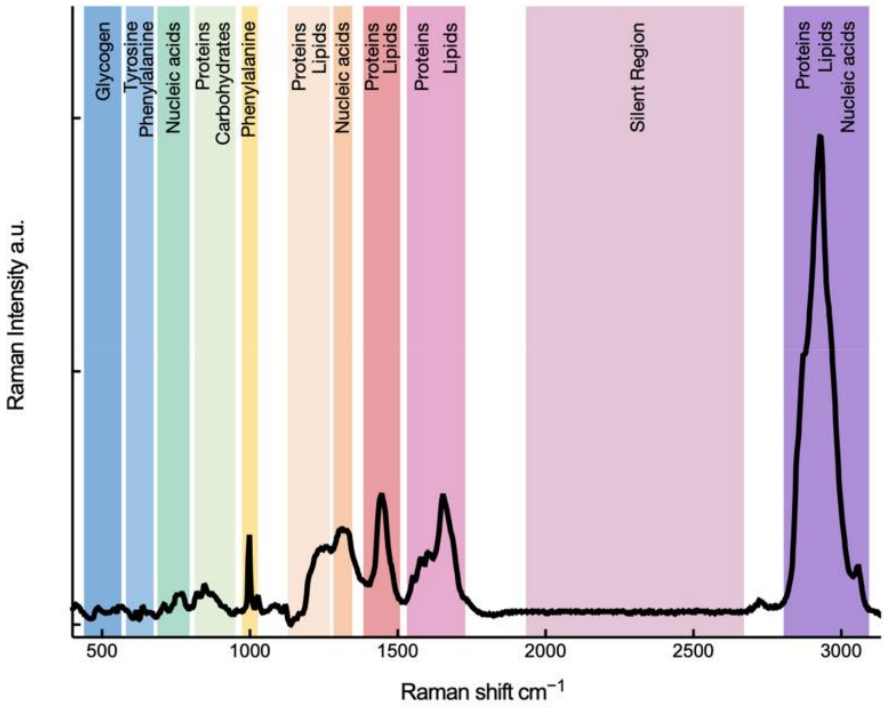

Figure 1.10. Typical Raman spectra of cells (Source[15])

Raman spectroscopy is non-destructive, label-free, rapid, sensitive, and low-labour technique and widely used to analyse various kinds of samples in various forms. As it is non-destructive, label-free and sensitive, it is a powerful tool to analyse biological samples such as cells and tissues. It enables characterization of the sample by identifying biochemical composition of it. Biological macromolecules i.e. proteins, lipids, nucleic

acids and so on, have unique signals in the Raman spectra. Hence, Raman spectroscopy provides detailed information about the biological samples. Combined with the multivariate analysis, it can be used in the discrimination of cells. The typical Raman spectra of cells can be divided into three subregions as can be seen in the Figure 1.10. The spectral region between 400 and 1800 cm^{-1} is fingerprint region, it gives information about the biochemical constituents of the cells. The spectral region between the 1800 and 2700 cm^{-1} do not contain signals except signals caused by triple bonds or stable isotopes and referred as silent region. The high wavenumber region contains signals arising owing to C-H groups of lipids and proteins and corresponds 2700-3200 cm^{-1} region.[15] Raman peaks observed in a typical cell spectra are listed in detail in the Table 1.1.

Table 1.1. Peak assignments of Raman signals found in a typical cell spectrum

Raman Shift (cm^{-1})	Biological Molecules
484	glycogen[16]
498	G, T[17]
623	Phe[17]
643	Tyr (C-C twisting)[18]
669	G, T[17], cysteine[18]
678	G[19]
702	cholesterol[17]
719	A, phospholipids,[20] choline $[(H_3C)N^+]$[17]
725	A[17,19]
746	T[19]
760	Trp[17,18]
785	C, T, Uracil, DNA backbone[19,21]
811	RNA backbone (PO_2^-), collagen[20]
831/852	Tyr[17,19]
936	α-helix (C-C stretching)[17,18]
1003	Phe[19,21]
1031	Phe[18,19]
1065	chain C-C (lipids)[17]

(Cont. on the next page)

Table 1.1. (cont.)

1090	PO_2^- (in DNA/RNA)[17,19,21]
1124	C-C stretching (lipids, proteins)[17,18]
1176	C, G, T, Tyr[18]
1208	A, T, amide III,[19] Tyr, Phe[17,18]
1260	amide III, =CH in plane bending (lipids)[21]
1303	CH_2 twisting & wagging in proteins and fatty acids[17,21]
1311	A[22]
1318	G[19]
1337	A, G[19], Trp[22]
1342	G (C-H deformation)[21]
1358	Trp (C-N stretching)[23]
1373	A, G, T[19]
1421	A, G[18,19]
1444	CH_2 deformation (lipids, proteins)[17,19,21]
1485	A, G[19]
1510	A[19]
1571	A, G (ring breathing)[17,21]
1581	pyrimidine ring[22]
1605	Phe, Tyr[18,19]
1616	Tyr, Trp[18]
1655-1680	amide I, C, G, T[17,19]
1657	C=C stretching (lipids)[17]
1671	cholesterol[17]
1739	C=O stretching (lipids)[17,21]
2854	CH_2 stretching (lipids)[17,21]
2886	CH_2 stretching (lipids)[17]
2936	CH_3 stretching (lipids)[17]
2960	CH_3 stretching (lipids)[17]

1.3. Regulation of Cell Cycle

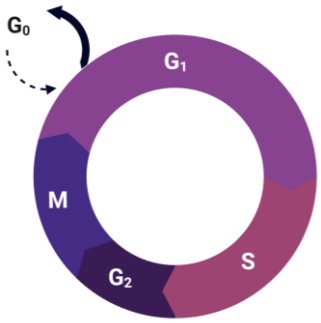

Figure 1.11. Cell cycle (Created with BioRender.com)

The eukaryotic cell cycle consists of four general phases as G_1, S, G_2, and M which can be seen in the Figure 1.11. G_1 refers to gap phase 1 and it prepares cells to DNA replication. In G_1 phase, cells decide to whether cell cycle will be continued. Cells can become quiescent by exiting from cell cycle and this case is described with G_0 phase. In the S phase DNA replication takes place. In the second gap phase, G_2, cells prepare themselves for division. In the M phase, which refers to mitosis, doubled chromosomes are segregated and cytokinesis takes place.[24]

Cell cycle is regulated via several factors. Cyclins, CDKs, CDK inhibitors (CKI) are key agents that regulate cell cycle. Activations of CDKs are governed by cyclic creation and degradation of cyclins and CKIs are also involved in these processes. D-type cyclins, their amounts are governed by growth factors, stimulate quiescent cells to enter the G_1 phase. Rb (retinoblastoma tumor suppressor) protein, regulates event in the G_1 phase, is the main substrate for D-type cyclin kinases. D-type cyclins are involved in phosphorylation of Rb and regulation of CDK4 and CDK6. E2F transcription factors are responsible to express encoding cyclin E, cyclin A, CDK1 which are part of progression of cell cycle and genome replication.[24] Cyclin E-CDK2 complex enables transition from G_1 to S phase. Cyclin A is involved in initiation of S and M phase, and it is also required to complete S phase.[24,25] Cyclin B is involved in completion of G_2 and entering M phase. [26] Dysregulations of cyclin related signalling pathways have important contributions to the development of cancer. Cyclin box domain is homologic region found in cyclins. They are responsible in activation of CDKs by binding them. CDKs and cyclins are not only responsible for regulation of cell cycle but also DNA repair, transcriptional regulation,

apoptosis, and differentiation processes. Phosphorylation of CDKs also affects their activity. Moreover, proteolysis governed by ubiquitin is an irreversible process targets regulating agents of cell cycle and constrains cells to next steps. CKIs can be divided into two groups as Cip/Kip and INK4 family[24]. p21, p27, and p57 are members of Cip/Kip family. In the case of DNA damage p21 is activated by p53 and cells are arrested at G_1 phase to repair their DNA.[24,27,28] Moreover, in senescent cells p21 is found as accumulated.[24] INK4 family, includes p16, p15, p18, and p19, only interact with CDK4 and CDK6 and disables them from forming complexes with D-type cyclins.[24,27] p16 is highly involved in regulation of Rb and is found as inactivated form in many tumors.[24,25] Mutations in tumor suppressor genes are also contributed to development of cancer. p53, regulates cell cycle checkpoint, is the most altered gene in carcinogenesis. It allows DNA repair by G_1 and G_2 arrest.[24,27]

Control of checkpoints is another important factor for cell cycle regulation to arrest cells in the cases of problems in replication of DNA and segregation of chromosomes to prevent accumulations of mutations.[29,30] Cell size is an important factor for division. G_1 and G_2 phases include cell size checkpoints. DNA damage checkpoints are also involved to cell cycle and regulated by p53 and Chk1. The latter one is takes part in all cases of DNA damage and its efficacy is higher in S and G_2 phases compared to G_1 phase.[31] Mitotic spindles control segregation of sister chromatids mechanically during anaphase and it is important to ensure bi-polar oriented spindles is created and chromosomes are properly aligned at the metaphase plate before initiation of anaphase. That process is controlled by SAC (spindle assembly checkpoint) and APC/C (anaphase-promoting complex/cyclosome), Aurora, Polo and Nek related kinases are involved in SAC.[29,31] Cancer cells exhibit continuous division due to impairments in the checkpoints. Tumor suppressors and oncogenes are mutated in cancer and signalling pathways are disrupted. Accelerated S phase entry cause oncogene induced replication stress and that led to genome and chromosomal instability. Moreover, aneuploidy is another common problem in cancer.[30]

1.4. The Cancer Stem Cell Model

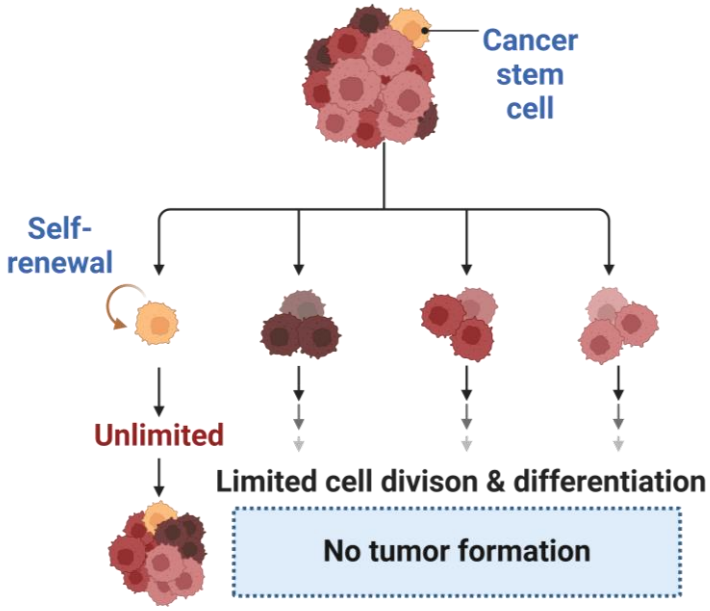

Figure 1.12. Cancer stem cell (CSC) model (Created with BioRender.com)

Cancer stem cells (CSCs) are small subpopulation in cancer cells and responsible for initiation, metastasis, recurrence, and resistance to therapy of cancer. As can be seen in Figure 1.12, they have self-renewal ability, and they can differentiate into heterogenous cell types like normal stem cells.[32–34] They asymmetrically divide, one of the resulting cells retain its stemness and quiescence while the other one continues dividing and differentiate post-mitotically.[35,36] CSCs can generate xenografts when they transplanted into animal host. To achieve this, CSCs are injected to SCID (severe combined immunodeficient) and NOD/SCID (non-obese diabetic SCID) mice due to their highly low immune response properties. It was seen that xenografts were formed in the mice.[35,37] Additionally, only a small percentage of cells isolated from different heterogeneous cancer cell population can form colonies in agar plates which supports that CSCs are constitutes a small percentage of cancer cells.[38,39] Indeed, the frequency of CSCs are on the order of one CSC per a million cancer cells.[36] CSCs can be isolated from bulk population with the help of cell surface markers they express such as CD44, CD29, and CD133 with flow cytometry or other immunologic methods.[35,40]

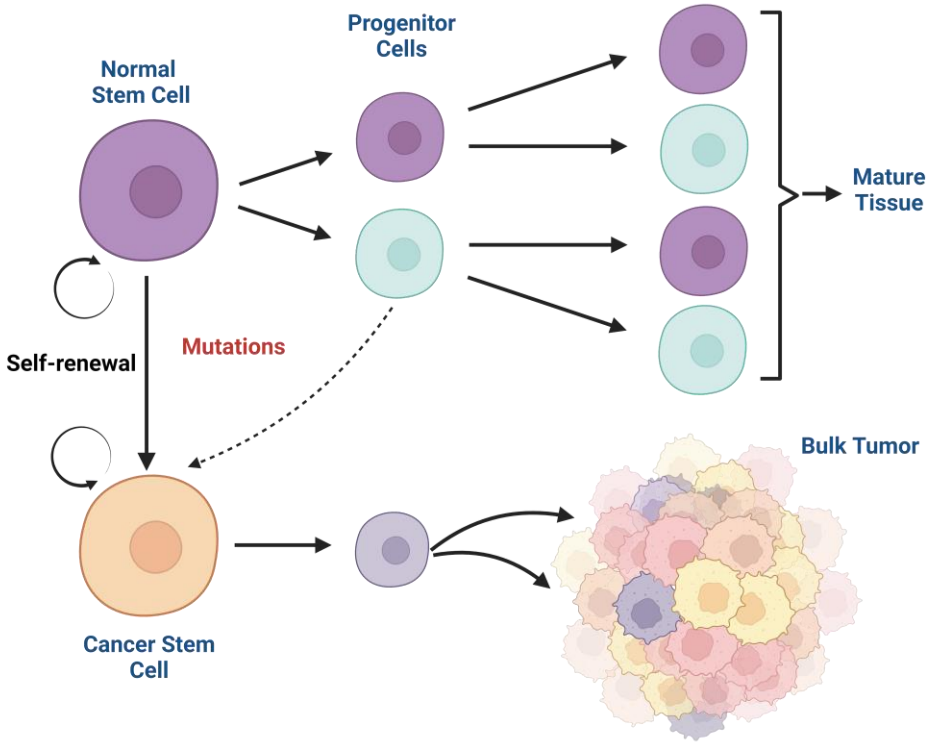

Figure 1.13. Origins of CSCs. Normal SCs and progenitor cells can be transformed into CSCs via mutations[41] [Reproduced with BioRender.com]

As can be seen in the 1.13, CSCs originate from normal stem cells and progenitor (transit-amplifying) cells that acquired self-renewal ability via mutations.[32,34,41] SCs are susceptible to accumulations of mutations since they are longest life span compared to other cells in many tissues.[39,40] Self-renewal pathways including WNT, Hedgehog, NOTCH, BMI1, PTEN, BMF, TGF-β, and telomerase play key roles in these transformations.[37,39] Interactions between CSCs and their niche -microenvironment- highly affects the activation of pathways.[37] Oncogenes are upregulated and tumor suppression is inactivated during the CSC transformation which result in uncontrolled cell growth.[33] miRNAs and EMT are another important factors that have roles in the regulation of CSCs.[35]

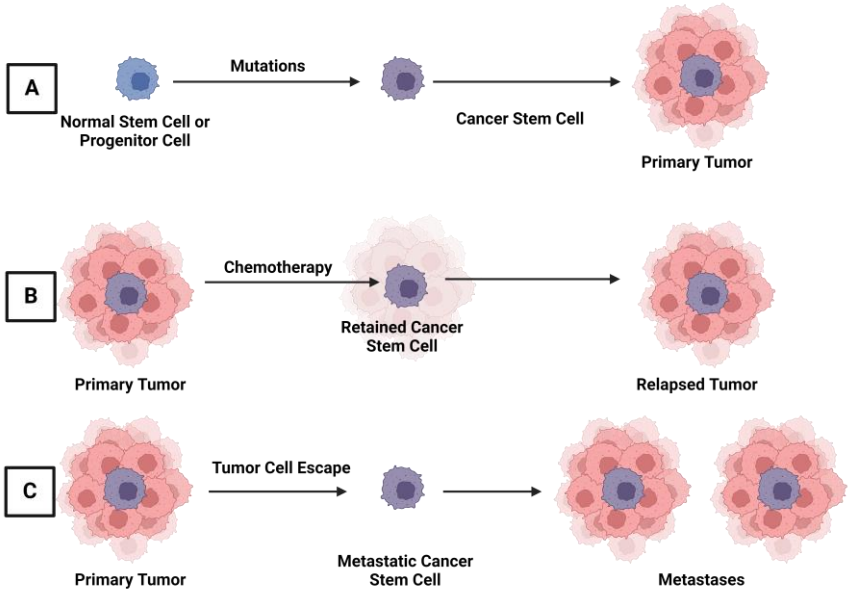

Figure 1.14. Examples demonstrating fates of CSCs: CSCs can form a primary tumor (A), CSCs can be refracted after the chemotherapy and cancer can relapse (B), CSCs can emigrate distant tissues and cause the metastasis of cancer[41] [Reproduced with BioRender.com]

Traditional cancer therapeutic approaches target bulk population of cancer cells and may not completely eliminate CSCs.[32] As can be seen in the Figure 1.14, cancer can relapse after the chemotherapy if some of the CSCs are retained (Figure 1.14-A). Also, CSCs can emigrate and cause metastases to distant tissues which makes challenging the therapy (Figure 1.14-B).[41] CSCs can survive through chemotherapy as chemotherapy is designed for actively cycling cells, but CSC are in general quiescent (in G_0 phase).[38,42,43] CSCs have high plasticity (hierarchy of differentiation).[33,36] This makes them highly tolerant to environmental stress via phenotypic alterations, multidrug resistance and quiescence.[36,42]

1.5. Malignant Melanoma

Malignant melanoma (MM), which is responsible of about %5 of the cutaneous cancer burden is accounting for over %60 of the skin cancer related deaths. Although it is in the third rank amongst the skin cancer cases, it is the main cause of skin cancer related mortality and morbidity. Its incidence has reached epidemic levels in some

countries such as Australia and United States.[44,45] Its incidence is increasing at a higher rate than other cancers. Early diagnoses with increasing public awareness have contributions to that statistics but still increase rate is alarming.[44,46] Also, median diagnostic age of melanoma is 57, which is lower than many other cancer types and this raises public health concerns.[47]

Melanoma has four general clinical subtypes as superficial spreading MM, lentigo MM, nodular, and acral lentiginous melanoma; desmoplastic, amelanotic, and ocular melanoma are rare types of MM.[45,46,48,49] Clinicians use ABCD(E) criteria to determine whether an atypic nevi is suspicious for MM and biopsy should be considered. A, B, C, D, and E stand for (a)symmetry, irregular (b)order, (c)olor variegation, (d)iameter that exceeds 6 mm, and (e)volution or (e)levation.[45,50]

Malignant melanoma is resulting from combination of multiple factors including environmental, genetic, and epigenetic factors. The main risk factor is UV (ultraviolet) radiation exposure.[47] UV light can be divided into three categories as UVA, UVB, and UVC which contain spectral regions between 315-400, 280-315, and 100-280 nm respectively.[48] UVC, and most of the UVB radiation is completely blocked by the ozone layer, while all the UVA radiation can pass through the ozone layer.[45] Depletion of ozone layer and climate change may be some of the reasons of increasing cutaneous cancer cases.[45,51] It is found that constant UV exposure can generally cause other types of cutaneous cancers, while malignant melanoma is generally related with intermittent sun exposures causing blistering burns.[44–46]

Melanocytes are originated from neural crest and responsible for melanin production which is the pigment gives color to skin. They are found in the epidermis at basal layer.[47,50] The process that melanocytes become melanoma is called melanogenesis. Accumulated mutations disturb cell cycle and melanocytes become more susceptible to UV radiation.[48]

A high base mutation frequency found in melanoma samples compared to other cancers. UV radiation is an agent that has high mutagenic potential. It causes mutations in DNA base-pairing by forming pyrimidine dimers and converting C to T via deamination. Moreover, UV radiation can cause oxidative stress and DNA mutations by leading to formation of ROS (reactive oxygen species).[50]

Another risk factors for melanoma are having fair skin and more than 100 moles.[45,48] It is found that only one third of the MM cases develop from a pre-existing mole, while others arise from de novo.[45,49] Individuals with xeroderma pigmentosa

disease are more susceptible to MM as their DNA repair systems are disrupted.[45,46] No correlation was found between MM and factors such as stress, diet, and smoking.[44]

Primary melanoma can be cured by surgery. However, the mortality rate is high at the advanced stages as the MM is aggressively metastatic. MM melanoma cells have stemness properties. Thus, failures in the treatment and recurrence are common problems for MM.[51]

Mutations in BRAF and NRAS (neuroblastoma-RAS) genes are common in MM cases. In general, mutations in only one of the oncogenes are found in the MM patients. BRAF is classified as proto-oncogene. It is responsible for encoding serine/threonine kinase and that protein takes place in RAS-RAF-MEK-ERK kinase signalling pathway and cause proliferation and growth of the cells. If BRAF is subjected to an activation mutation it becomes self-sufficient and permanently activated which results in uncontrolled proliferation of the cells and this is the case for about a half of the MM cases. These can lead to tumour development. The most common BRAF mutation is V600E missense mutation, accountable for %90 of the activating mutations and represents transformation of valine to glutamic acid, is responsible about half of the metastatic MM cases. Another common mutation is the V600K mutation, a missense mutation that alters valine to lysine.[50] However, BRAF alterations are also found in over the half (up to 80%) of the benign nevi.[47,50] Hence, whether the BRAF alterations are responsible for carcinogenesis is not clear. Moreover, it was found that in the radial growth phase of melanoma, which is early stage of MM, BRAF mutation rate is %10. Thus, BRAF may not be responsible for initiation of MM.[50]

Alterations in NRAS GTPase and NRAS are other possible key contributors to MM development. About %20 of the MM cases NRAS GTPase mutations are detected, in the G12/13 and Q60/61 codons in most of the cases. NRAS takes part in the mitogen activating protein kinase (MAPK) signalling pathway and regulates Raf activity. Which means BRAF and RAF take place in the same pathway. There is a correlation between NRAS mutations and higher levels of proliferation. Mutations in NRAS also found in normal moles frequently, so it may not take place in the initiation of MM. Consequently, transition into metastatic MM from initial stages might be promoted by BRAF and NRAS mutations in the MAPK pathway.[50] Hence, MAPK pathway is the most disrupted pathway in MM. The second most disrupted pathway is PI3K (phosphoinositol-3-kinase) pathway which is responsible for maintaining homeostasis.[47,52] Together with BRAF and NRAS, NF1 tumor suppressor gene and KIT genes possess somatic mutations that can lead to

MM. NF1 is take place in regulation of RAS family loss of it cause hyperactivated NRAS, while alterations in KIT cause proliferation of MM.[47,52]

p53 gene is responsible for tumor suppression and it is involved in many cancer types. It encodes p53 protein which induces cell death after its activation with DNA damage or cell death. Its role in MM is controversial. p53 mutations are not found in many MM cases. However, MM cells do not response radiation therapy and chemotherapy in general which suggests that p53 cannot perform its tumor suppressing functions.[50]

CDK4 (Cyclin-dependent kinase 4) and CDKN2A take place in inheritance of the MM. CDKN2A encodes $p16^{INK4a}$ protein responsible for tumor suppression. CDK4, CDK6, pRb, and $p16^{INK4a}$ take place in regulation of S phase transition from the G1 phase during the cell cycle. CDK4 promotes cell proliferation by promoting S phase transition, while p16INK4a arrests S phase by blocking action of CDK4. p16INK4 was found inactivated in about 25-60% of the inherited MM cases.[50]

MC1R (melanocortin 1 receptor) is found in melanocytes and responsible in determining the pigmentation of skin by acting as G-protein coupled receptor. Upon UV radiation exposure MC1R becomes activated, and melanin is produced. Mutations in MC1R decrease the amount of melanin formed. Hence, the amount of melanin is not enough to overcome negative effects of ROS which resulting in DNA damage owing to excess oxidative stress. Having MC1R variant alleles increase the risk of acquisition of CDKN2A, BRAF, and NRAS mutations. Over the 80% of the MM patients with MC1R mutation have CDKN2A mutations. However, since it is a germline mutation in general which cause inheridition of MM it cannot be said that MC1R mutation cause CDKN2A mutations.[50] CDKN2A gene which found on chromosome 9 and encodes p16INK4A, mutations in that gene are considered most penetrant mutation in MM. Additionally, TERT (telomerase reverse transcriptase), POT1, MITF, TERF2IP, and RB1 mutations are linked with the familial MM.[47]

Epithelial to mesenchymal transition (EMT) take place in the metastasis of MM to distant sites throughout the body. E-cadherin etc. molecules connect melanocytes to basal keratinocytes in normal conditions. EMT transition occurs and E-cadherin switch to N-cadherin form during the metastatic transition of MM and cause invasion, migration, and excess proliferation of MM.[46,50] Vimentin can be used as EMT marker as most of the epithelial cells express it.[51] Moreover, since MM cells have stemness properties their interactions with their niche highly affect their activity. CAFs induce EMT and various

transcription factors and are involved in crosstalk between tumor cells and CAFs via various signalling pathways. Moreover, keratinocytes and infiltrating leukocytes affect MM cells by crosstalking.[51]

Several biomarkers including S100 which has limited specificity but high sensitivity, Melan A, SOX10 which has both high specificity and sensitivity, HMB45, MITF, tyrosinase, BRAF V600E, NK1/C3, and PRAME can be helpful in the detection and subtyping of MM. Moreover, several miRNAs and exosomes could be used as biomarkers.[52]

1.6. Aim of the Study

Cell cycle which is a highly controlled process [24] is dysregulated in cancer cells. Cells become cancerous due to accumulation of mutations. Dysregulations of cell cycle leads to uncontrolled proliferation of cancer cells. Hence, decoding mechanism of cell cycle in cancer cells of importance. Cancer stem cells are a small subpopulation of cancer cells have ability of self-renewal and differentiation as normal stem cells. They are highly responsible for metastasis, recurrence, and failure in the treatment of cancer.[53–55]

Vibrational spectroscopic techniques, IR and Raman spectroscopy, are robust techniques and they give comprehensive information about the biochemical and biophysical compositions of cells. They are label-free, fast, low labour, sensitive, and non-invasive methods. These makes vibrational spectroscopy a powerful tool for cellular research.[7,15]

In this study, it was aimed to examine cell cycle, biochemical, and biophysical properties of cancer stem cells on malignant melanoma model using vibrational spectroscopy. Cancer stem cells, non-stem cancer cells, and bulk population of cells were analysed with ATR-FTIR and Raman spectroscopy at 11^{th}, 24^{th}, 48^{th}, and 72^{nd} hours of cell cycle. Recorded spectra were pre-processed and obtained peaks in the spectra were assigned. Moreover, multivariate statistical analyses i.e. HCA and PCA were used to statistically interpret the collected data.

CHAPTER 2

METHODOLOGY

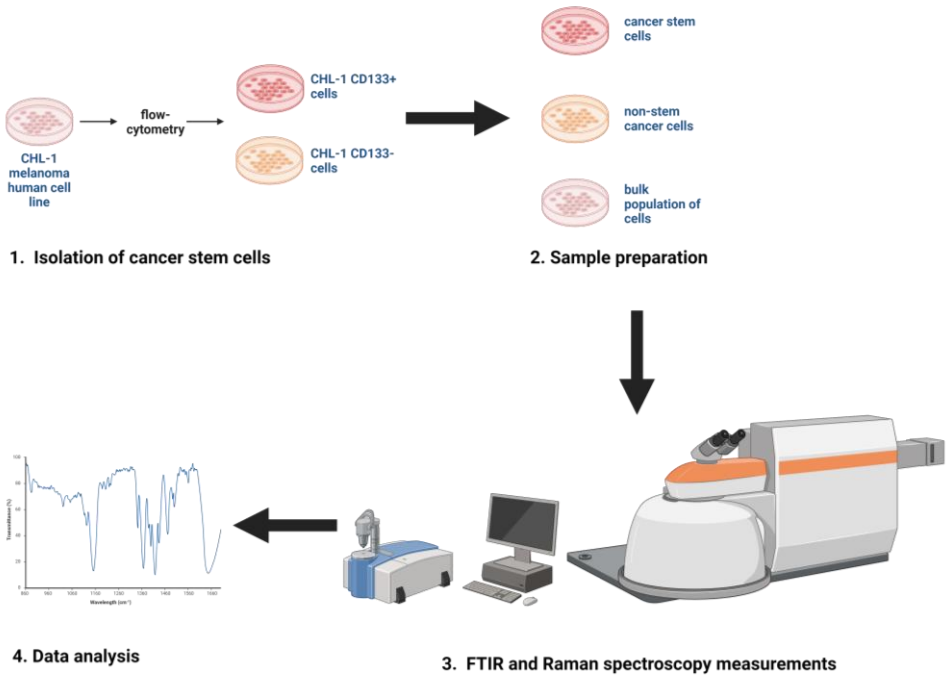

Figure 2.1. Workflow of the study

Figure 2.1 shows the generalized workflow followed in this study. Firstly CD133+ CSCs was isolated from the CHL-1 melanoma human cell line. Afterwards, cell samples were prepared for spectroscopy measurement. Then, ATR-FTIR and Raman spectroscopy measurements were performed, and obtained data was analysed.

2.1. Sample Preparation

The samples used in this work were gently provided and prepared for measurements by Prof. Dr. Hüseyin Aktuğ and Dr. Berrin Özdil. MM CSCs were isolated from CHL-1 cell line by using flow cytometry, by this way CSCs and non-stem cancer

cells were separated. CSCs were regarded as CD133+ cells, while CD133- cells were regarded as non-stem cancer cells. Three groups of cells were used in the experiments as CD133+, CD133-, and CHL-1 bulk population cells. Cells were cultured in EMEM (Eagle's minimal essential medium) with %10 FBS and %1 L-glutamine during the preparation medium was removed and cells were washed with NaCl solution. Each group of cells were prepared as ~10^6 cells/ml concentration with four groups corresponding to 11^{th}, 24^{th}, 48^{th}, and 72^{nd} hours of the cell cycle.

2.2 ATR-FTIR Spectroscopic Measurements

Figure 2.2. ATR-FTIR spectrometer used in the study

ATR-FTIR measurements were performed by using PerkinElmer-UATR Two FTIR spectrometer with diamond ATR unit (USA) (1 reflection) which can be seen in the Figure 2.2. CD133+, CD133-, and CHL-1 cells at 11^{th}, 24^{th}, 48^{th}, and 72^{nd} hours of the cell cycle were analysed as three replicas. Firstly, samples were gently homogenized with vortex for 10 seconds and then 3 µl of samples were dropped into the centre of ATR crystal. Spectra were recorded in the 4000-650 cm^{-1} spectral range with 20 scans and 4 cm^{-1} resolution. Spectra were recorded to track whether the sample was dried by observing the O-H stretching mode. Then at least 5 spectra were recorded for dried sample for each sample group and these spectra were used in the data analysis.

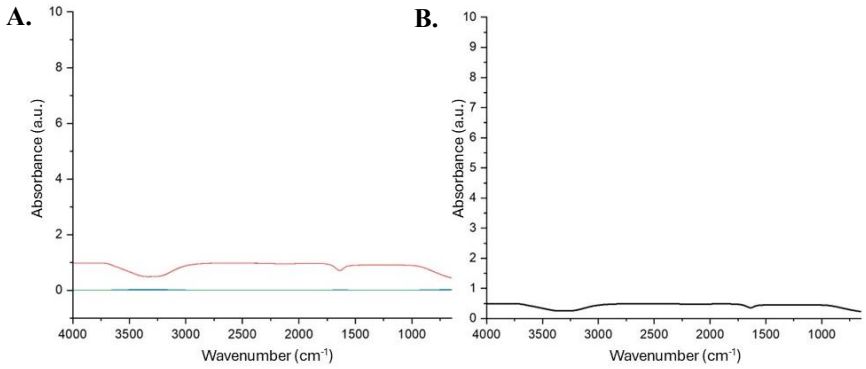

Figure 2.3. The IR spectra of (A) NaCl solution used in experiments and (B) their averages in the 4000-400 cm^{-1} spectral ranges

Figure 2.3-A shows the IR spectra recorded for NaCl solution and Figure 2.3-B shows average spectrum of them. It can be seen from the Figure 2.3, NaCl solution signals have negligible effects in the in the 3100-2800 and 1800-805 cm^{-1} spectral range.

2.3. IR Data Pre-processing

Spectra were pre-processed and analysed using MATLAB-based Kinetics and OriginLab softwares.[56–59] All spectra were normalized with respect to the area 1715 and 1485 cm^{-1} which corresponds to the area under amid I and amid II bands. Then baseline correction was performed using the baseline points corresponding to 3970, 3700, 2995, 2800, 2700, 1800, 1765, 1480, 1353, 1276, 1185, 943, and 805 cm^{-1}.

2.4. IR Data Analysis

Mean spectra were calculated by averaging all spectra for each cell types for 11^{th}, 24^{th}, 48^{th}, and 72^{nd} hours and each hour for cell types CD133+, CD133-, and CHL-1 in the spectral ranges 3100-2800 and 1800-805 cm^{-1}. Student's t-test, a widely used statistical analysis technique, tests null hypothesis (H_0) states the mean difference of two groups are the same, whereas alternative hypothesis (H_1) states that mean difference

differs from each other with statistically significant level. There are several types of t-tests. In this work, unpaired t-test was used which is used for two independent groups.[60]

Student's t test was performed on 3100-2800 and 1800-805 cm^{-1} ranges at a confidence level $\alpha = 0.1$ and difference spectra of CD133(+) − CD133(-), CD133(+) − CHL-1, and CD133(-) − CHL-1 were calculated at all hours to determine differences and similarities between the cell groups at each hour (Alpha (α) level is determined by before conducting t-test to determine threshold for significance of differences between the means of groups.).[61] Additionally, difference spectra of $24^{th} - 11^{th}$, $48^{th} - 24^{th}$, and $72^{nd} - 48^{th}$ hours were calculated using same spectra to track differences in each cell group with time.

Principal component analysis (PCA) is an old and popular multivariate analysis method, and it identifies patterns in a data set. It reduces dimension by compressing data and during this reduction information is conserved overall. PCA represents variances in the data sets with principal components (PCs) and in general first two PC, i.e. PC1 and PC2, contains most of the information regarding to the variations in the data set.[62] Hierarchical clustering analysis (HCA) clusters samples according to distances between the samples. Several linkage rules such as Ward's and centroid methods can be used to depict the data grouped as natural clusters and form a hierarchy between these clusters.[62] In this work, PCA was performed in the spectral ranges 3050-2800 and 1800-805 cm^{-1}. Finally, HCA was performed in the same spectral ranges according to Euclidian distances between the spectra by using Ward's clustering algorithm and results were represented with dendrograms. Each analysis i.e. PCA and HCA was performed both for according to hours and cell groups using the same data set.

2.5. Raman Spectroscopic Measurements

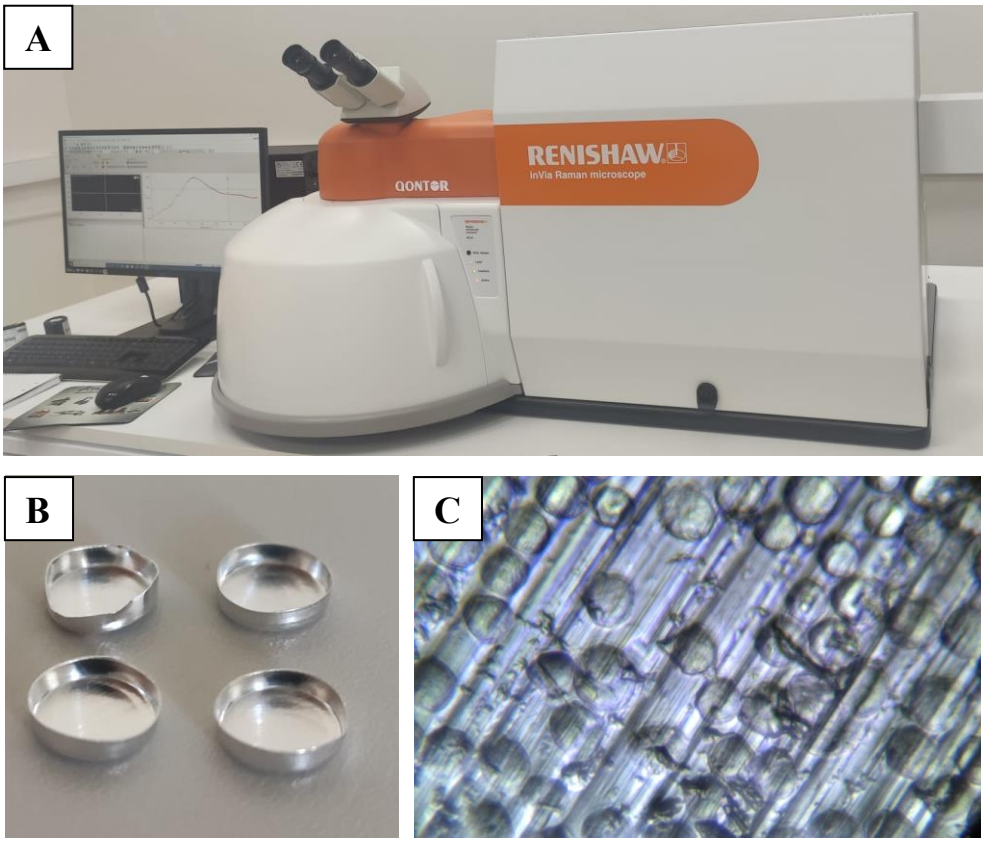

Figure 2.4. Confocal Raman system (A) and aluminium pans (B) used in the study. Raman microscopic images of CD133+ cells acquired with 532 nm laser and x50L objective (C).

Raman measurements were performed by using Renishaw inVia Qontor confocal Raman spectrometer and PerkinElmer standard aluminium pans which can be seen in the Figure 2.4-A and B, respectively. Each cell types at 11^{th}, 24^{th}, 48^{th}, and 72^{nd} hours of the cell cycle were analysed. 30 µl of samples were homogenized and put into aluminium pans. Before each measurement with the aid of the microscope focused on single cell and microscopic images were recorded as in the Figure 2.4-C. All spectra were recorded in the 400-4000 cm^{-1} range with 20 seconds accumulation time using 532 nm laser, 50% laser power, and x50L objective of the microscope. At least 15 spectra were recorded for each sample group.

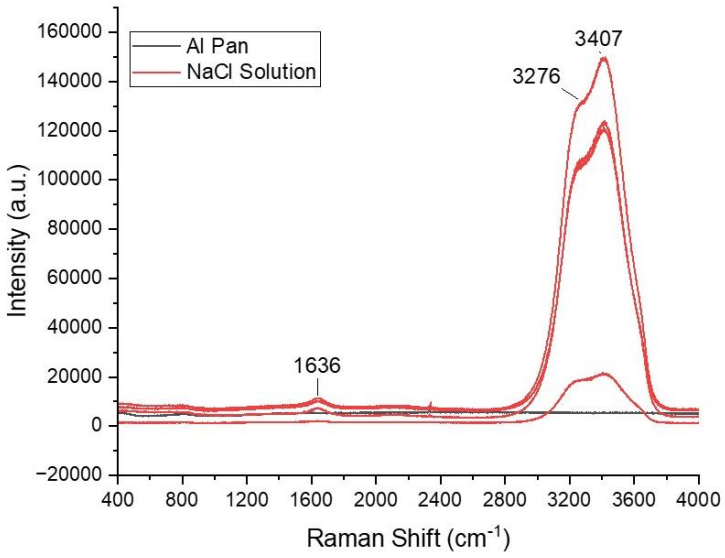

Figure 2.5. The Raman spectra of empty Al pan and NaCl solution in Al pan in the 400-4000 cm^{-1} ranges

Figure 2.5 shows the Raman spectra recorded for empty aluminium pan (black spectrum) and aluminium pan with NaCl solution in it (red spectra). It can be seen from Figure 2.5, NaCl solution signals have negligible effects in the in the 400-1800 and 2800-3000 cm^{-1} spectral ranges. There is only a small contribution of O-H bending vibration at 1636 cm^{-1}. Additionally, there are O-H stretching vibrations at 3276 and 3407 cm^{-1},[63] which are not in the analysis range.

2.6. Raman Data Pre-processing

Spectral pre-processing was performed using Origin Pro software. All spectra were normalized 0 to 1 in 400-3000 cm^{-1} ranges and smoothed with Savitzky-Golay method with 15 points of window and polynomial order of 2. Then, asymmetric least squares smoothing baselines were calculated and subtracted from the spectra with 0.001 asymmetric factor, 0.05 threshold, 10 iterations, and smoothing factor of 4.

2.7. Raman Data Analysis

Analysis of Raman data was performed using Origin Pro software. All analyses were performed both for each cell groups at 11^{th}, 24^{th}, 48^{th}, and 72^{nd} hours to compare cells at different hours of cell cycle and for each hour for CD133+, CD133-, and CHL-1 cells to track time dependent changes in each cell group. Mean spectra were calculated in the spectral ranges 400-1800 and 2800-3000 cm^{-1}. Difference spectra were calculated by subtracting mean spectra from each other. PCA was applied in the spectral ranges 400-1800 and 2800-3000 cm^{-1}. Score plots with 95% confidence ellipses and loading plots of PC1 and PC2 were obtained.

CHAPTER 3

RESULTS & DISCUSSION

3.1. ATR-FTIR Spectroscopy

3.1.1 Analysis of IR Spectra at 11th Hour

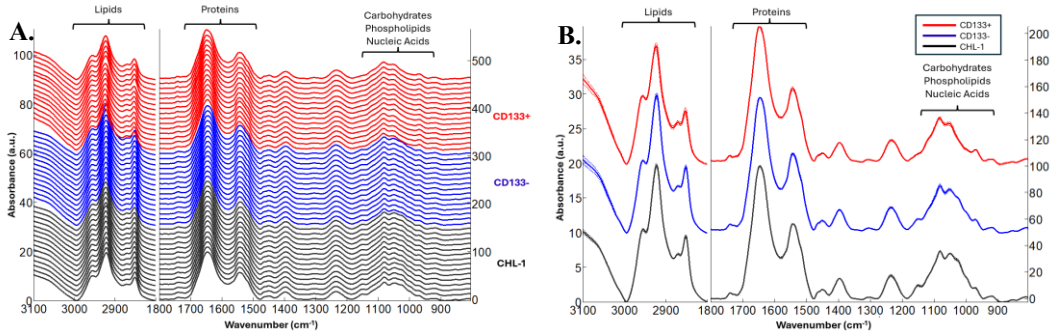

Figure 3.1. (A) All collected IR spectra in the 3100-2800 and 1800-805 cm^{-1} spectral ranges at 11th hour for CD133+ (red), CD133- (blue), and CHL-1 (black) cells and (B) mean spectra obtained by averaging them

Figure 3.1-A represents all recorded and pre-processed IR spectra for CD133+ (red), CD133- (blue), and CHL-1 (black) cells at the 11th hour of cell cycle in the 3100-2800 and 1800-805 cm^{-1} spectral ranges. Mean spectra are shown in Figure 3.1-B calculated by averaging all collected spectra. As it can be seen from the Figure 3.1, a typical FT-IR spectrum of melanoma cells includes lipid signals in the higher wavenumber region. Protein signals are predominated in the 1700-1500 cm^{-1} spectral range, whereas signals arising from nucleic acids, phospholipids, and carbohydrates are predominated in the 1200-900 cm^{-1} spectral range.[7]

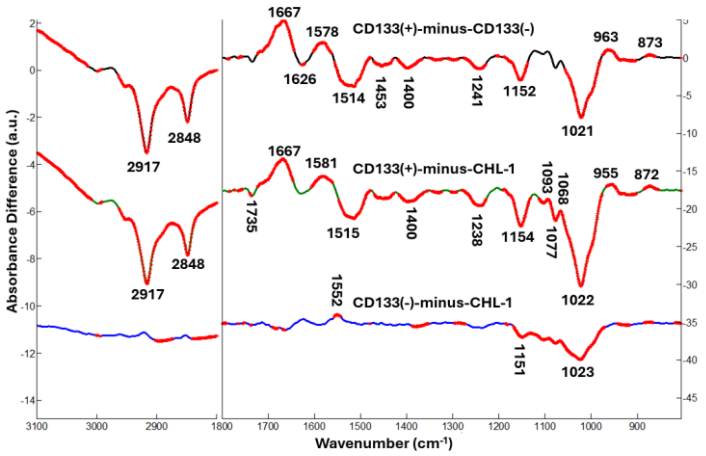

Figure 3.2. FT-IR difference spectra obtained by Student's t-test with confidence level of $\alpha = 0.1$ in the 3100-2800 and 1800-805 cm^{-1} spectral ranges at 11th hour using all spectra. Significant differences are shown in red.

Figure 3.2 depicts FT-IR difference spectra in the 3100-2800 and 1800-805 cm^{-1} ranges for 11th hour. Significant differences were determined by Student's t-test with 0.1 confidence level. The difference spectrum of CD133+ cells and CD133- cells reveals that the peaks centred at 1667, 1578, 963, and 873 cm^{-1} are higher in CD133+ cells compared to CD133- cells which are arising from amide I and amide II bands of the proteins, C-O in DNA backbone,[64] and another DNA signal,[65] respectively. The IR signals detected at 2917 and 2848 cm^{-1} can be attributed to asymmetric and symmetric vibrations of CH_2 groups in lipids,[64] respectively, and they are higher in CD133- cells. Peaks detected at 1626 cm^{-1} (amino acids), 1514 cm^{-1} (Tyr C-C ring vibrations),[66] 1453 cm^{-1} (CH_2 /CH_3 bending in proteins and lipids), 1400 cm^{-1} (COO^- vibrations of amino acids and/or lipids), 1241 cm^{-1} (vibrations of phosphate groups of nucleic acids and/or phospholipids), 1152 cm^{-1} (COH vibrations of carbohydrate derivatives), and 1021 cm^{-1} (C-O stretching in carbohydrates)[67] are also higher in CD133- cells compared to CD133+ cells. The difference spectra of CD133+ and CHL-1 cells shows similar profile with the difference spectrum of CD133+ and CD133- cells. The IR signals absorbing at 2917 and 2848 cm^{-1} due to vibrations of CH_2 groups in lipids[64] are also higher in CHL-1 cells compared to CD133+ cells. The signal at 1735 cm^{-1} caused by C=O stretching vibrations in lipids[67] is also higher in CHL-1 cells. The IR signals absorbing at 1667 cm^{-1} (amide I), 1581 cm^{-1} (amino acids and/or NH bending of nucleic acid bases),[65] 1093 cm^{-1} (symmetric stretching of PO_2^- found in nucleic acids and phospholipids), 1068 cm^{-1} (phosphate groups), 955 cm^{-1} (P-O vibrations in phosphorylated proteins),[67] and 872 cm^{-1} (DNA)[65]

are higher in CD133+ cells compared to CHL-1 cells. Whereas signals at 1515 cm^{-1} (Tyr C-C ring vibrations),[66] 1400 cm^{-1} (COO^- vibrations of amino acids and/or lipids), 1238 cm^{-1} (vibrations of phosphate groups of nucleic acids and/or phospholipids), 1154 cm^{-1} (COH vibrations of carbohydrate derivatives), 1077 cm^{-1} (symmetric stretching of PO_2^- groups in nucleic acids and/or phospholipids), and 1022 cm^{-1} (C-O stretching of carbohydrates)[67] are higher in CHL-1 cells. According to the difference spectra of CD133- and CHL-1, there is not much biochemical difference between them. The IR signal absorbing at 1552 cm^{-1} caused by amide II band[64] is slightly higher in CD133- cells, while the signals at 1151 cm^{-1} (COH vibrations of carbohydrate derivatives) and 1023 cm^{-1} (carbohydrates)[67] are higher in CHL-1 cells. The triplet IR bands absorbing at 1151, 1040, and 1023 cm^{-1} are due to glycogen and polysaccharide derivatives.[56] Overall, difference spectra revealed that amount of protein and nucleic acids are higher in CD133+ cells, while amount of lipids and glycogen are lower at 11th hour.

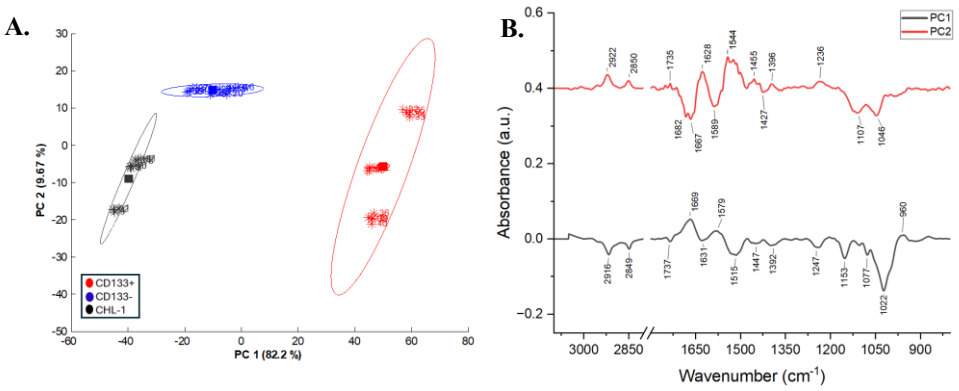

Figure 3.3. Results of PCA performed at 11th hour in the spectral ranges 3050-2800 and 1800-805 cm^{-1} (A) score plot and (B) loading plots for PC1 and PC2

Figure 3.3 depicts results of PCA performed in the spectral ranges 3050-2800 and 1800-805 cm^{-1} using all spectra collected at the 11th hour. According to the score plot shown in the Figure 3.3-A, CD133+ cells discriminated from other groups with 82.2% score for PC1, while PC2 has 9.67% score for separation of the cell groups. Hence, CD133+ cells might be in different phase from other groups at 11th. PCA loading plots shown in the Figure 3.3-B, show that PC1 clustered cells mainly based on the variations in lipid signals absorbing at 2916 and 2849 cm^{-1}, protein signals at 1669,[64] 1579,[65] and 1515[66] cm^{-1}, nucleic acid signal at 960 cm^{-1},[64] and carbohydrate signals detected at 1153

and 1022 cm^{-1}.[67] PC2 clustered cells according to variations in the lipid signals at 2922 and 2850 cm^{-1}, protein signals at 1682, 1667, 1628, 1589, and 1544 cm^{-1},[64] common contributions of macromolecules at 1107 and 1046 cm^{-1}.[65] Loading plots of PC1 and PC2 mostly overlaps with the difference spectra of cells at 11th hour.

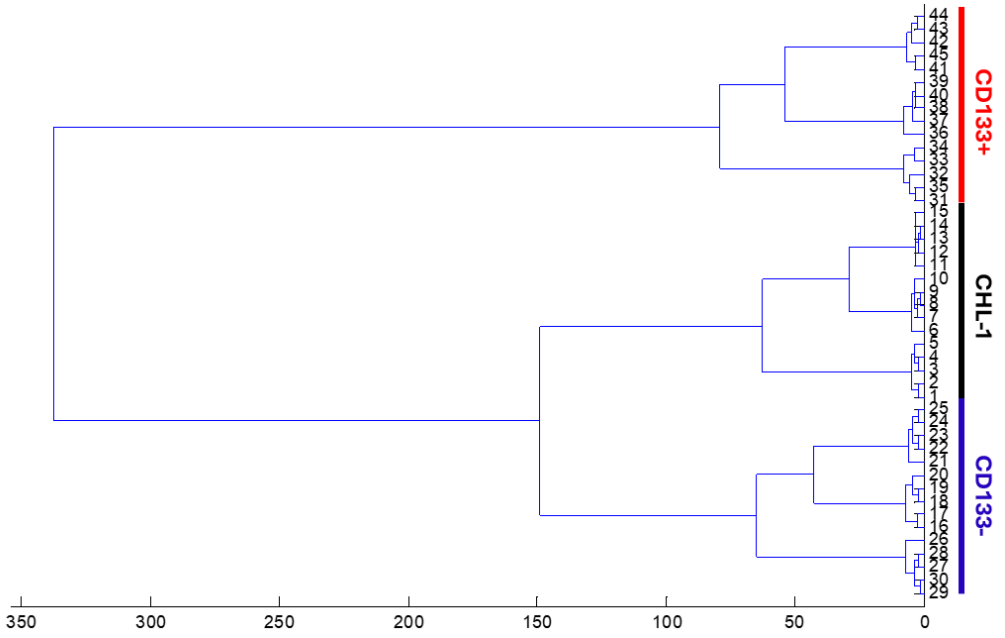

Figure 3.4. HCA dendrogram for 11th hour performed by using all recorded IR spectra in the 3050-2800 and 1800-805 cm-1 ranges according to Euclidian distances between the spectra. (1-15: CHL-1, 16-30: CD133-, and 31-45: CD133+)

Figure 3.4. represents HCA results obtained by using all collected spectra at 11th hour in the 3050-2800 and 1800-805 cm^{-1} spectral ranges. According to the dendrogram obtained, CD133- and CHL-1 cells are connected to the same node but not in the same group, while CD133+ cells are placed to a different branch. It can be said that HCA discriminates CD133+ cells from other groups at 11th hour according to IR spectroscopy results. CD133+ cells might be in a different phase of the cell cycle and CD133- and CHL-1 cells might be in the same phase as they are connected to the same node directly. HCA results are consistent with PCA results at 11th hour.

3.1.2. Analysis of IR Spectra at 24th Hour

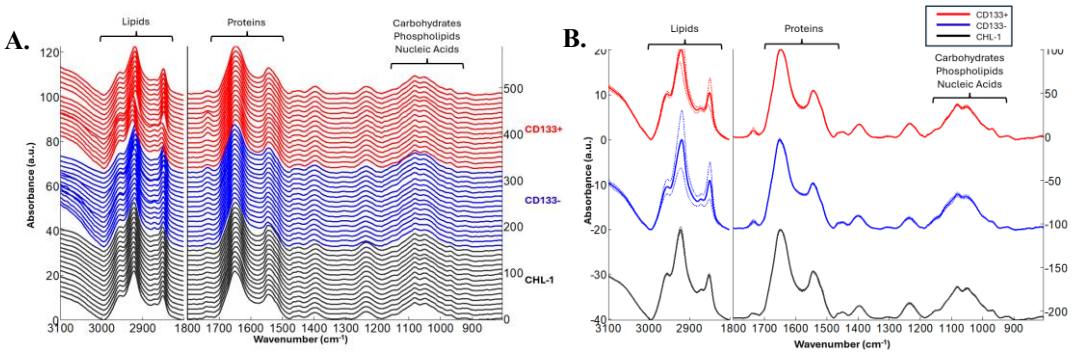

Figure 3.5. (A) All recorded IR spectra in the 3100-2800 and 1800-805 cm^{-1} spectral ranges at 24th hour for CD133+ (red), CD133- (blue), and CHL-1 (black) cells and (B) mean spectra obtained by averaging them

Figure 3.5-A shows all recorded spectra in the pre-processed form for CD133+ (red), CD133- (blue), and CHL-1 (black) cells at 24th hour in the 3100-2800 and 1800-805 cm^{-1} spectral ranges. Figure 3.5-B shows mean spectra calculated by using all collected spectra for each cell group.

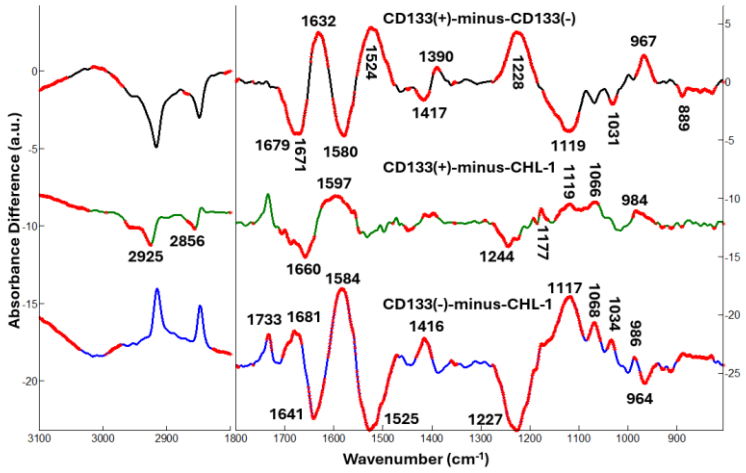

Figure 3.6. FT-IR difference spectra obtained by Student's t-test with confidence level of $\alpha = 0.1$ in the 3100-2800 and 1800-805 cm^{-1} spectral ranges at 24th hour using all spectra. Significant differences are shown in red.

Figure 3.6 shows difference spectra in the 3100-2800 and 1800-805 cm^{-1} ranges at the 24th hour. According to the difference spectrum of CD133+ and CD133- cells the IR absorbance signals centred at 1632 cm^{-1} (amino acids), 1524 cm^{-1} (Tyr C-C ring vibrations),[66] 1390 cm^{-1} (COO^- vibrations of amino acids and/or lipids), 1228 cm^{-1} (vibrations of phosphate groups of nucleic acids and/or phospholipids), and 967 cm^{-1} (C-O vibrations in DNA backbone)[67] are higher in CD133+ cells compared to CD133- cells. Whereas signals caused by proteins at 1679 cm^{-1}, 1671 cm^{-1} (amide I), 1580 cm^{-1} (amide II)[64], 1417 cm^{-1} (COO^- vibrations of amino acids and/or lipids),[67] 1119 cm^{-1} (nucleic acids and carbohydrates),[65] 1031 cm^{-1} (C-O stretching of carbohydrates),[67] and 889 cm^{-1} (deoxyribose in DNA)[65] are higher in CD133- cells. It can be seen from the difference spectrum of CD133+ and CHL-1 cells, the IR signals absorbing at 2925 and 2856 cm^{-1} due to asymmetric and symmetric vibrations of CH_2 groups in lipids, at 1660 cm^{-1} due to amide I band[64] and at 1244 cm^{-1} due to vibrations of phosphate groups of nucleic acids and/or phospholipids[67] are higher in CHL-1 cells; while signals at 1597 cm^{-1} (amide II),[64] 1119 cm^{-1} (due to nucleic acids and carbohydrates),[65] 1068 cm^{-1} (phosphate groups), and 984 cm^{-1} (mainly caused by nucleic acids)[67] are higher in CD133+ cells. It can be seen in the difference spectrum of CD133- and CHL-1 cells that absorbances at 1733 cm^{-1} (C=O stretching of phospholipids),[67] 1681 cm^{-1} (amide I), 1584 cm^{-1} (amide II),[64] 1416 cm^{-1} (lipids),[67] 1117 cm^{-1} (nucleic acids and carbohydrates),[65] 1068 cm^{-1} (phosphate groups in nucleic acids and phospholipids), 1034 cm^{-1} (carbohydrate derivatives), and 986 cm^{-1} (nucleic acids) are higher in CD133- cells, while signals caused by proteins at 1641 and 1525 cm^{-1}, and nucleic acids at 1227 and 964 cm^{-1} are higher in CHL-1 cells.[67] Overall, it can be said that concentrations of proteins and nucleic acids are higher in CD133+ cells, while amount of lipids are lower compared to CD133- and CHL-1 cells at 24th hour.

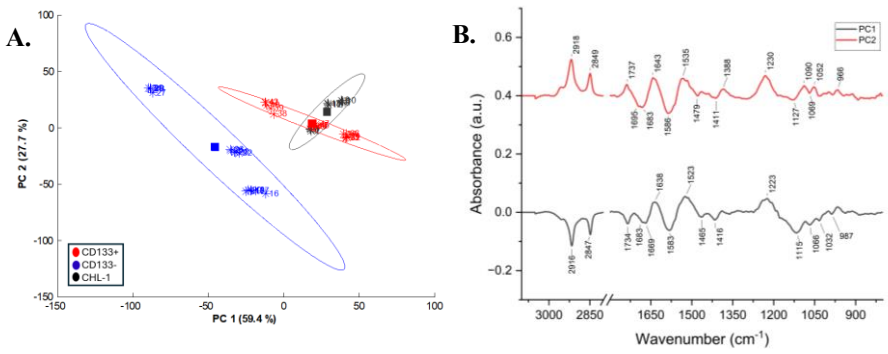

Figure 3.7. Results of PCA performed at 24th hour in the spectral ranges 3050-2800 and 1800-805 cm^{-1} (A) score plots and (B) loading plots for PC1 and PC2

Figure 3.7 shows PCA results performed in the spectral ranges 3050-2800 and 1800-805 cm^{-1} using all spectra for 24th hour. It can be seen score plots in the Figure 3.7-A, PC1 discriminated CD133- cells with 59.4% score. CD133+ and CHL-1 cells are more closely related to each other. PC2 discriminated CD133+ & CHL-1 cells with 27.7% score. According to the score plots CD133+ and CHL-1 cells might be in the same phase of the cell cycle, and they might be similar in term of their biochemistry. Loading plots shown in the Figure 3.7-B revealed that PC1 clustered cells mainly by variations in lipid signals at 2916, 2847,[64] 1734, 1416, and 1388 cm^{-1}, protein signals at 1683, 1669, 1638, 1583, and 1523 cm^{-1},[67] carbohydrate signals at 1115[65] and 1032 cm^{-1}, and nucleic acid signals at 1223, 1066, and 966 cm^{-1}.[67] PC2 separated cells according to variations at 2918, 2849,[64] and 1737 cm^{-1} which can be attributed to lipids, at 1695, 1683, 1643, 1586, and 1535 cm^{-1} can be attributed to proteins,[67] at 1127 cm^{-1} are mainly due to carbohydrates,[65] and at 1230, 1090, 1052, and 966 cm^{-1} are caused by nucleic acids.[67] Loading plots of PC1 and PC2 support difference spectra at 24th hour.

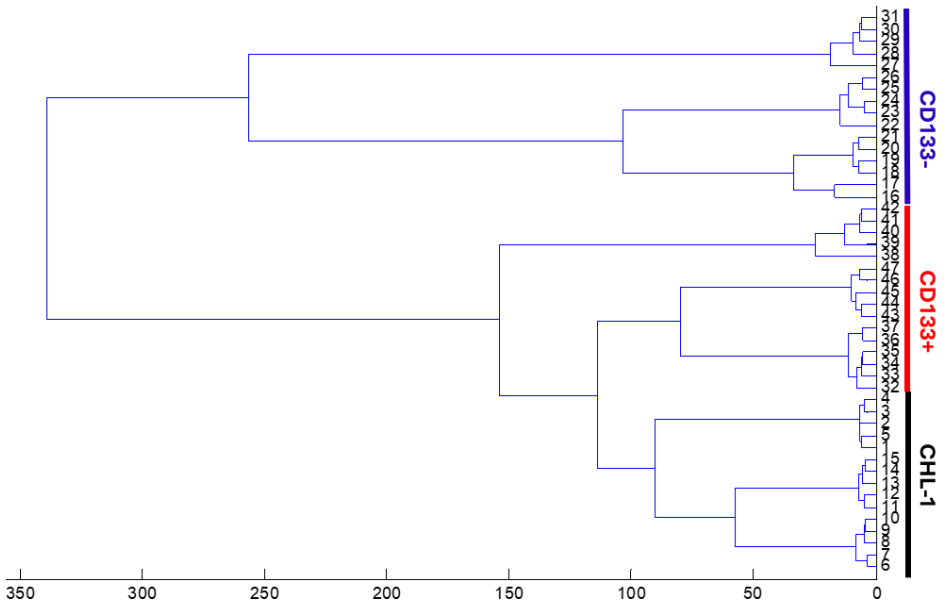

Figure 3.8. HCA dendrogram for 24th hour performed in the 3050-2800 and 1800-805 cm^{-1} ranges by using all recorded spectra (1-15: CHL-1, 16-31: CD133-, and 32-47: CD133+)

Figure 3.8 shows the HCA dendrogram for 24th hour in the 3050-2800 and 1800-805 cm^{-1} spectral ranges. CD133+ and CHL-1 cells have common node, while CD133- cells are separated from them. According to HCA results CD133- cells are more different from other groups at 24th hour. At 24th hour all cells might be in the different phases of cell cycle. HCA results support PCA results at 24th hour.

3.1.3. Analysis of IR Spectra at 48th Hour

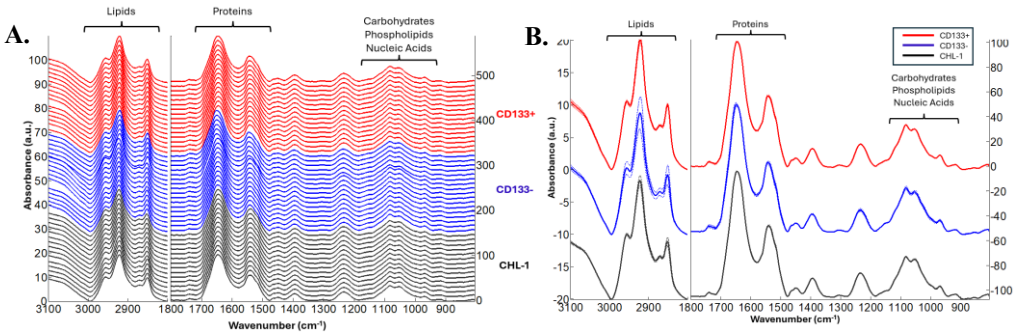

Figure 3.9. (A) All collected IR spectra in the 3100-2800 and 1800-805 cm^{-1} spectral ranges at 48th hour for CD133+ (red), CD133- (blue), and CHL-1 (black) cells and (B) mean spectra obtained by averaging them

Figure 3.9-A shows all recorded and pre-processed spectra for CD133+ (red), CD133- (blue), and CHL-1 (black) cells at the 48th hour in the 3100-2800 and 1800-805 cm^{-1} spectral ranges. Mean spectra are shown in the Figure 3.9-B which were calculated by averaging all recorded spectra for each cell group.

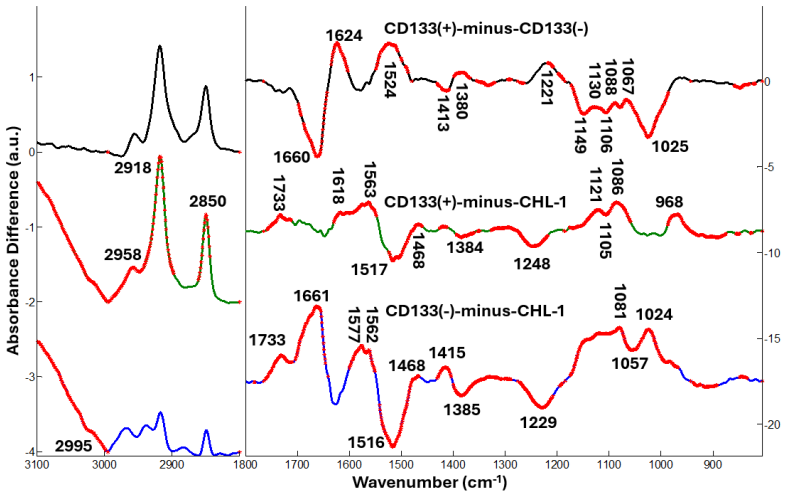

Figure 3.10. FT-IR difference spectra obtained by Student's t-test with confidence level of $\alpha = 0.1$ in the 3100-2800 and 1800-805 cm^{-1} spectral ranges at the 48th hour using all recorded spectra. Significant differences are shown in red.

Figure 3.10 presents difference spectra in the 3100-2800 and 1800-805 cm^{-1} ranges for 48th hour. According to the difference spectrum of CD133+ and CD133- cells the IR absorbance signals peaked at 1624 cm^{-1} (amino acids), 1524 cm^{-1} (Tyr C-C ring vibrations),[66] 1380 cm^{-1} (CH_3 vibrations in lipids), 1221 cm^{-1} (vibrations of phosphate groups of nucleic acids and/or phospholipids),[67] 1130 cm^{-1} (carbohydrates),[65] 1088 cm^{-1} (nucleic acids and/or phospholipids), and 1067 cm^{-1} (phosphate group vibrations)[67] are higher in CD133+ cells; while the signals obtained at 1660 cm^{-1} (amide I),[64] 1149 cm^{-1} (COH vibrations of carbohydrate derivatives),[67] 1106 cm^{-1} (nucleic acids and carbohydrates),[65] and 1025 cm^{-1} (carbohydrate derivatives) are higher in CD133- cells. Difference spectra of CD133+ and CHL-1 cells shows that lipid signals at 2958, 2918, 2850, and 1733 cm^{-1}, protein signals at 1618 and 1563 cm^{-1},[67] carbohydrate signal at 1121 cm^{-1},[65] and nucleic acid signals at 1066 and 968 cm^{-1} are higher in CD133+ cells,[67] whereas the signals absorbing at 1517 and 1248 cm^{-1} due to Tyr ring vibrations[66] and phosphate groups of nucleic acids and phospholipids, respectively were lower in in CD133+ cells. The difference spectra of CD133- and CHL-1 cells shows that the lipid signals at 1733, 1468, and 1415 cm^{-1}, protein signals at 1661, 1577 and 1562 cm^{-1}, nucleic acid signal at 1081, and carbohydrate signal at 1024 cm^{-1} are higher in CD133- cells;[67] while signals at 1516 and 1229 cm^{-1} due Tyr ring[66] and phosphate group vibrations, respectively, the lipid signal detected at 1385 cm^{-1}, and C-O stretching signal observed at 1057 cm^{-1} are lower.[67] Overall, lipid concentration was higher in CD133+ cells. Moreover, protein and nucleic acid amounts were higher in CD133+ cells though the differences between CD133+ cells and other groups were lower compared to 11th and 24th hours.

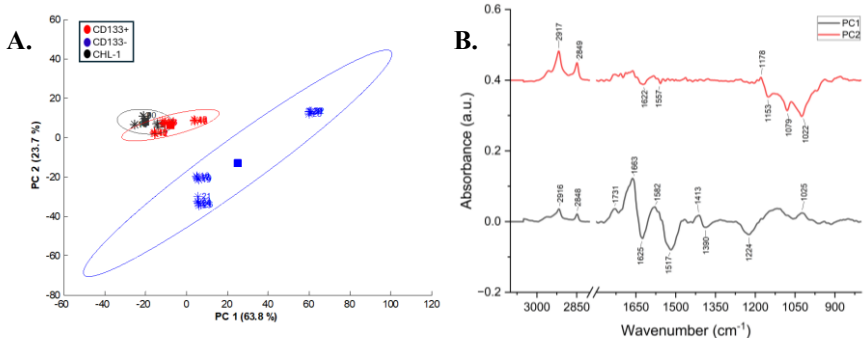

Figure 3.11. Results of PCA performed at 48th hour in the spectral ranges 3050-2800 and 1800-805 cm^{-1} (A) score plots and (B) loading plots for PC1 and PC2

Figure 3.11 shows PCA results performed in the spectral ranges 3050-2800 and 1800-805 cm^{-1} using all spectra for 48th hour. It can be seen in score plots shown in the Figure 3.11-A, PC1 discriminated cells with 63.8% score, and PC2 discriminated cells with 23.7% score. According to PC1 and PC2 CD133+ and CHL-1 cells are more similar to each other statistically, and CD133- cells are different from them. Hence, CD133+ and CHL-1 cells might be in the same phase of the cell cycle, while CD133- ones are in the different phase from them. According to the loading plot shown in the figure 3.11-B, PC1 separated cells according to the absorbance variations in lipid signals at 2916, 2948,[64] 1731, 1413, and 1390 cm^{-1}, protein signals at 1663, 1625, 1582, and 1517 cm^{-1}, nucleic acid signal at 1224 cm^{-1} and carbohydrate signals at 1025 cm^{-1}.[67] PC2 groups cells according to the variations in lipid signals at 2917 and 2849 cm^{-1},[64] protein signal at 1622 cm^{-1}, variations at 1178, 1153, 1079, 1064, and 1022 cm^{-1} are due to differences in amount of nucleic acids and carbohydrates.[67] PCA loading plots matches with the difference spectra at 48th hour.

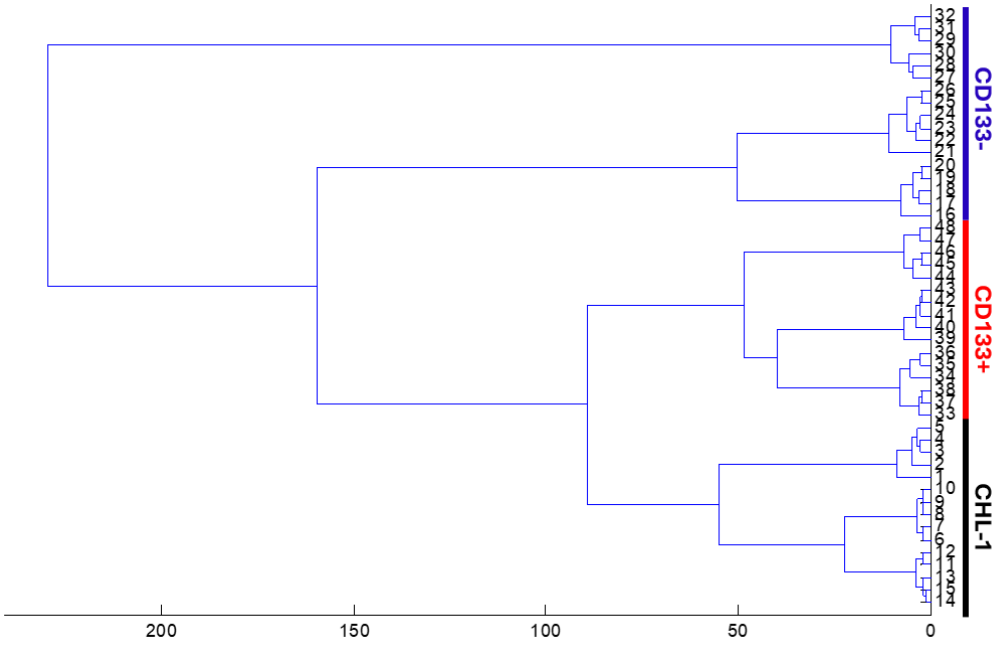

Figure 3.12. HCA results performed in the 3050-2800 and 1800-805 cm^{-1} ranges by using all recorded spectra at 48th hour (1-15: CHL-1, 16-32: CD133-, and 33-48: CD133+)

Figure 3.12 shows HCA results at the 48th hour in the 3050-2800 and 1800-805 cm^{-1} spectral ranges. CD133- cells are placed to different branches from other groups. CD133+ and CHL-1 cells are more closely related with each other, so they might be in the same phase of cell cycle. HCA results support PCA results at 48th hour.

3.1.4. Analysis of IR Spectra at 72nd Hour

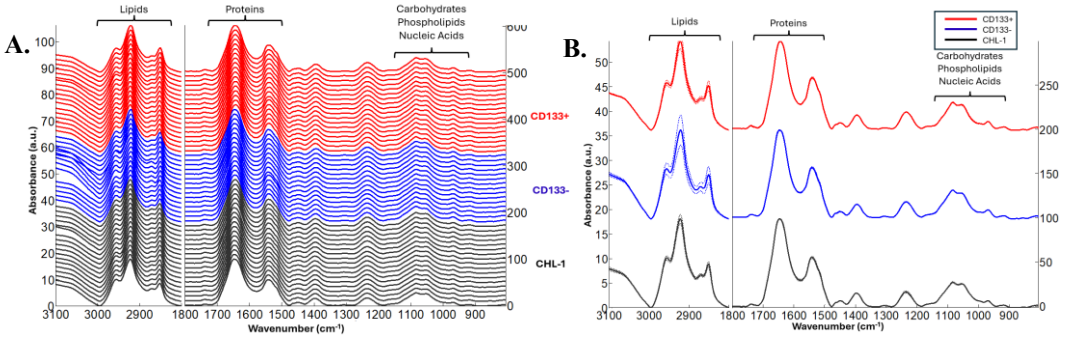

Figure 3.13. (A) All collected IR spectra in the 3100-2800 and 1800-805 cm^{-1} spectral ranges at 72nd hour for CD133+ (red), CD133- (blue), and CHL-1 (black) cells and (B) mean spectra obtained by averaging them

Figure 3.13-A shows all recorded and pre-processed IR spectra for CD133+ (red), CD133- (blue), and CHL-1 (black) cells at the 72nd hour in the 3100-2800 and 1800-805 cm^{-1} spectral ranges. Mean spectra are shown in the Figure 3.13-B calculated by averaging all recorded spectra for each cell type at 72nd hour.

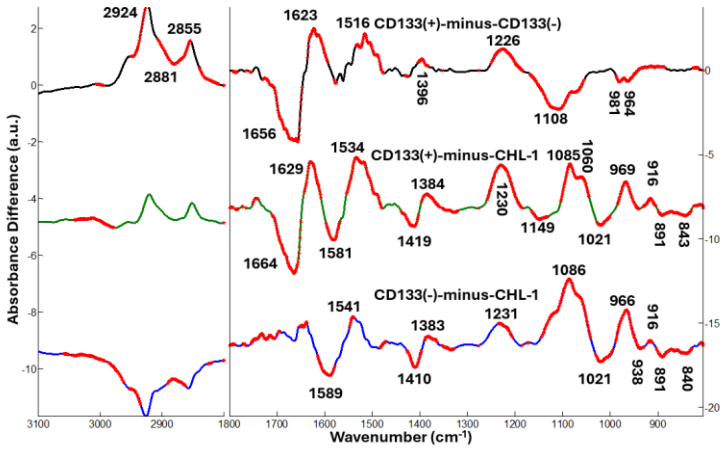

Figure 3.14. FT-IR difference spectra obtained by Student's t-test with confidence level of α = 0.1 in the 3100-2800 and 1800-805 cm^{-1} spectral ranges at the 72nd hour using all spectra. Significant differences are shown in red.

Figure 3.14 presents IR difference spectra in the 3100-2800 and 1800-805 cm^{-1} ranges for 72nd hour. According to the difference spectrum of CD133+ and CD133-, CD133+ cells have higher lipid amount from CD133- cells as the signals absorbing at 2924 and 2855 cm^{-1} due to the asymmetric and symmetric vibrations of CH_2 groups in lipids are higher in them.[64] The protein signals at 1623 and 1516 cm^{-1} are higher in CD133+ cells, while protein signal at 1656 cm^{-1} is lower. The IR signal absorbing at 1396 cm^{-1} which can be attributed to COO^- vibrations of amino acids and/or lipids is slightly higher in CD133+ cells,[67] while the carbohydrate signal at 1108 cm^{-1} is lower.[65] The nucleic acid signals at 1226, 981 and 964 cm^{-1} are also higher in CD133- cells. The difference spectra of CD133+ and CHL-1 depicts that the protein signals at 1629 and 1534 cm^{-1} are higher in CD133+ cells, while the protein signals at 1664 and 1581 cm^{-1} are lower. The lipid signal at 1419 cm^{-1} is higher in CHL-1 cells, while the lipid signal at 1384 cm^{-1} is lower. The carbohydrate signals at 1021 cm^{-1} are higher in CHL-1 cells, whereas at 1149 cm^{-1} is lower.[67] Nucleic acid signals at 891 and 843 cm^{-1} are slightly lower in CD133+ cells,[65] while nucleic acid signals at 1230, 1085, 1060, 969,[67] and 916 cm^{-1} are higher.[65] The difference spectra of CD133- and CHL-1 cells depicts that lipid and protein signals show decreasing trend in CD133- cells compared to CHL-1 cells, while nucleic acid signals at 1086, 966,[67] and 916 cm^{-1} are higher in CD133- cells.[65] Overall, at the 72nd hour CD133- cells have lower amounts of lipid composition compared to the other groups and showed increasing trend in the amount of nucleic acids.

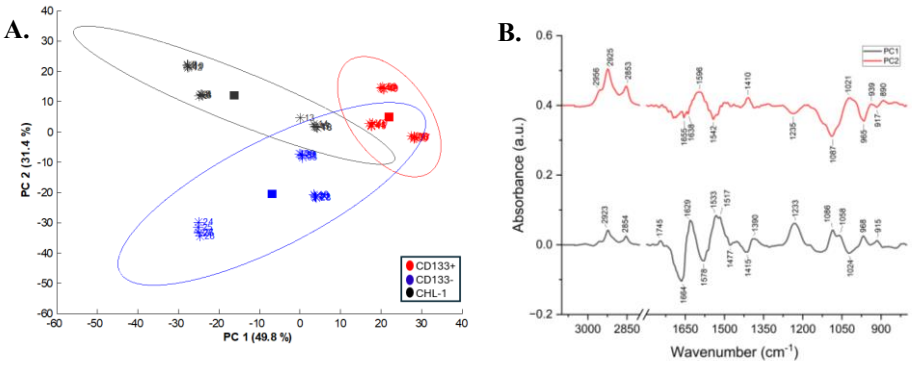

Figure 3.15. Results of PCA performed at 72nd hour in the spectral ranges 3050-2800 and 1800-805 cm^{-1} (A) score plots and (B) loading plots of PC1 and PC2

Figure 3.15 shows PCA results performed in the spectral ranges 3050-2800 and 1800-805 cm^{-1} using all spectra recorded at the 72nd hour. It can be seen from the score plots shown in the Figure 3.15-A, PC1 separated cells with 49.8% score, and PC2 distinguished cells with 31.4% score. According to PC1 CD133+ cells are less similar to other cell groups, while PC2 clusters cells as CHL-1 cells and CD133+ & CD133- cells. Loading plot for PC1 show that spectra have variances at 2923, 2854,[64] 1745, 1477, 1415, and 1390 cm^{-1} correspond to lipid signals, 1664, 1629, 1578, 1533, and 1517 cm^{-1} correspond to protein signals, 1024 cm^{-1} correspond to carbohydrate signals, and 1233, 1086, 1058, 968, and 915 cm^{-1} correspond to nucleic acids[67] and cell groups were clustered according to the absorbance variances at these wavenumbers for PC1. Loading plot for PC2 revealed that PC2 clustered cells mainly based on the lipid signals at 2956, 2925, 2853, and 1410 cm^{-1}, protein signals at 1596 and 1542 cm^{-1}, and nucleic acid signals at 1087 and 965 cm^{-1}.[67] Score plots are in line with the difference spectra for 72nd hour.

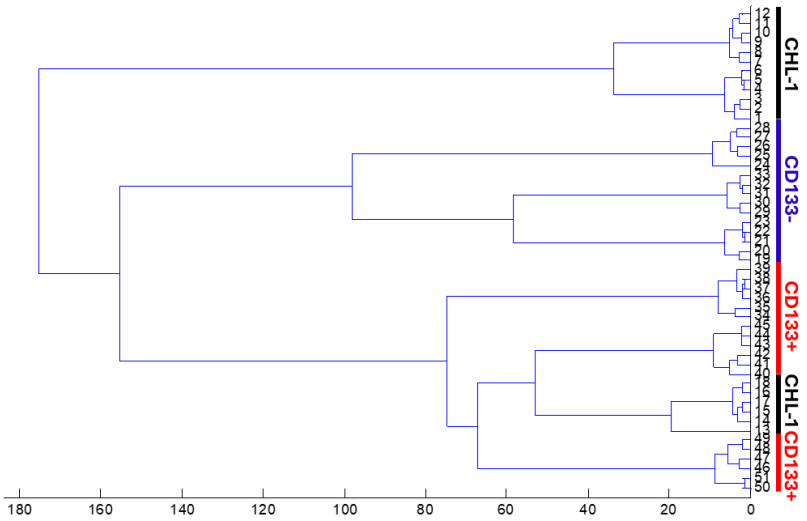

Figure 3.16. HCA results performed in the 3050-2800 and 1800-805 cm^{-1} ranges by using all collected spectra at 72nd hour (1-18: CHL-1, 19-33: CD133-, and 34-51: CD133+)

Figure 3.16 shows HCA results for the 72nd hour in the 3050-2800 and 1800-805 cm^{-1} spectral ranges. According to the dendrogram CD133+ and CHL-1 cells cannot be separated to distinct clusters at the 72nd hour as in PCA, while CD133- cells were clustered in a different group.

3.1.5. Analysis of IR Spectra for CD133(+) Cells

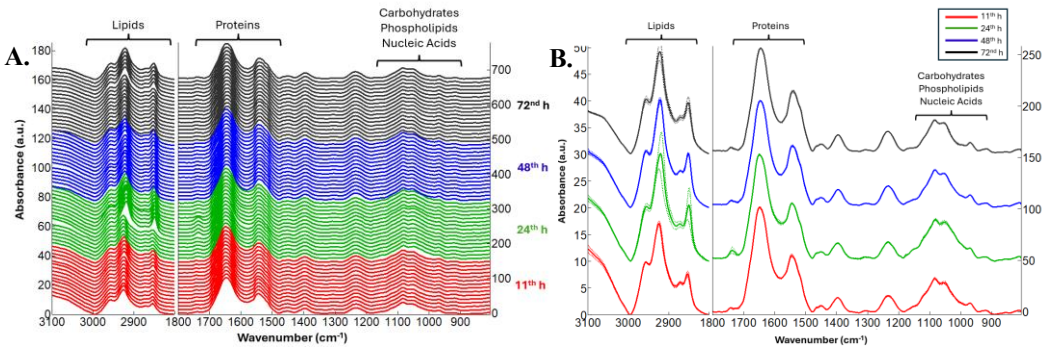

Figure 3.17. (A) All collected IR spectra for CD133+ cells in the 3100-2800 and 1800-805 cm^{-1} spectral ranges for all hours and (B) mean spectra obtained by averaging them

Figure 3.17-A shows all recorded and pre-processed spectra for CD133+ cells for all hours in the 3100-2800 and 1800-805 cm^{-1} spectral ranges. Mean spectra are shown in the Figure 3.17-B calculated by averaging all recorded spectra at the 11^{th}, 24^{th}, 48^{th}, and 72^{nd} hours.

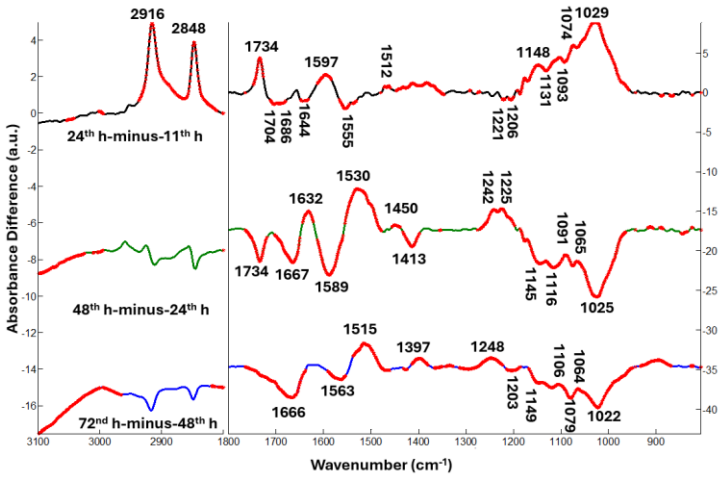

Figure 3.18. FT-IR difference spectra for CD133+ cells obtained by Student's t-test with confidence level of $\alpha = 0.1$ in the 3100-2800 and 1800-805 cm^{-1} spectral ranges. Significant differences are shown in red.

Figure 3.18 shows difference spectra for CD133+ cells in the 3100-2800 and 1800-805 cm^{-1} ranges. According to the difference spectrum of cells in 24^{th} hour and 11^{th} hour, lipid signals absorbing at 2916 cm^{-1} (asymmetric vibrations of CH_2 groups), 2848 cm^{-1} (symmetric vibrations of CH_2 groups),[64] and 1734 cm^{-1} (C=O stretching), protein signals at 1597 cm^{-1}, carbohydrate signals at 1148 cm^{-1} (COH vibrations) and 1029 cm^{-1} (C-O stretching), and nucleic acid signals at 1074 cm^{-1} (symmetric stretching of PO_2^- groups) were increased, while protein signals at 1686, 1644, and 1555 cm^{-1} were slightly decreased at 24^{th} hour. The difference spectrum of 48^{th} hour and 24^{th} hour depicts that lipid signals at 1734 cm^{-1} (C=O stretching) and 1413 cm^{-1} (COO^- vibrations), protein signals at 1667 and 1589 cm^{-1}, carbohydrate signals at 1145,[67] 1116,[65] and1025 cm^{-1} were decreased at 48^{th} hour, whereas protein signals at 1632 and 1530 cm^{-1}, and nucleic acid signals absorbing at 1242 and 1225 cm^{-1} were increased. The difference spectrum of 72^{nd} and 48^{th} hour shows that at 72^{nd} hour lipid signals observed at 2996 and 1397 cm^{-1}, protein signals at 1515 cm^{-1}, and nucleic acid signals at 1248 cm^{-1} were slightly increased at 72^{nd} hour, while the protein signals at 1666 and 1563 cm^{-1}, nucleic acid signals at 1079 cm^{-1},

and carbohydrate signals at 1149 and 1022 cm^{-1} were decreased.[67] Overall, lipid, protein, nucleic acid and carbohydrate absorbances have showed highest increase in between 11^{th} and 24^{th} hours for CD133+ cells.

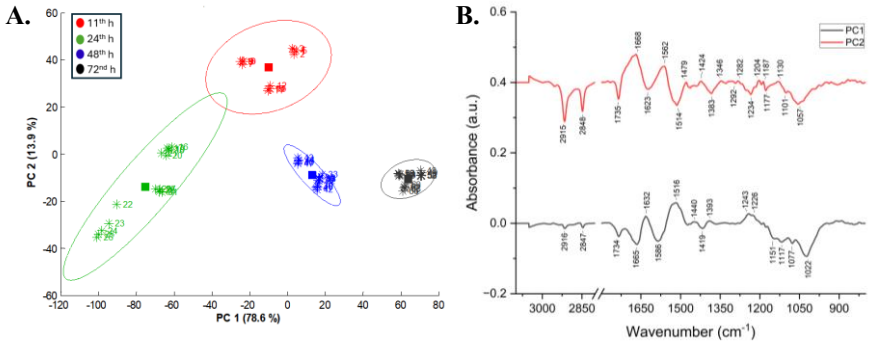

Figure 3.19. Results of PCA performed for all hours for CD133+ cells in the spectral ranges 3050-2800 and 1800-805 cm^{-1} (A) score plots and (B) loading plots for PC1 and PC2

Figure 3.19 shows PCA results performed in the spectral ranges 3050-2800 and 1800-805 cm^{-1} using all spectra recorded for CD133+ cells at 11^{th}, 24^{th}, 48^{th}, and 72^{nd} hours. It can be seen from the score plot shown in the Figure 3.19-A, PC1 separated cells with 78.6% score and PC2 distinguished cells with 13.9% score. PC1 separated cells at 24^{th} hour from other cells, though cells at 48^{th} and 72^{nd} hours are more related to each other. PC2 separates cells at 11^{th} hour and cannot distinguish cells at other hours. It can be said that CD133+ cells at 24^{th} hour is more different from others by considering the score values, and cells might be in a different phase of the cell cycle. Loading plots of PC1 and PC2, show that PC1 clusters cells mainly based on the absorbance variations at 1734 and 1419 cm^{-1} corresponding to lipids, 1665, 1632, 1586, and 1516 cm^{-1} corresponding to proteins, 1243 and 1077 cm^{-1} due to nucleic acids, and 1022 cm^{-1} due to carbohydrates. PC2 distinguishes cells mainly based on the absorbance variations in lipid signals at 2915, 2848, 1735, and 1383 cm^{-1}, protein signals at 1668, 1623, 1562, and 1514 cm^{-1}, carbohydrate signals at 1177 cm^{-1}, and nucleic acid signals at 1234 and 1057 cm^{-1}.[67] Loading plots and difference spectra are consistent with each other for CD133+ cells.

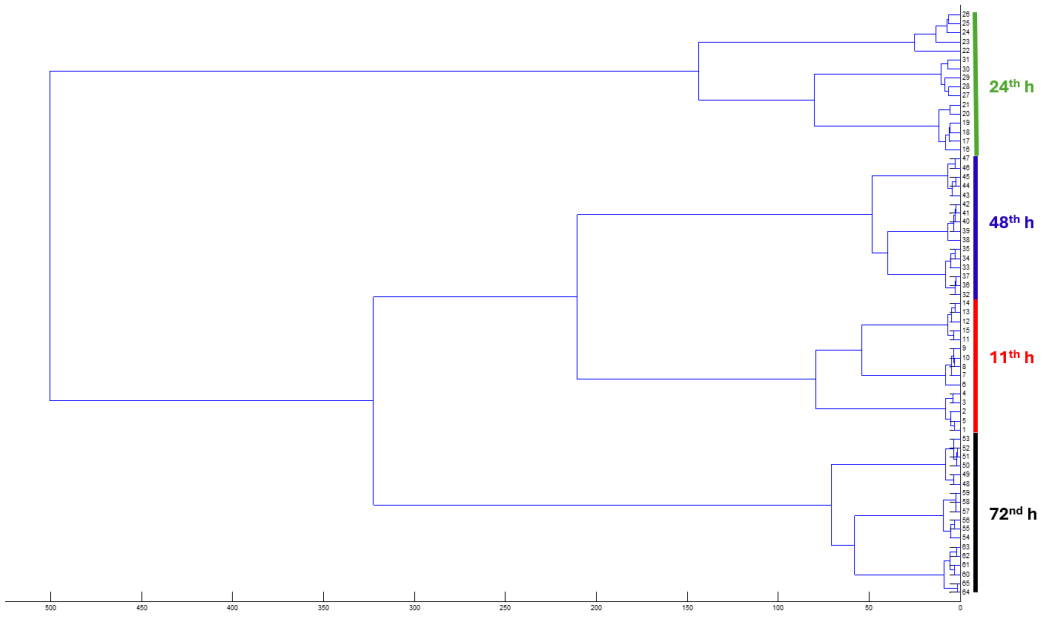

Figure 3.20. HCA results for CD133+ cells at different hours performed in the 3050-2800 and 1800-805 cm^{-1} ranges (1-15: 11th hour, 16-31: 24th hour, 32-47: 48th hour, and 48-65: 72nd hour)

Figure 3.20 shows HCA results performed using all spectra for CD133+ cells at 11th, 24th, 48th, and 72nd hours in the 3050-2800 and 1800-805 cm^{-1} spectral ranges. CD133+ cells were separated into a different branch at 24th hour, so they might be in different phase of cell cycle and biochemically different. At the 11th and 48th hours, cells are more closely related to each other so they might be in the same phase. Cells in the 72nd hour of the cell cycle are connected to same node with cells in 11th and 48th hours. Hence, they are statistically more related with each other compared to 24th hour.

3.1.6. Analysis of IR Spectra for CD133(-) Cells

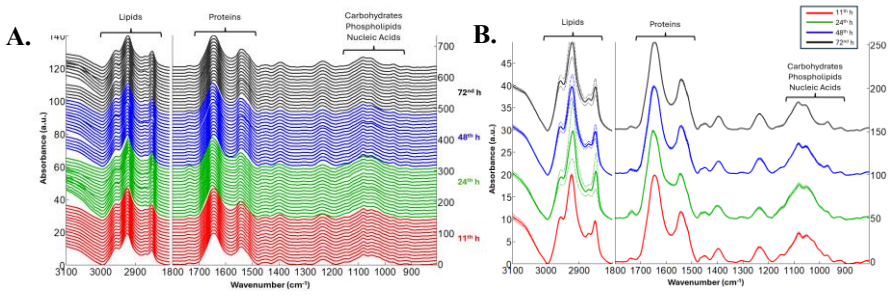

Figure 3.21. (A) All collected IR spectra for CD133- cells in the 3100-2800 and 1800-805 cm^{-1} spectral ranges for all hours and (B) mean spectra obtained by averaging them

Figure 3.21-A shows all recorded and pre-processed IR spectra for CD133- cells for all hours in the 3100-2800 and 1800-805 cm^{-1} spectral ranges. Mean spectra are shown in the Figure 3.21-B calculated by averaging all recorded spectra at the 11th, 24th, 48th, and 72nd hours.

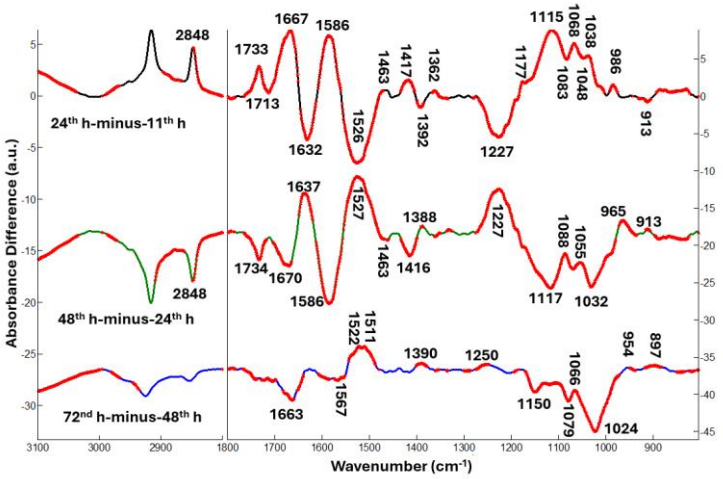

Figure 3.22. FT-IR difference spectra for CD133- cells obtained by Student's t-test with confidence level of $\alpha = 0.1$ in the 3100-2800 and 1800-805 cm^{-1} spectral ranges at 11th, 24th, 48th, and 72nd hours using all spectra. Significant differences are shown in red.

Figure 3.22 presents difference spectra for CD133- cells in the 3100-2800 and 1800-805 cm^{-1} ranges for all hours. Difference spectrum of 24th and 11th hour depicts that at 24th hour lipid signals at 2848, 1733, 1463, and 1417 cm^{-1}, protein signals at 1667 and 1586 cm^{-1}, nucleic acid signals at 1115, 1068, and 986 cm^{-1}, and the signal mostly caused by carbohydrates at 1038 cm^{-1} were increased at 24th hour in CD133- cells; while the protein signals at 1632 and 1526 cm^{-1}, lipid signals at 1392 cm^{-1}, and nucleic acid signals at 1227 and 913 cm^{-1} were decreased. According to difference spectrum of 48th and 24th hours at 48th hour, there is a decreasing trend in lipid signals and the signals at 2848, 1734 and 1416 cm^{-1} were lower and found statistically significant. Protein signals at 1637 and 1527 cm^{-1} were higher in 48th hour, while protein signals at 1670 and 1586 cm^{-1} were higher in 24th hour.[67] Moreover, carbohydrate signals absorbing at 1117[65] and 1032 cm^{-1}, were lower in 48th hour, while the signals at 1227, 965 and 913 cm^{-1} were slightly higher.[67] The difference spectrum of the 72nd and 48th hours show that the amide I signal at 1663 cm^{-1} was lower in 72nd hour,[64] while the protein signal caused by Tyr ring vibrations at 1522 cm^{-1} was higher.[66] Nucleic acid signals at 1079 cm^{-1}, and carbohydrate signals at 1150 and 1024 cm^{-1} were also lower at 72nd hour compared to 48th hour.[67] Overall, the lipid and carbohydrate amounts showed a decreasing trend after 48th hour, and between 48th and 72nd hours cells were not change too much.

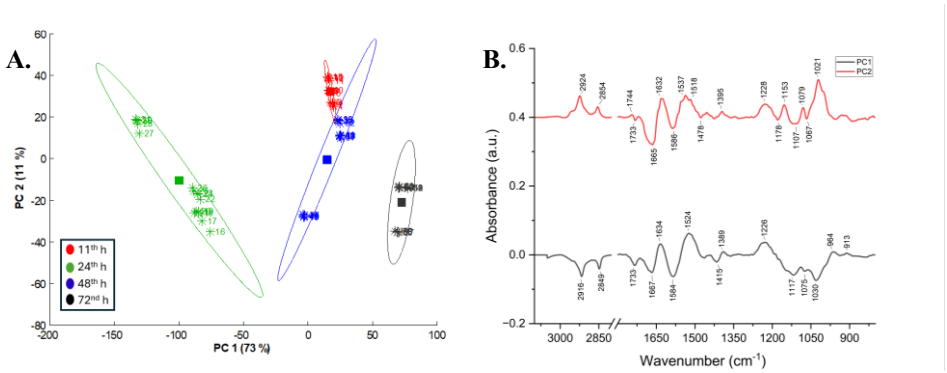

Figure 3.23. Results of PCA performed for CD133- cells at all hours in the spectral ranges 3050-2800 and 1800-805 cm^{-1} (A) score plots and (B) loading plots for PC1 and PC2

Figure 3.23 shows PCA results performed in the spectral ranges 3050-2800 and 1800-805 cm^{-1} using all recorded spectra for CD133- cells. It can be seen from the score plot shown in the Figure 3.23-A, PC1 discriminated cells with 73% score, while PC2

discriminated cells only with 11% score. According to PC1 CD133- cells at 24th hour separated from other hours and cells at 11th and 48th hours are more relevant to each other. Hence, at 11th and 48th hours percentage of CD133- cells that in the same phase of the cell cycle might be higher. PC2 cannot separated cells, though it was able to separate cells at the 11th and 72nd hours. Figure 3.23-B shows loading plots for PC1 and PC2. PC1 discriminated cells according to the variations in lipid signals at 2916, 2849, 1733, 1415, and 1389 cm^{-1}, protein signals at 1667, 1634, 1584, and 1524 cm^{-1}, and nucleic acid and carbohydrate signals at 1226, 1117, 1030, 964, and 913 cm^{-1}. PC2 distinguished cells based on absorbance differences at 2924, 2854, 1733, 1478, and 1395 cm^{-1} due to lipids, at 1665, 1632, 1586, and 1537 cm^{-1} due to proteins, and variations at 1228, 1178, 1153, 1107, 1079, 1067, and 1021 cm^{-1} due to carbohydrates and nucleic acids.[67] The peaks in loading plots match with the peaks at difference spectra for CD133- cells.

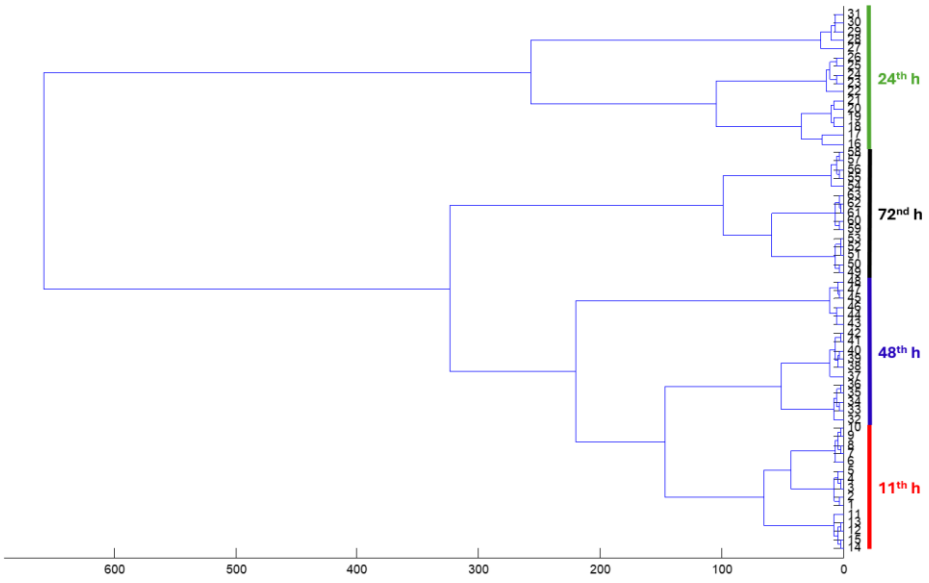

Figure 3.24. HCA results for CD133- cells at different hours performed in the 3050-2800 and 1800-805 cm^{-1} ranges (1-15: 11th hour, 16-31: 24th hour, 32-48: 48th hour, and 49-63: 72nd hour)

Figure 3.24 represents the dendrogram obtained with HCA performed using all spectra for CD133- cells at the 11th, 24th, 48th, and 72nd hours in the 3050-2800 and 1800-805 cm^{-1} spectral ranges. CD133- cells at the 11th and 48th hours might have higher percentage of cells that are in the same phase of cell cycle as their clusters are closer to

each other. At the 24th hour cells are separated to a different branch. Thus, they might be in different phase than other hours. At the 72nd hour, CD133- cells are placed to different branch from cells at the 11th and 48th hours but more related with them compared to the 24th hour. The findings in HCA are consistent with PCA performed for CD133- cells.

3.1.7. Analysis of IR Spectra for CHL-1 Cells

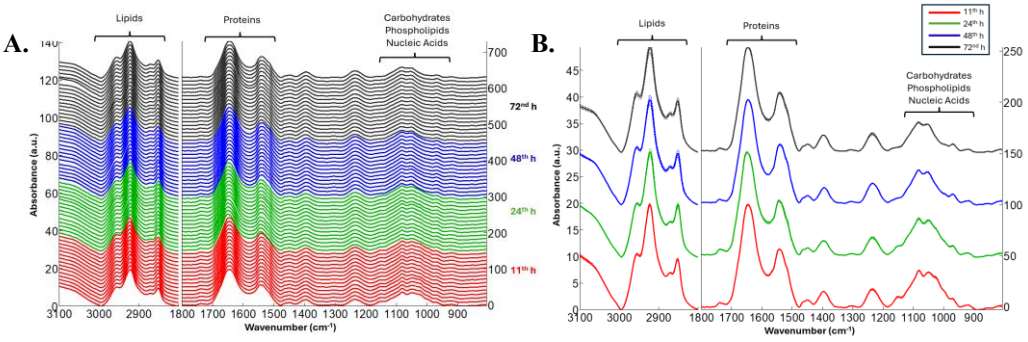

Figure 3.25. (A) All collected IR spectra for CHL-1 cells in the 3100-2800 and 1800-805 cm^{-1} spectral ranges for all hours and (B) mean spectra obtained by averaging them

Figure 3.25-A shows all recorded and pre-processed IR spectra for CHL-1 cells for all hours in the 3100-2800 and 1800-805 cm^{-1} spectral ranges. Mean spectra are shown in the Figure 3.25-B were calculated by averaging all recorded spectra at the 11th, 24th, 48th, and 72nd hours.

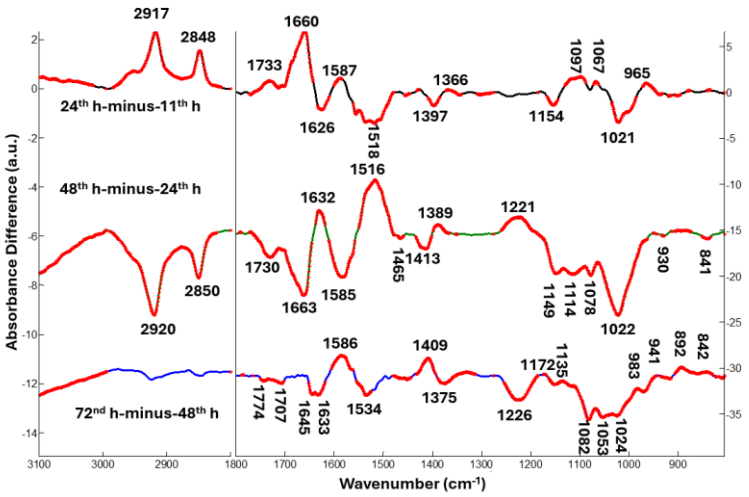

Figure 3.26. FT-IR difference spectra for CHL-1 cells obtained by Student's t-test with confidence level of α = 0.1 in the 3100-2800 and 1800-805 cm^{-1} spectral ranges at 11th, 24th, 48th, and 72nd hours using all spectra. Significant differences are shown in red.

Figure 3.26 shows difference spectra for CHL-1 cells in the 3100-2800 and 1800-805 cm^{-1} ranges for all hours. According to the difference spectrum of 24th and 11th hours lipid signals at 2917, 2848, 1733, and 1397 cm^{-1}, protein signals at 1660 and 1587 cm^{-1}, and nucleic acid signals at 1097, 1067, and 965 cm^{-1} were increased at 24th hour, while protein signals at 1626 and 1518 cm^{-1}, and carbohydrate signals at 1154, and 1021 cm^{-1} were decreased. The difference spectrum of 48th and 24th hours shows that protein signals at 1632 and 1516 cm^{-1}, lipid signals at 1389 cm^{-1}, and nucleic acid signal absorbing at 1221 cm^{-1} were increased at 48th hour, lipid signals at 2920, 2850, 1730 and 1413 cm^{-1}, protein signals at 1663 and 1585 cm^{-1}, and carbohydrate and nucleic acid signals at 1149,[67] 1114,[65] 1078, 1022, 930,[67] and 841 cm^{-1} showed a decreasing trend.[65] The difference spectrum of the 72nd and 48th hours shows that the protein signal at 1586 cm^{-1} was increased at 72nd hour, the protein signals at 1645, 1633, and 1534 cm^{-1} were decreased. The signal at 1409 cm^{-1} partly caused by absorption of lipids was increased and the lipid signal at 1375 cm^{-1} was decreased. The nucleic acid and carbohydrate signals at 1172[67] and 892 cm^{-1} were increased,[65] while at 1226, 1082, 1053 and 1024 cm^{-1} were decreased at 72nd hour.[67] Overall, at 24th hour lipid amount in CHL-1 cells shows increasing trend, while at 48th hour it shows a decreasing trend and stabilized at 72nd hour. Protein amounts showed decreasing trend at 24th hour, increased at 48th hour, and

stabilized at 72nd hour. The nucleic acid and carbohydrate amounts decreased after 48th hour.

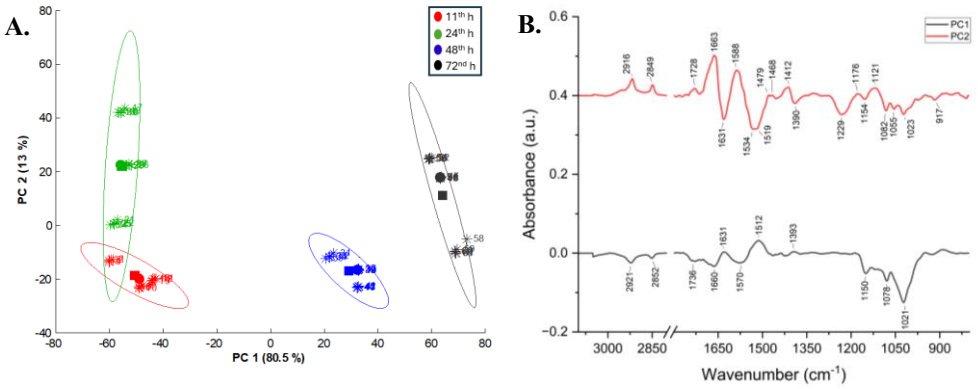

Figure 3.27. Results of PCA performed for all hours for CHL-1 cells in the spectral ranges 3050-2800 and 1800-805 cm^{-1} (A) score plots and (B) loading plots for PC1 and PC2

Figure 3.27 represents PCA results performed in the spectral ranges 3050-2800 and 1800-805 cm^{-1} using all spectra for CHL-1 cells at 11th, 24th, 48th, and 72nd hours. It can be seen from the score plots shown in the figure 3.27-A, PC1 was able to separate cells with 80.5% score, while PC2 distinguished cells with 13% score. PC1 separates CHL-1 cells as cells in 11th & 24th and 48th & 72nd hour. Especially, cells at 11th and 24th might have higher cell percentage in the same phase of the cell cycle. PC2 poorly separates cells at 11th and 48th from other cells. According to the loading plots depicted in the Figure 3.27-B, PC1 grouped cells mainly based on the absorbance variations caused by lipids at 2921, 2852, and 1736 cm^{-1}, by proteins at 1660, 1631, 1570, and 1512 cm^{-1}, by carbohydrates at 1150 and 1021 cm^{-1}, and by nucleic acids at 1078 cm^{-1}. PC2 distinguished cells based on the variances at 2916, 2849, 1728, and 1412 cm^{-1} due to lipids, at 1663, 1631, 1588, 1534, and 1519 cm^{-1} due to proteins, and 1390, 1229, 1154, 1082, 1055, 1023, and 917 cm^{-1} due to nucleic acids and carbohydrates.[67] Loading plots support difference spectra for CHL-1 cells as the peaks contained in them match with each other.

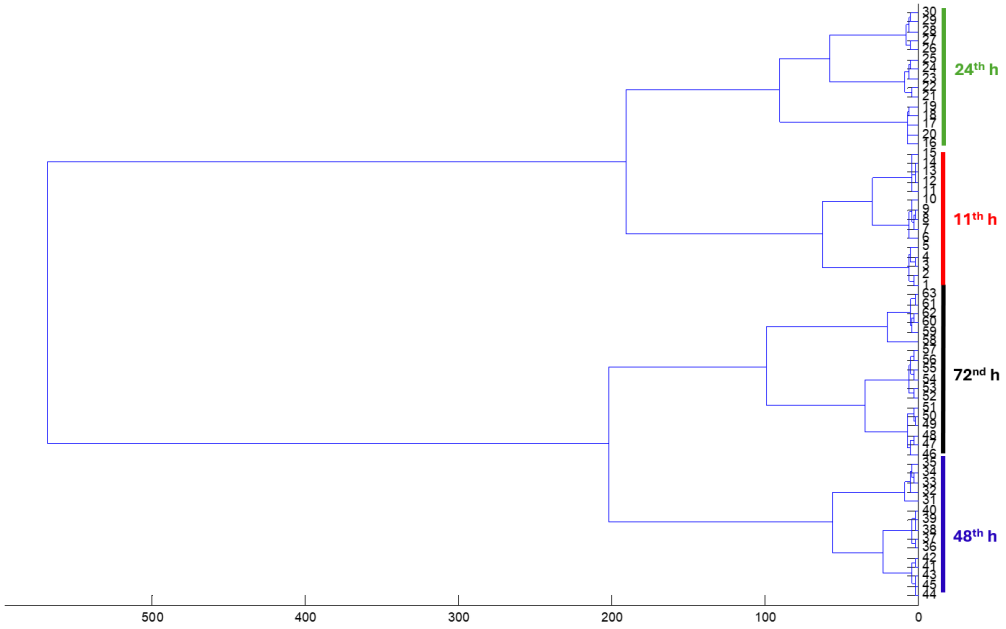

Figure 3.28. HCA dendrogram for CHL-1 cells at different hours performed in the 3050-2800 and 1800-805 cm^{-1} spectral ranges (1-15: 11^{th} hour, 16-30: 24^{th} hour, 31-45: 48^{th} hour, and 46-63: 72^{nd} hour)

Figure 3.28 depicts HCA results performed using all spectra for CHL-1 bulk population of cells at the 11^{th}, 24^{th}, 48^{th}, and 72^{nd} hours in the 3050-2800 and 1800-805 cm^{-1} spectral ranges. CHL-1 cells were separated into two general groups as cells at 11^{th} & 24^{th} hours and 48^{th} & 72^{nd} hours. Hence, at 11^{th} & 24^{th} and 48^{th} & 72^{nd} hours cells might be in the same phase of the cell cycle. Resulting dendrogram of HCA and PCA score plot for PC1 with 80.5% score support each other.

3.2. Raman Spectroscopy

3.2.1. Analysis of Raman Spectra at 11th Hour

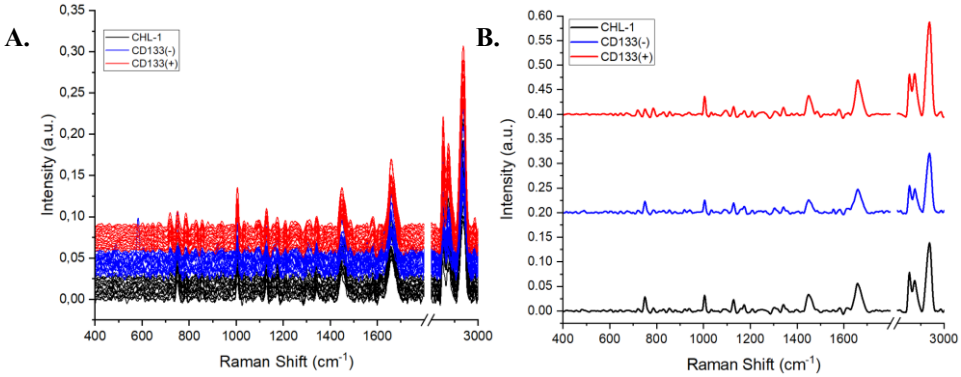

Figure 3.29. (A) All collected Raman spectra in the 400-1800 and 2800-3000 cm^{-1} spectral ranges at 11th hour for CD133+ (red), CD133- (blue), and CHL-1 (black) cells and (B) mean spectra obtained by averaging them

Figure 3.29-A shows all recorded and pre-processed Raman spectra for CD133+ (red), CD133- (blue), and CHL-1 (black) cells at the 11th hour in the 400-1800 and 2800-3000 cm^{-1} spectral ranges. Mean spectra are shown in the Figure 3.29-B were calculated by averaging all recorded spectra for each cell group at the 11th hour.

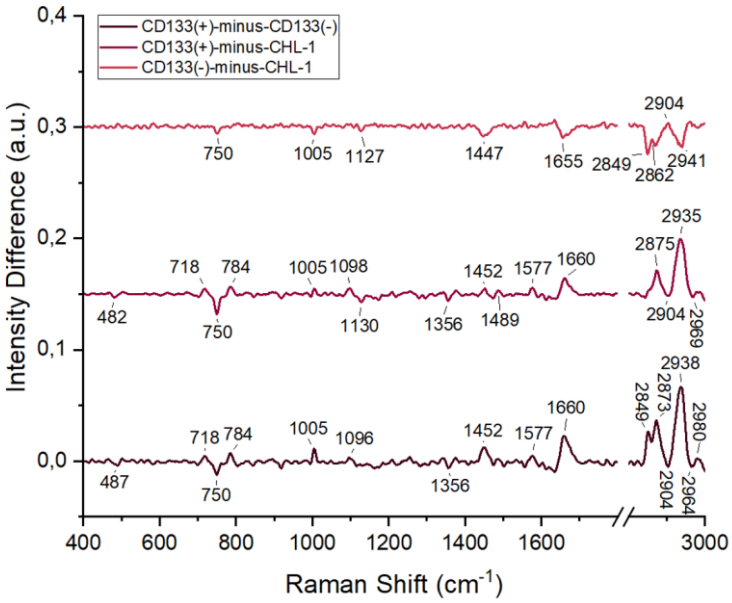

Figure 3.30. Raman difference spectra of cells obtained using average spectra at the 11th hour in the 400-1800 and 2800-3000 cm^{-1} spectral ranges.

Figure 3.30 shows the Raman difference spectra in the 400-1800 and 2800-3000 cm^{-1} spectral ranges for 11th hour. According to the difference spectrum of CD133+ and CD133- cells Raman intensity is higher in CD133+ cells at the wavenumbers 718 cm^{-1} (choline),[17] 784 cm^{-1} (C, T, and U bases),[21] 1005 cm^{-1} (Phe),[19] 1096 cm^{-1} (PO_2^- in nucleic acids),[19] 1452 cm^{-1} (CH_2 deformation mode of lipids),[17] 1577 cm^{-1} (pyrimidine rings in nucleic acids),[22] 1660 cm^{-1} (amide I[19] and C=C stretching of lipids[17]), 2849 cm^{-1} (CH_2 stretching of lipids), 2873 cm^{-1} (CH_2 stretching of lipids), 2938 cm^{-1} (CH_3 stretching of lipids);[17] while Raman intensity is higher in CD133- cells at 487 cm^{-1} (glycogen),[16] 750 cm^{-1} (T),[19] 1356 cm^{-1} (nucleic acids),[68] and 2964 cm^{-1} (CH_3 stretching of lipids).[17] According to the difference spectrum of CD133+ and CHL-1 cells, the Raman signals at 718 cm^{-1} (choline),[17] 784 cm^{-1} (C, T, and U), 1005 cm^{-1} (Phe),[19] 1098 cm^{-1} (PO_2^- in nucleic acids),[21] 1452 cm^{-1} (lipids), 1489 cm^{-1} (A and G),[19] 1577 cm^{-1} (pyrimidine ring vibrations),[22] 1660 cm^{-1} (amide I and C-C stretching in lipids), 2875 cm^{-1} (lipids), and 2935 cm^{-1} (lipids) are higher in CD133+ cells;[17] whereas the signals at 482 cm^{-1} (glycogen),[16] 750 cm^{-1} (T),[19] 1130 cm^{-1} (C-C stretching in lipids),[18] and 1356 cm^{-1} (nucleic acids)[68] are higher in CHL-1 cells. The difference spectrum of CD133- and CHL-1 cells revealed that the signals at 750 cm^{-1} (T), 1005 cm^{-1} (Phe),[19] 1127 cm^{-1} (lipids),[18] 1447 cm^{-1} (lipids), 1655 cm^{-1} (amide I), 2849 cm^{-1} (lipids), 2862 cm^{-1} (lipids), and 2941 cm^{-1} (lipids) are higher in CHL-1 cells compared to CD133- cells at 11th hour.[17]

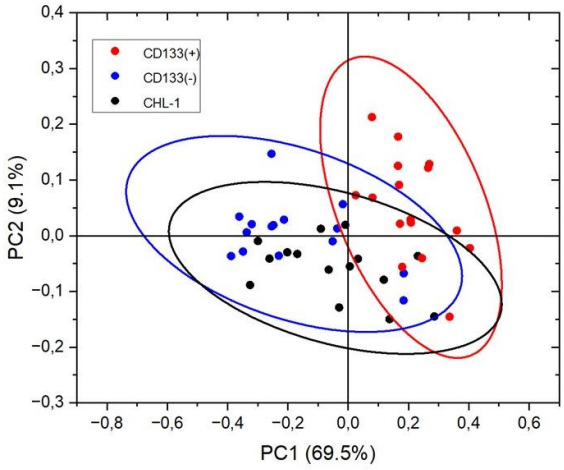

Figure 3.31. Score plot for PCA performed at 11th hour for in the spectral ranges 400-1800 and 2800-3000 cm^{-1} with 95% confidence ellipses

Figure 3.31 represents PCA score plot for 11th hour. PC1 separated cells with 69.5% score, while PC2 was able to distinguish them with only 9.1% score. According to PC1 CD133+ cells are different from other cells, and they might be in the different phase of cell cycle. Clusters of CD133- and CHL-1 cells almost overlapped so they might be in the same phase of the cell cycle.

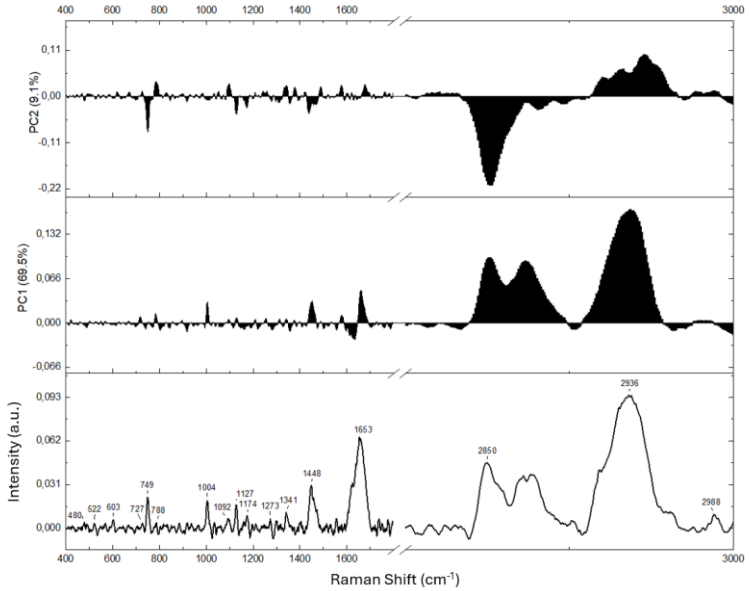

Figure 3.32. Loading plots of PC1 and PC2 for PCA performed in the spectral ranges 400-1800 and 2800-3000 cm^{-1} at 11th hour

Figure 3.32 represents loading plots of PC1 and PC2 in the ranges 400-1800 and 2800-3000 cm^{-1}. According to loading plots PC1 and PC2 distinguished cells mainly variations at 480 cm^{-1} (glycogen),[16] 727 cm^{-1} (A), 749 cm^{-1} (T), 788 cm^{-1} (DNA backbone),[19] 1004 cm^{-1} (Phe),[21] 1092 cm^{-1} (PO_2^-),[19] 1127 cm^{-1} (lipids), 1174 cm^{-1} (C,G, Tyr),[18] 1341 (A, G, and Trp), 1448 cm^{-1} (lipids), 1653 cm^{-1} (amide I),[19] 2850 cm^{-1} (lipids), 2936 cm^{-1} (lipids), and 2988 cm^{-1} (lipids) at 11th hour.[17] Loading plots and Raman difference spectra are consistent with each other.

3.2.2. Analysis of Raman Spectra at 24th Hour

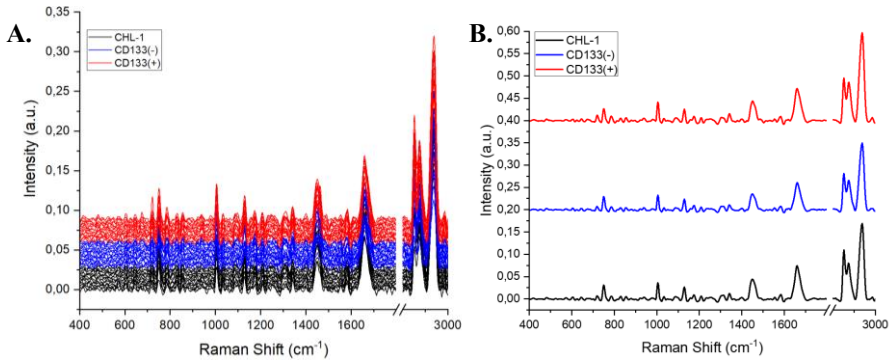

Figure 3.33. (A) All collected spectra in the 400-1800 and 2800-3000 cm^{-1} spectral ranges at 24th hour for CD133+ (red), CD133- (blue), and CHL-1 (black) cells and (B) mean spectra obtained by averaging them

Figure 3.33-A shows all recorded and pre-processed spectra for CD133+ (red), CD133- (blue), and CHL-1 (black) cells at the 24th hour in the 400-1800 and 2800-3000 cm^{-1} spectral ranges. Mean spectra are shown in the Figure 3.33-B calculated by averaging all recorded spectra for each cell type at 24th hour.

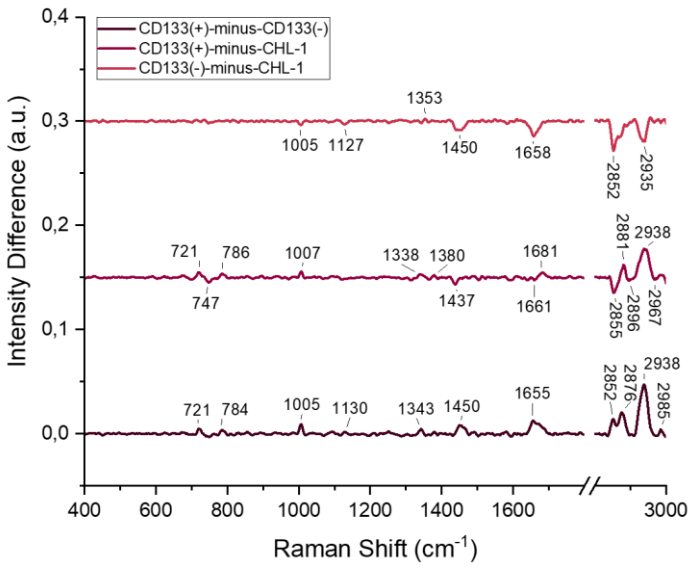

Figure 3.34. Difference spectra of cells obtained using average spectra at 24th hour in the 400-1800 and 2800-3000 cm^{-1} spectral ranges

Figure 3.34 shows difference spectra in the 400-1800 and 2800-3000 cm^{-1} ranges for 24th hour. According to the difference spectrum of CD133+ and CD133- cells Raman intensity is higher in CD133+ cells at 721 cm^{-1} (choline),[17] 784 cm^{-1} (C, T, and U bases), 1005 cm^{-1} (Phe),[19] 1130 cm^{-1} (C-C stretching in lipids),[17] 1343 cm^{-1} (A, G, and Trp),[21] 1450 cm^{-1} (CH_2 deformation mode of lipids), 1655 cm^{-1} (amide I),[19] 2852 cm^{-1} (CH_2 stretching of lipids), 2876 cm^{-1} (CH_2 stretching of lipids), 2938 cm^{-1} (CH_3 stretching of lipids), and 2985 cm^{-1} (lipids).[17] The difference spectrum of CD133+ and CHL-1 cells depicts that the signals at 721 cm^{-1} (choline),[17] 786 cm^{-1} (C, T, and U), 1007 cm^{-1} (Phe), 1338 cm^{-1} (A, G,[19] and Trp[22]), 1380 cm^{-1} (T),[19] 1681 cm^{-1} (lipids), 2881 cm^{-1} (lipids), and 2938 cm^{-1} (lipids) are higher in CD133+ cells,[17] while the signals at 747 cm^{-1} (T), 1437 cm^{-1} (phospholipids), 1661 cm^{-1} (amide I),[19] 2855 cm^{-1} (lipids), and 2967 cm^{-1} (lipids) are higher in CHL-1 cells.[17] The difference spectrum of CD133- and CHL-1 cells revealed that the signals at 1005 cm^{-1} (Phe),[21] 1127 cm^{-1} (lipids),[18] 1450 cm^{-1} (lipids),[21] 1658 cm^{-1} (amide I), 2852 cm^{-1} (lipids), and 2935 cm^{-1} (lipids) are higher in CHL-1 cells,[17] while the signal at 1353 cm^{-1} (C-N stretching of Trp) is lower.[23]

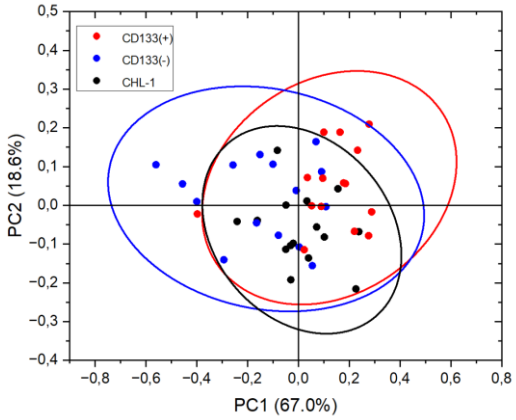

Figure 3.35. Score plot for PCA performed at 24th hour for in the spectral ranges 400-1800 and 2800-3000 cm^{-1} with 95 % confidence ellipses

Figure 3.35 depicts PCA score plot for 24th hour. PC1 separated cells with 67% score, while PC2 was able to distinguish them with 18.6% score. CD133+ and CHL-1 cells might be in the same phase of the cell cycle at the 24th hour as they are more similar to each other according to PC1.

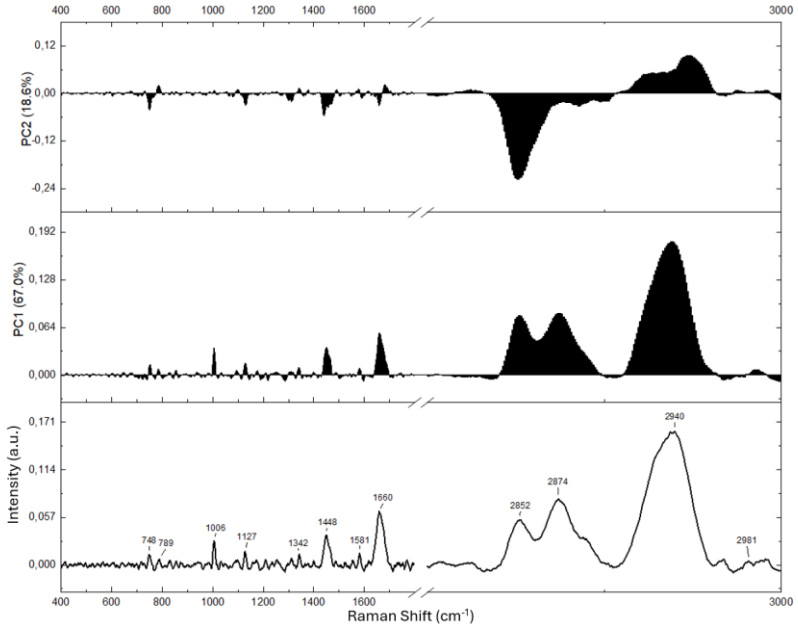

Figure 3.36. Loading plots of PC1 and PC2 for PCA performed in the spectral ranges 400-1800 and 2800-3000 cm^{-1} at 24th hour

Figure 3.36 represents loading plots of PC1 and PC2 in the spectral ranges 400-1800 and 2800-3000 cm^{-1}. Loading plots of PC1 and PC2 show that cells were distinguished mainly based on the variations at 748 cm^{-1} (T), 789 cm^{-1} (DNA backbone),

1006 cm^{-1} (Phe),[19] 1127 cm^{-1} (lipids),[18] 1342 cm^{-1} (A, G,[19] and Trp[69]), 1448 cm^{-1} (lipids),[19] 1581 cm^{-1} (pyrimidine rings),[22] 1660 cm^{-1} (amide I), 2852 cm^{-1} (lipids), 2874 cm^{-1} (lipids), and 2940 cm^{-1} (lipids) at 24th hour.[17] Loading plots and difference spectra contain similar peaks with each other.

3.2.3. Analysis of Raman Spectra at 48th Hour

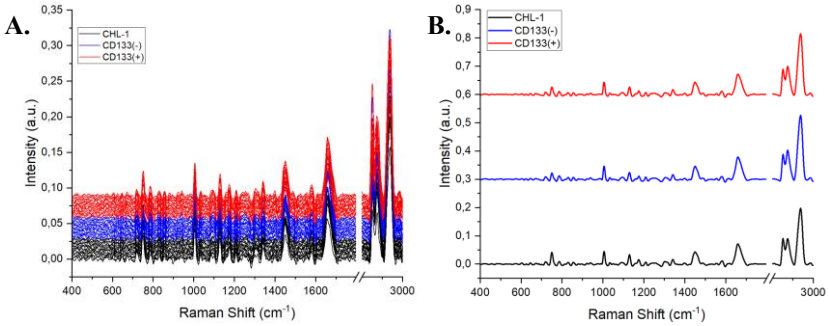

Figure 3.37. (A) All collected Raman spectra in the 400-1800 and 2800-3000 cm^{-1} spectral ranges at 48th hour for CD133+ (red), CD133- (blue), and CHL-1 (black) cells and (B) mean spectra obtained by averaging them

Figure 3.37-A shows all recorded and pre-processed Raman spectra for CD133+ (red), CD133- (blue), and CHL-1 (black) cells at the 48th hour in the 400-1800 and 2800-3000 cm^{-1} spectral ranges. Mean spectra are shown in the Figure 3.37-B calculated by averaging all recorded spectra for each cell group at the 48th hour.

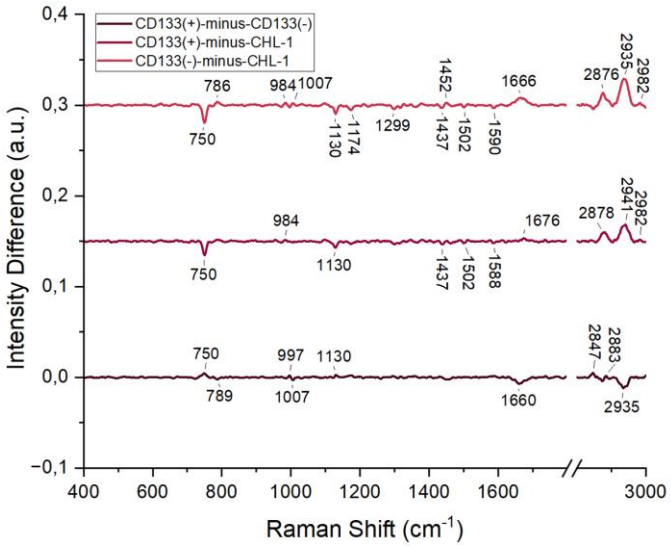

Figure 3.38. Raman difference spectra of cells obtained using average spectra at 48th hour in the 400-1800 and 2800-3000 cm^{-1} spectral ranges

Figure 3.38 shows the Raman difference spectra in the 400-1800 and 2800-3000 cm^{-1} ranges for 48th hour. It can be seen from the difference spectrum of CD133+ and CD133- cells Raman intensity is higher in CD133+ cells at 750 cm^{-1} (T),[19] 1130 cm^{-1} (C-C stretching in lipids), 2847 cm^{-1} (lipids), and 2883 cm^{-1} (lipids),[17] while higher in CD133- cells at 789 cm^{-1} (C, T, and U), 1007 cm^{-1} (Phe), 1660 cm^{-1} (amide I),[19] and 2935 cm^{-1} (lipids).[17] The difference spectrum of CD133+ and CHL-1 cells depicts that the signals detected at 750 cm^{-1} (T),[19] 1130 cm^{-1} (lipids),[18] and 1437 cm^{-1} (lipids),[17] are higher in CHL-1 cells, while the signals at 1676 cm^{-1} (cholesterol), 2878 cm^{-1} (lipids), and 2941 cm^{-1} (lipids)[17] are higher in CD133+ cells. The difference spectrum of CD133- and CHL-1 cells show that the signals at 786 cm^{-1} (nucleic acids),[19] 984 cm^{-1} (glutathione),[23] 1007 cm^{-1} (Phe), 1452 cm^{-1} (lipids), 1666 cm^{-1} (amid I[19] and lipids), 2876 cm^{-1} (lipids), and 2935 cm^{-1} (lipids)[17] are higher in CD133- cells, while the signals at 750 cm^{-1} (T),[19] 1130 cm^{-1} (lipids), 1174 cm^{-1} (nucleic acids),[18] 1299 cm^{-1} (CH_2 twisting vibration), 1437 cm^{-1} (lipids),[17] 1502 cm^{-1} (nucleic acids),[19] and 1590 cm^{-1} (nucleic acids)[22] are higher in CHL-1 cells.

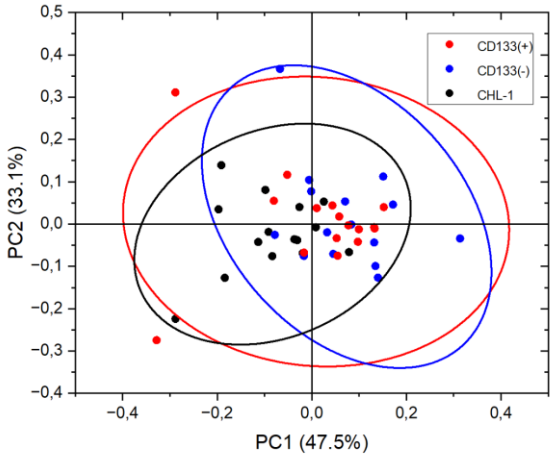

Figure 3.39. Score plot for PCA performed at 48th hour for in the spectral ranges 400-1800 and 2800-3000 cm^{-1} with 95 % confidence ellipses

Figure 3.39 shows PCA score plot for 48th hour. Cells are distinguished by PC1 with 47.5% score and by PC2 with 18.6% score. As can be seen from Figure 3.39, there are 2 outliers for CD133+ cells. CD133- and CD133+ cells are more similar to each other according to PC1, while CHL-1 is more different from them. Whereas CD133+ and CHL-1 are more similar according to PC2.

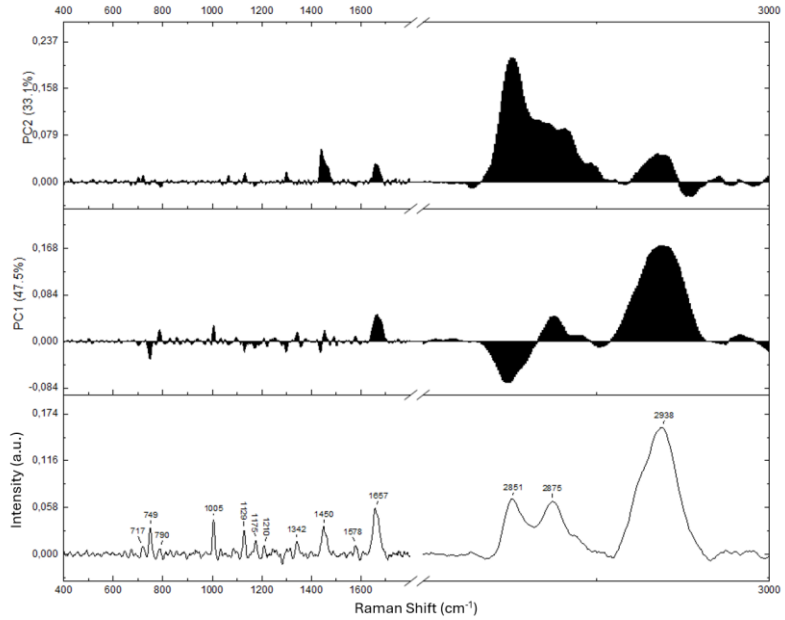

Figure 3.40. Loading plots of PC1 and PC2 for PCA performed in the spectral ranges 400-1800 and 2800-3000 cm^{-1} at the 48th hour

Figure 3.40 represents loading plots of PC1 and PC2 in the ranges 400-1800 and 2800-3000 cm^{-1}. Loading plots of PC1 and PC2 depict that cells were distinguished mainly based on variations at 717 cm^{-1} (choline),[17] 749 cm^{-1} (T), 790 cm^{-1} (DNA backbone vibrations), 1005 cm^{-1} (Phe),[19] 1129 cm^{-1} (lipids), 1175 cm^{-1} (C, G, and Tyr),[18] 1210 cm^{-1} (Tyr and Phe),[18] 1342 cm^{-1} (A, G, and Trp),[21] 1450 cm^{-1} (lipids),[17] 1578 cm^{-1} (pyrimidine rings),[22] 1657 cm^{-1} (amide I and lipids), 2851 cm^{-1} (lipids), 2875 cm^{-1} (lipids), and 2938 cm^{-1} (lipids)[17] at 48th hour. The peaks in the loading plots and difference spectra are consistent with each other.

3.2.4. Analysis of Raman Spectra at 72nd Hour

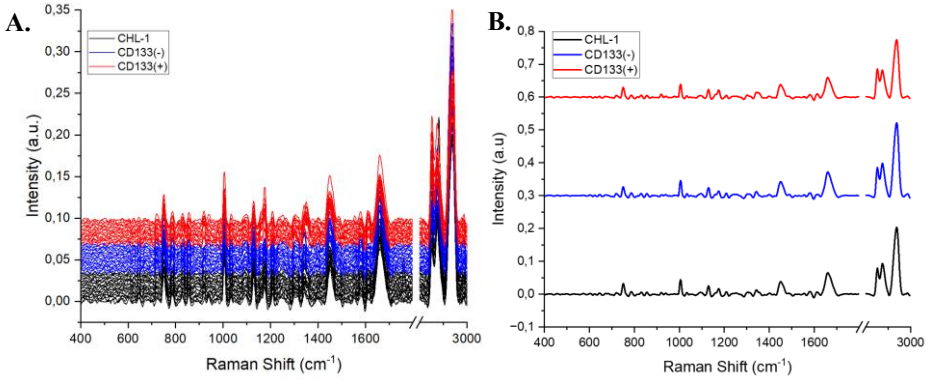

Figure 3.41. (A) All collected spectra in the 400-1800 and 2800-3000 cm^{-1} spectral ranges at 72nd hour for CD133+ (red), CD133- (blue), and CHL-1 (black) cells and (B) mean spectra obtained by averaging them

Figure 3.41-A shows all recorded and pre-processed spectra for CD133+ (red), CD133- (blue), and CHL-1 (black) cells at the 72nd hour in the 400-1800 and 2800-3000 cm^{-1} spectral ranges. Mean spectra are shown in Figure 3.41-B calculated by averaging all recorded spectra for each cell type at 72nd hour.

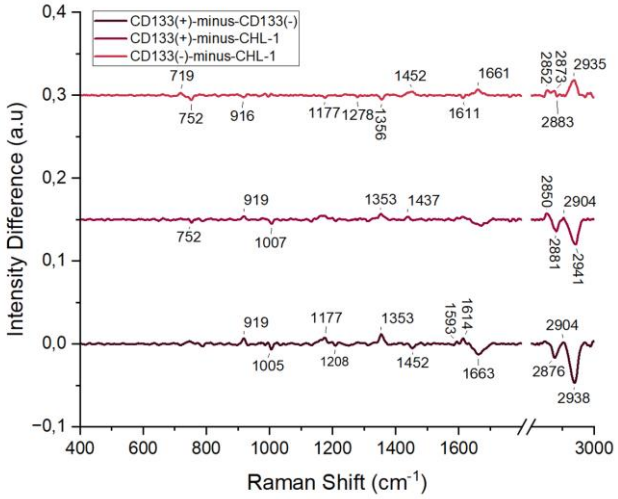

Figure 3.42. Difference spectra of cells obtained using average spectra at 72nd hour in the 400-1800 and 2800-3000 cm^{-1} spectral ranges

Figure 3.42 shows difference spectra in the 400-1800 and 2800-3000 cm^{-1} ranges for 72nd hour. It can be seen from the difference spectrum of CD133+ and CD133- cells Raman intensity is higher in CD133+ cells at 919 cm^{-1} (glutathione),[23] 1177 cm^{-1} (C, G, and Tyr),[18] 1353 cm^{-1} (Trp), 1593 cm^{-1} (nucleic acids),[23] and 1614 cm^{-1} (proteins);[18] while higher in CD133- cells at 1005 cm^{-1} (Phe), 1208 cm^{-1} (Tyr and Phe), 1452 cm^{-1} (lipids),[19] 1663 cm^{-1} (lipids and proteins), 2876 cm^{-1} (lipids), and 2938 cm^{-1} (lipids).[17] The difference spectrum of CD133+ and CHL-1 cells shows that the signals at 919 cm^{-1} (glutathione), 1353 cm^{-1} (Trp),[23] 1437 cm^{-1} (lipids), and 2850 cm^{-1} (lipids)[17] are higher in CD133+ cells; while the signals at 752 cm^{-1} (T), 1007 cm^{-1} (Phe),[19] 2881 cm^{-1} (lipids), and 2941 cm^{-1} (lipids)[17] are higher in CHL-1 cells. The difference spectrum of CD133- and CHL-1 cells are revealed that the signals at 719 cm^{-1} (choline), 1452 cm^{-1} (lipids), 1661 cm^{-1} (amide I and lipids), 2852 cm^{-1} (lipids), 2873 cm^{-1} (lipids), and 2935 cm^{-1} (lipids)[17] are higher in CD133- cells, whereas the signals at 752 cm^{-1} (T),[19] 916 cm^{-1} (glutathione),[23] 1177 cm^{-1} (C, G, and Tyr),[18] 1278 cm^{-1} (lipids), 1356 cm^{-1} (Trp),[23] 1611 cm^{-1} (proteins),[18] and 2883 cm^{-1} (lipids)[17] are lower.

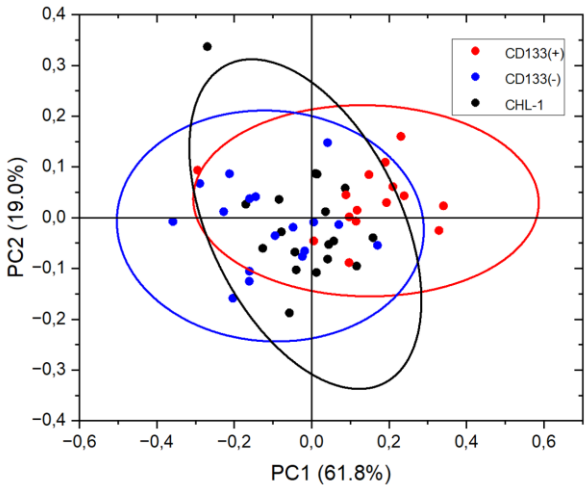

Figure 3.43. Score plot for PCA performed at the 72nd hour for in the spectral ranges 400-1800 and 2800-3000 cm^{-1} with 95 % confidence ellipses

Figure 3.43 shows PCA score plot for 72nd hour. Cells are distinguished by PC1 with 61.8% score and by PC2 with 19% score. As can be seen from Figure 3.43, there is an outlier for CHL-1 cells. CD133+ cells are different from the other groups according to PC1.

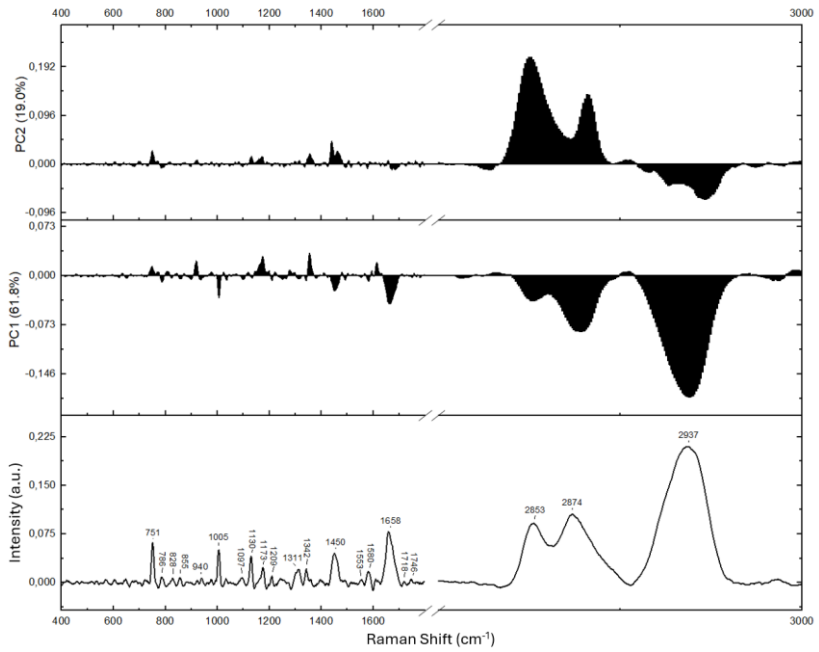

Figure 3.44. Loading plots of PC1 and PC2 for PCA performed in the spectral ranges 400-1800 and 2800-3000 cm^{-1} at the 72nd hour

Figure 3.44 represents loading plots of PC1 and PC2 at 72nd hour in the spectral ranges 400-1800 and 2800-3000 cm^{-1}. Loading plots show that cells were distinguished mainly based on the variations at 751 cm^{-1} (T), 786 cm^{-1} (DNA backbone), 828 cm^{-1} (Tyr), 855 cm^{-1} (Tyr),[19] 940 cm^{-1} (α-helix),[18] 1005 cm^{-1} (Phe), 1097 cm^{-1} (nucleic acids),[19] 1130 cm^{-1} (lipids), 1173 cm^{-1} (C, G, and Tyr), 1209 cm^{-1} (Tyr and Phe),[18] 1311 cm^{-1} (A),[22] 1342 cm^{-1} (A, G,[19] and Trp[22]), 1450 cm^{-1} (lipids),[17] 1553 cm^{-1} (proteins),[23] 1580 cm^{-1} (pyrimidine rings),[22] 1658 cm^{-1} (amide I and lipids),[17] 1718 cm^{-1} (C=O stretching),[23] 1746 cm^{-1} (lipids), 2853 cm^{-1} (lipids), 2874 cm^{-1} (lipids), and 2937 cm^{-1} (lipids)[17] at the 72nd hour. The loading plots and difference spectra present similar peaks.

3.2.5. Analysis of Raman Spectra for CD133(+) Cells

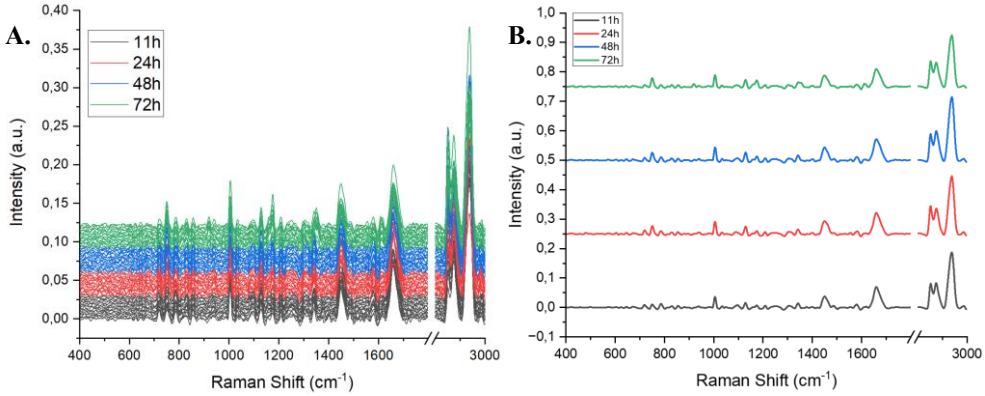

Figure 3.45. (A) All collected Raman spectra in the 400-1800 and 2800-3000 cm^{-1} spectral ranges at for CD133+ cells and (B) mean spectra obtained by averaging them at 11th, 24th, 48th, and 72nd hours

Figure 3.45-A shows all recorded and pre-processed spectra for CD133+ cells at 11th, 24th, 48th, and 72nd hours in the 400-1800 and 2800-3000 cm^{-1} spectral ranges. Mean spectra are shown in the Figure 3.45-B calculated by averaging all recorded spectra at different hours.

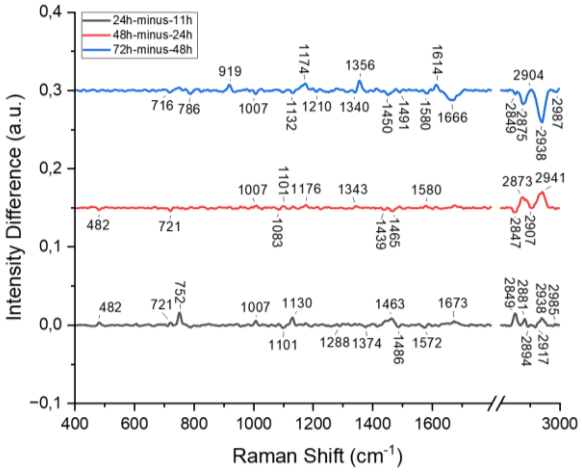

Figure 3.46. Raman difference spectra of CD133+ cells obtained using average spectra at the 11th, 24th, 48th, and 72nd hours in the 400-1800 and 2800-3000 cm^{-1} spectral ranges

Figure 3.46 shows Raman difference spectra for CD133+ cells in the 400-1800 and 2800-3000 cm^{-1} spectral ranges. According to the difference spectrum of the 24th and 11th hours Raman intensity was increased at 482 cm^{-1} (glycogen),[16] 721 cm^{-1} (choline),[17] 752 cm^{-1} (T), 1007 cm^{-1} (Phe),[19] 1130 cm^{-1} (lipids),[17] 1463 cm^{-1} (lipids),[23] 1673 cm^{-1} (cholesterol), 2849 cm^{-1} (lipids), 2881 cm^{-1} (lipids), and 2938 cm^{-1} (lipids),[17] and decreased at 1101 cm^{-1} (nucleic acids),[19] 1288 cm^{-1} (cytochrome c),[23] 1374 cm^{-1} (T), 1486 cm^{-1} (A, G),[19] 1572 cm^{-1} (nucleic acids), 2894 cm^{-1} (lipids), and 2917 cm^{-1} (lipids)[17] at 24th hour. It can be seen from difference spectra of 48th and 24th hours that signals at 482 cm^{-1} (glycogen),[16] 721 cm^{-1} (choline),[17] 1083 cm^{-1} (phospholipids and nucleic acids),[23] 1439 cm^{-1} (lipids),[19] 1465 cm^{-1} (lipids),[23] and 2847 cm^{-1} (lipids)[17] were decreased, while at 1007 cm^{-1} (Phe), 1101 cm^{-1} (nucleic acids),[19] 1176 cm^{-1} (C, G, and Tyr),[18] 1343 cm^{-1} (G),[21] 1580 cm^{-1} (pyrimidine rings),[22] 2873 cm^{-1} (lipids), and 2941 cm^{-1} (lipids)[17] were increased at 48th hour. According to the difference spectrum of the 72nd and 48th hours Raman intensity was increased at 919 cm^{-1} (glutathione),[23] 1174 cm^{-1} (C, G, and Tyr),[18] 1356 cm^{-1} (Trp),[23] and 1614 cm^{-1} (Tyr)[18] cm^{-1}, and decreased at 716 cm^{-1} (choline),[17] 786 cm^{-1} (C, T, and U), 1007 cm^{-1} (Phe),[19] 1132 cm^{-1} (lipids), 1210 cm^{-1} (Tyr and Phe),[17] 1340 cm^{-1} (A, G,[19] and Trp[22]), 1450 cm^{-1} (lipids), 1491 cm^{-1} (nucleic acids),[19] 1580 cm^{-1} (nucleic acids),[22] 1666 cm^{-1} (proteins and lipids), 2849 cm^{-1} (lipids), 2875 cm^{-1} (lipids), 2938 cm^{-1} (lipids), and 2987 cm^{-1} (lipids)[17] at 72nd hour.

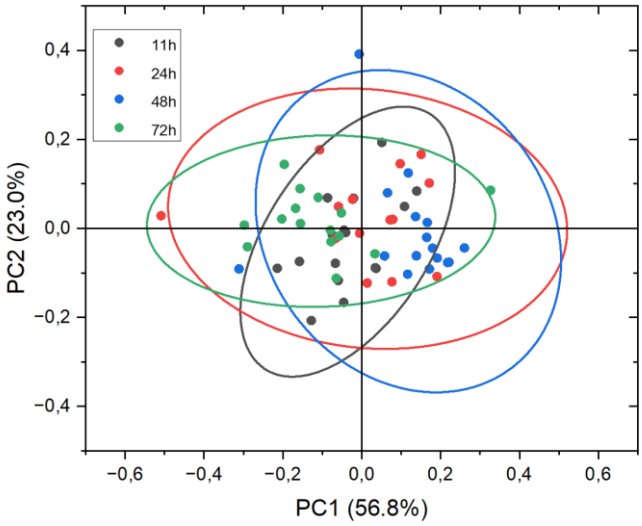

Figure 3.47. Score plot for PCA performed for CD133+ cells at all hours in the spectral ranges 400-1800 and 2800-3000 cm^{-1} with 95 % confidence ellipses

Figure 3.47 shows PCA score plot for CD133+ cells at all hours. Cells are distinguished by PC1 with 56.8% score and by PC2 with 23% score. PC1 almost separates cells at 48th and 72nd hours so they are statistically more different from each other.

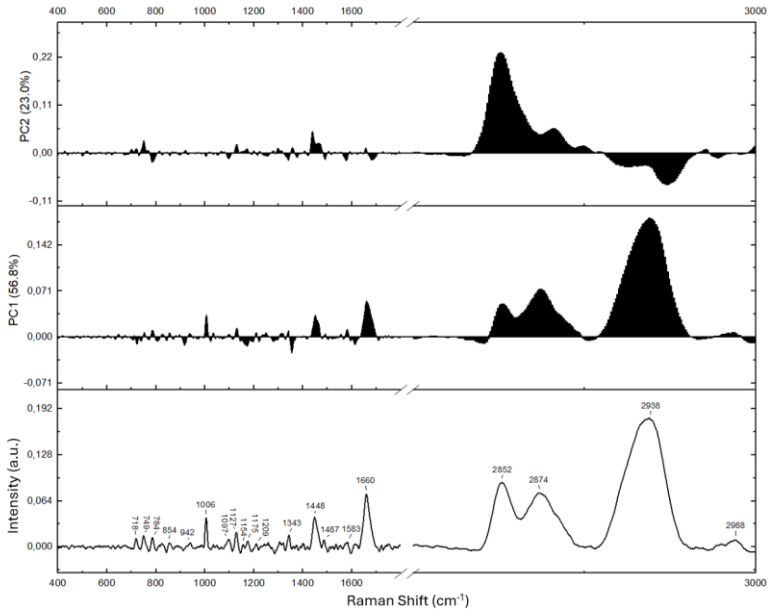

Figure 3.48. Loading plots of PC1 and PC2 for PCA performed in the spectral ranges 400-1800 and 2800-3000 cm^{-1} for CD133+ cells

Figure 3.48 represents loading plots of PC1 and PC2 for CD133+ cells at different hours in the ranges 400-1800 and 2800-3000 cm^{-1}. According to the loading plots CD133+ cells at different hours were distinguished mainly based on the variations in signals at 716 cm^{-1} (choline),[17] 749 cm^{-1} (T), 784 cm^{-1} (DNA backbone), 854 cm^{-1} (Tyr),[19] 942 cm^{-1} (proteins),[18] 1006 cm^{-1} (Phe), 1097 cm^{-1} (nucleic acids),[19] 1127 cm^{-1} (lipids), 1153 cm^{-1} (proteins), 1175 cm^{-1} (C, G, and Tyr),[18] 1209 cm^{-1} (Tyr and Phe),[17] 1343 cm^{-1} (G), 1448 cm^{-1} (lipids),[21] 1487 cm^{-1} (A, G),[19] 1583 cm^{-1} (pyrimidine rings),[22] 1660 cm^{-1} (amide I and lipids), 2852 cm^{-1} (lipids), 2874 cm^{-1} (lipids), and 2938 cm^{-1} (lipids).[17] The loading plots and difference spectra are consistent with each other.

3.2.6. Analysis of Raman Spectra for CD133(-) Cells

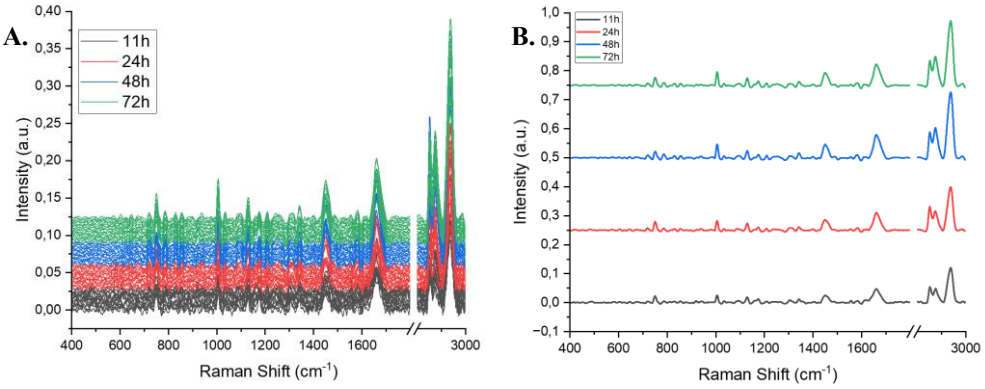

Figure 3.49. (A) All collected spectra in the 400-1800 and 2800-3000 cm^{-1} spectral ranges at 11th, 24th, 48th, and 72nd hours for CD133- cells and (B) mean spectra obtained by averaging them

Figure 3.49-A shows all recorded and pre-processed spectra for CD133- cells at 11th, 24th, 48th, and 72nd hours in the 400-1800 and 2800-3000 cm^{-1} spectral ranges. Mean spectra are shown in Figure 3.49-B calculated by averaging all recorded spectra at different hours.

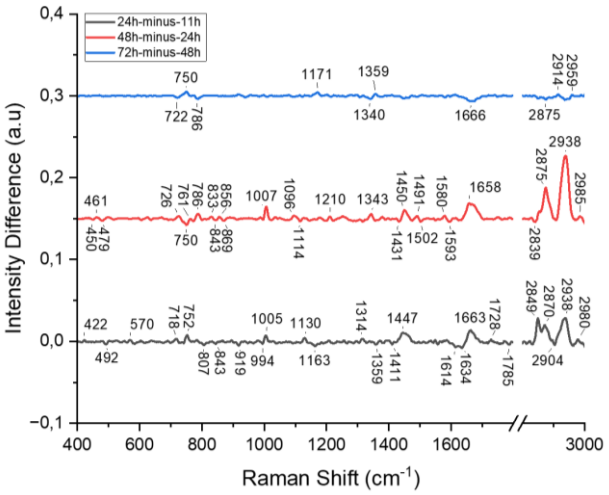

Figure 3.50. Raman difference spectra of CD133- cells obtained using average spectra at 11th, 24th, 48th, and 72nd hours in the 400-1800 and 2800-3000 cm^{-1} spectral ranges

Figure 3.50 depicts the difference spectra for CD133- cells in the 400-1800 and 2800-3000 cm^{-1} spectral ranges. The difference spectrum of 24th and 11th hours shows that at 24th hour Raman intensity was increased at 750 cm^{-1} (T),[19] 1171 cm^{-1} (C, G, and Tyr),[18] 1359 cm^{-1} (Trp),[23] and 2959 cm^{-1} (lipids); while decreased at 722 cm^{-1} (choline),[17] 786 cm^{-1} (nucleic acids), 1340 cm^{-1} (A, G,[19] and Trp[22]), 1666 cm^{-1} (amide I), and 2875 cm^{-1} (lipids).[17] The difference spectrum of 48th and 24th hour presents that at the 48th hour the peaks detected at 726 cm^{-1} (A), 786 cm^{-1} (C,T, and U), 833 cm^{-1} (Tyr), 856 cm^{-1} (Tyr), 1007 cm^{-1} (Phe), 1096 cm^{-1} (nucleic acids),[19] 1210 cm^{-1} (Tyr, Phe)[17], 1343 cm^{-1} (G), 1450 cm^{-1} (lipids),[21] 1491 cm^{-1} (nucleic acids),[19] 1580 cm^{-1} (nucleic acids),[22] 1658 cm^{-1} (proteins and lipids), 2875 cm^{-1} (lipids), and 2938 cm^{-1} (lipids)[17] were increased, while 479 cm^{-1} (glycogen),[16] 750 cm^{-1} (T),[19] 1431 cm^{-1} (lipids), and 2839 cm^{-1} (lipids) decreased. According to the difference spectrum of the 72nd and 48th hours the signals at 718 cm^{-1} (choline),[17] 752 cm^{-1} (T), 1005 cm^{-1} (Phe),[19] 1130 cm^{-1} (lipids),[18] 1314 cm^{-1} (A),[22] 1447 cm^{-1} (lipids), 1663 cm^{-1} (proteins & lipids), 1728 cm^{-1} (lipids), 2849 cm^{-1} (lipids), 2870 cm^{-1} (lipids), and 2938 cm^{-1} (lipids) were increased, whereas the signals at 492 cm^{-1} (nucleic acids),[17] 807 cm^{-1} (nucleic acids),[20] 919 cm^{-1} (glutathione),[23] 994 cm^{-1} (nucleic acids), 1359 cm^{-1} (Trp),[23] 1614 cm^{-1} (proteins),[18] and 1634 cm^{-1} (proteins) were decreased at 72nd hour.[23]

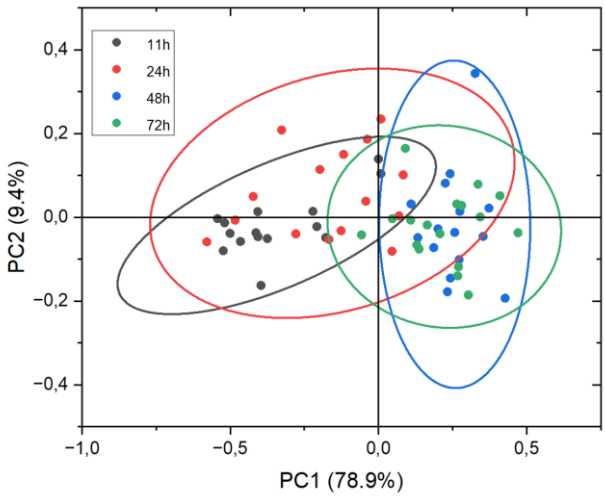

Figure 3.51. Score plot for PCA performed for CD133- cells at all hours in the spectral ranges 400-1800 and 2800-3000 cm^{-1} with 95 % confidence ellipses

Figure 3.51 shows PCA score plot for CD133- cells at all hours. Cells are distinguished by PC1 with 78.9% score and by PC2 with only 9.4% score. PC1 separated cells as cells in 11^{th} & 24^{th} hours and 48^{th} & 72^{nd} hours.

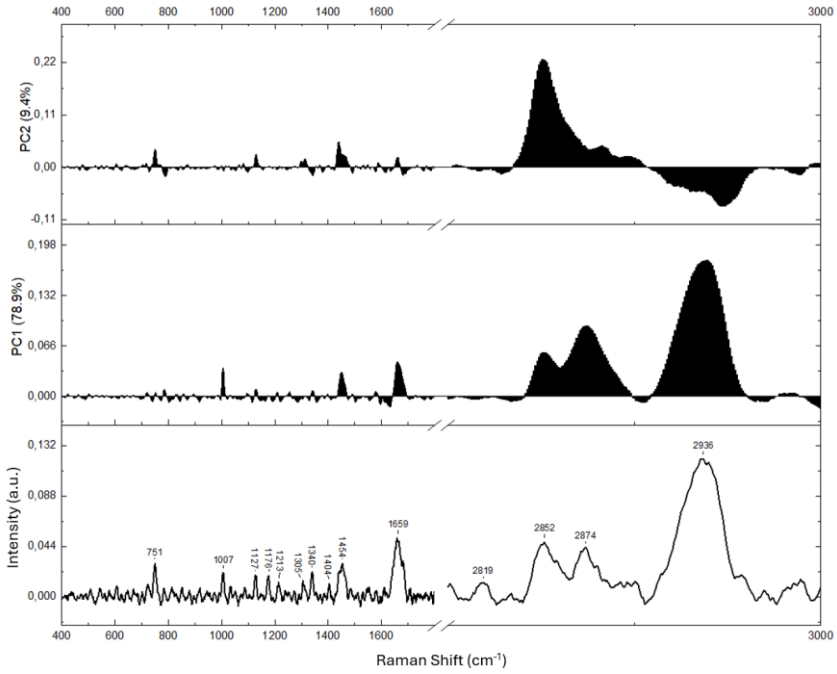

Figure 3.52. Loading plots of PC1 and PC2 for PCA performed in the spectral ranges 400-1800 and 2800-3000 cm^{-1} for CD133- cells

Figure 3.52 represents loading plots of PC1 and PC2 for CD133- cells at different hours in the spectral ranges 400-1800 and 2800-3000 cm^{-1}. It can be seen from the loading plots CD133- cells at different hours were distinguished mainly based on the variations in signals at 751 cm^{-1} (T), 1007 cm^{-1} (Phe),[19] 1127 cm^{-1} (lipids), 1176 cm^{-1} (C, G, and Tyr),[18] 1213 cm^{-1} (Tyr and Phe), 1305 cm^{-1} (lipids),[17] 1340 cm^{-1} (A, G,[19] and Trp[22]), 1454 cm^{-1} (lipids), 1659 cm^{-1} (amide I and lipids), 2852 cm^{-1} (lipids), 2874 cm^{-1} (lipids), and 2936 cm^{-1} (lipids).[17] The loading plots and difference spectra present similar peaks for CD133- cells at different hours.

3.2.7. Analysis of Raman Spectra for CHL-1 Cells

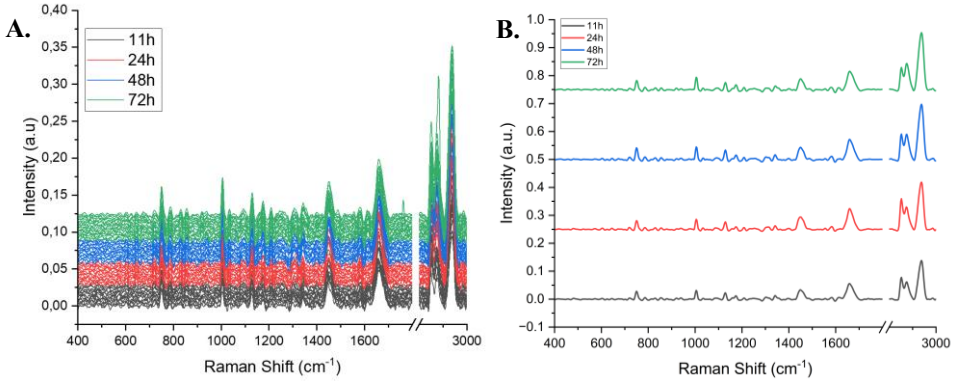

Figure 3.53. (A) All collected Raman spectra in the 400-1800 and 2800-3000 cm^{-1} spectral ranges at 11th, 24th, 48th, and 72nd hours for CHL-1 cells and (B) mean spectra obtained by averaging them

Figure 3.53-A shows all recorded and pre-processed spectra for CHL-1 cells at 11th, 24th, 48th, and 72nd hours in the 400-1800 and 2800-3000 cm^{-1} spectral ranges. Mean spectra are shown in the Figure 3.53-B calculated by averaging all recorded spectra at different hours.

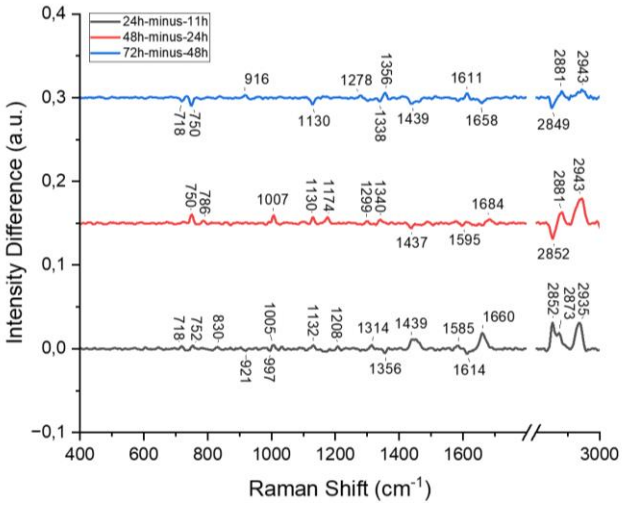

Figure 3.54. Raman difference spectra of CHL-1 cells obtained using average spectra at 11th, 24th, 48th, and 72nd hours in the 400-1800 and 2800-3000 cm^{-1} spectral ranges

Figure 3.54 represents difference spectra for CHL-1 cells in the 400-1800 and 2800-3000 cm^{-1} ranges. The difference spectrum of 24th and 11th hours show that Raman intensity was increased at 718 cm^{-1} (choline),[17] 752 cm^{-1} (T), 830 cm^{-1} (Tyr), 1005 cm^{-1} (Phe),[19] 1132 cm^{-1} (lipids), 1208 cm^{-1} (Tyr and Phe),[18] 1314 cm^{-1} (A),[22] 1439 cm^{-1} (lipids),[19] 1588 cm^{-1} (proteins),[23] 1660 cm^{-1} (proteins and lipids), 2852 cm^{-1} (lipids), 2873 cm^{-1} (lipids), and 2935 cm^{-1} (lipids),[17] and was decreased at 921 cm^{-1} (glutathione),[23] 997 cm^{-1} (nucleic acids), 1356 cm^{-1} (Trp),[23] and 1614 cm^{-1} (proteins)[18] at 24th hour. It can be seen from difference spectra of 48th and 24th hours that signals at 750 cm^{-1} (T), 786 cm^{-1} (C, T, and U), 1007 cm^{-1} (Phe),[19] 1130 cm^{-1} (lipids), 1174 cm^{-1} (C, G, and Tyr),[18] 1299 cm^{-1} (CH_2 twisting),[17] 1340 cm^{-1} (A, G,[19] and Trp[22]), 1684 cm^{-1} (proteins),[23] 2881 cm^{-1} (lipids), and 2943 cm^{-1} (lipids) were increased, while the signals at 1437 cm^{-1} (lipids),[17] 1595 cm^{-1} (nucleic acids),[23] and 2852 cm^{-1} (lipids)[17] were increased at 48th hour. The difference spectrum of 72nd and 48th hours shows that Raman intensity was increased at 916 cm^{-1} (glutathione), 1278 cm^{-1} (phospholipids), 1356 cm^{-1} (Trp),[23] 1611 cm^{-1} (Tyr),[18] 2881 cm^{-1} (lipids), and 2943 cm^{-1} (lipids), and was decreased at 718 cm^{-1} (choline),[17] 750 cm^{-1} (T),[19] 1130 cm^{-1} (lipids),[18] 1338 cm^{-1} (A, G,[19] and Trp[22]), 1439 cm^{-1} (lipids), 1658 cm^{-1} (proteins and lipids), and 2849 cm^{-1} (lipids)[17] at the 72nd hour.

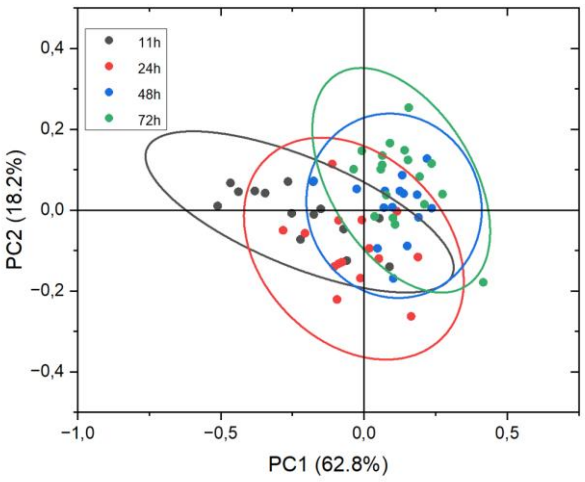

Figure 3.55. Score plot for PCA performed for CHL-1 cells at all hours in the spectral ranges 400-1800 and 2800-3000 cm^{-1} with 95 % confidence ellipses

Figure 3.55 shows PCA score plot for CHL-1 cells at all hours. Cells are distinguished by PC1 with 62.8% score and by PC2 with 18.2% score. PC1 separated cells as cells in 11^{th} & 24^{th} hours and 48^{th} & 72^{nd} hours with 62.8% score.

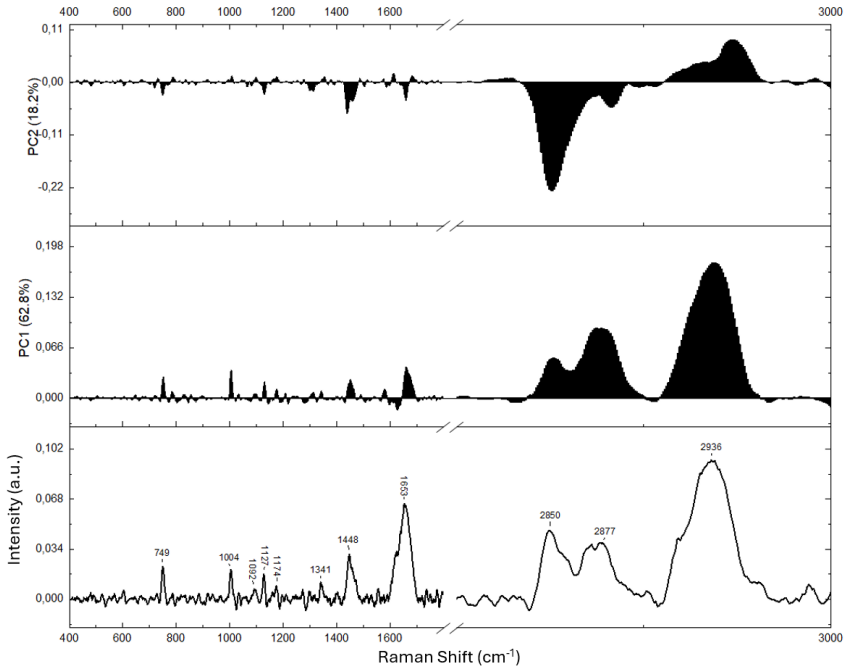

Figure 3.56. Loading plots of PC1 and PC2 for PCA performed in the spectral ranges 400-1800 and 2800-3000 cm^{-1} for CD133- cells

Figure 3.56 represents loading plots of PC1 and PC2 for CHL-1 cells at different hours in the ranges 400-1800 and 2800-3000 cm^{-1}. According to the loading plots CHL-1 cells at different hours were clustered mainly based on the variations in signals at 749 cm^{-1} (T), 1004 cm^{-1} (Phe),[19] 1092 cm^{-1} (nucleic acids),[21] 1127 cm^{-1} (lipids), 1174 cm^{-1} (C, G, and Tyr),[18] 1341 cm^{-1} (A, G,[19] and Trp[22]), 1448 cm^{-1} (lipids), 1653 cm^{-1} (amide I and lipids), 2850 cm^{-1} (lipids), 2877 cm^{-1} (lipids), and 2936 cm^{-1}(lipids).[17] The loading plots and difference spectra contain similar peaks for CHL-1 cells at different hours.

3.3. Interpretation and Comparison of IR and Raman Spectroscopy Results

IR and Raman spectroscopy are both vibrational techniques and complementary to each other. IR spectroscopy works based on dipole moment changes in the molecules, while Raman spectroscopy detects changes related to polarization of the molecules. Both techniques give excellent insights composition, structure, and dynamics of the molecule. While Raman data presents more specific information about the components of the sample, IR data has lower S/N (signal-to-noise) ratio and enables to perform statistical analysis more confidently.[7,15] In this study, malignant melanoma CSCs (CD133+), non-stem cancer cells (CD133-), and bulk population of cells (CHL-1) cells were examined IR and Raman spectroscopy techniques at different hours after passaging. Resulted data were pre-processed, and statistical analysis were applied.

All spectra collected at 11^{th}, 24^{th}, 48^{th}, and 72^{nd} hours for all cell groups were compared statistically for each hour to compare biochemical and biophysical properties of cells and gain insights about the cell cycle of the cells. According to IR and Raman difference spectra signals of CHL-1 cells are higher than other cells at 11^{th} hour. Hence, CHL-1 cells present higher amounts of biological components compared to CD133+ and CD133- cells, while CD133+ cells present the lowest amount. The percentage of cells in S phase might be higher in CHL-1 cells, they might be preparing themselves to division by synthesizing cellular materials and replicating their genomes.[24] While multivariate analyses revealed that CD133+ cells are statistically different, and CD133- and CHL-1 cells are more related to each other in all analyses.

The results for 24th hour revealed that according to the difference spectra there is not much difference between CD133+ and CHL-1 cells in terms of the amounts of biochemical ingredients. Nucleic acid signals observed to increase in both analyses, which can be interpreted as especially CD133+ and CD133- cells are likely leaving G_1 phase at 24th hour.[24] PCA and HCA show that CD133+ and CHL-1 cells statistically more relevant with each other, whereas CD133- cells more different. At this stage, cancer stem cell population in the bulk population might be increased.

Analyses at 48th hour show that the divergence between the cells were decreased hour and CD133+ and CHL-1 cells are more similar biochemically at 48th hour according to the difference spectra. Moreover, CHL-1 cells have higher amounts of components which suggests they are dividing more rapidly from other groups. The multivariate analyses revealed that CD133+ and CHL-1 cells are statistically more similar to each other, though CD133- cells partially share common properties with them.

Analyses at 72nd hour revealed that CD133+ and CD133- cells have higher amount of nucleic acid composition than CHL-1 cells according to the difference spectra which suggests that CHL-1 cells more likely to have higher percentage of cells in G_1 phase at 72nd hour.[24] PCA and HCA revealed that though CD133+ and CHL-1 cells are more relevant cell groups cannot be separated to different clusters at 72nd hour, which suggest that they share common properties that disable to statistical differentiation of them at 72nd hour.

After comparing spectra at different hours, spectra were compared according to cell types i.e. all spectra collected at different hours analysed for each cell type to track changes with time in each cell type. The analysis of spectra of CD133+ cells revealed that according to the difference spectra contents of CD133+ cells were increased overall between the 11th and 24th hours, which suggests that synthesis occurs at most in between 11th and 24th hours in CD133+ cells. Moderate synthesis took place in between 24th and 48th hours, while little synthesis took place in between 48th and 72nd hours. Moreover, multivariate analyses revealed that at 24th hour cells are statistically different from other hours. These findings suggest that the time that the greatest percentage of the CD133+ cells in S phase might be 24th hour.[24]

The analysis of all spectra of CD133- cells shows that most amount synthesis of genetic materials and cellular components took place between the 11th and 24th hours, while little synthesis take place between the 48th and 72nd hours and cells were almost stabilized according to the difference spectra. Multivariate statistical analyses revealed

that cells are more different from other hours at 24th hour. It can be suggested that the highest percentage of the cells transitioning from G_1 to S phase occurred at 24th hour.[24]

The analysis of all spectra of CHL-1 cells revealed that more synthesis take place in between 11th and 24th hours and 24th and 48th hours according to the difference spectra of CHL-1 cells, while there are small variations in the difference spectrum of 72nd and 48th hours. It can be suggested that the percentage of CHL-1 cells in S phase decreased at 72nd hour.[24] PCA and HCA analyses show that CHL-1 cells at 11th hour more resemble to cells at 24th hour, while cells at 48th hour are more similar to cells at 72nd hour.

CHAPTER 4

CONCLUSION

Cancer stem cells highly responsible for resistance to therapy, metastasis, and reoccurrence of cancer, although they consist of a small percentage of cancer cells. In this study, it was aimed to probe biochemical and biophysical properties of cancer stem cells and gain insights regarding to cell cycle of cancer stem cells on malignant melanoma model which is a highly aggressive cancer using vibrational spectroscopy and multivariate analysis methods. Vibrational spectroscopy is an excellent tool for cellular studies as it gives highly informative spectra regarding to composition and metabolism of cells, combined with statistical tools it offers various applications in cell biology as well as other biological studies. In this work, cancer stem cells (CD133+) and non-stem cancer cells (CD133-) were separated from CHL-1 MM cell line (bulk population) by flow-cytometry with the help of CD133+ marker. Cells were cultured and prepared for measurements with about 10^6 cells/ml concentration. Both IR and Raman spectroscopy experiments were conducted with 12 experimental groups as CD133+, CD133-, and CHL-1 cells at 11^{th}, 24^{th}, 48^{th}, and 72^{nd} hours. Afterwards, all spectra were pre-processed, difference spectra of groups were calculated, and multivariate analyses were performed based on both at each hour to determine differences between cell groups and for each cell group to tract time-dependent changes in each cell group. Findings show that vibrational spectroscopy combined with multivariate analyses is a suitable tool to characterise cells. Vibrational spectroscopy provides highly comprehensive and both qualitative and quantitative information regarding to biochemical components and their amounts in the cells, while multivariate analyses offer evaluation of statistical significance of data and interpretation of relationships between the samples.

REFERENCES

1. Andrews, D. L. Electromagnetic Radiation. *Elsevier Ltd.* **1999**, 451–455.

2. Hollas, M. *Modern Spectroscopy*, 4th ed.; John Wiley & Sons, **2004**.

3. Thompson, J. *Infrared Spectroscopy*; Taylor & Francis, **2018**.

4. Larkin, P. J. Basic Principles. *Infrared and Raman Spectroscopy* **2018**, 7–28.

5. Dutta, A. Fourier Transform Infrared Spectroscopy. In *Spectroscopic Methods for Nanomaterials Characterization*; Elsevier, **2017**; Vol. 2, pp 73–93.

6. Smith, B. *Fundamentals of Fourier Transform Infrared Spectroscopy*, 2nd ed.; CRC Press, **2011**.

7. Baker, M. J.; Trevisan, J.; Bassan, P.; Bhargava, R.; Butler, H. J.; Dorling, K. M.; Fielden, P. R.; Fogarty, S. W.; Fullwood, N. J.; Heys, K. A.; Hughes, C.; Lasch, P.; Martin-Hirsch, P. L.; Obinaju, B.; Sockalingum, G. D.; Sulé-Suso, J.; Strong, R. J.; Walsh, M. J.; Wood, B. R.; Gardner, P.; Martin, F. L. Using Fourier Transform IR Spectroscopy to Analyze Biological Materials. *Nat Protoc* **2014**, *9* (8), 1771–1791.

8. Sitnikova, V. E.; Kotkova, M. A.; Nosenko, T. N.; Kotkova, T. N.; Martynova, D. M.; Uspenskaya, M. V. Breast Cancer Detection by ATR-FTIR Spectroscopy of Blood Serum and Multivariate Data-Analysis. *Talanta* **2020**, *214*.

9. Krüger, A.; Bürkle, A.; Hauser, K.; Mangerich, A. Real-Time Monitoring of PARP1-Dependent PARylation by ATR-FTIR Spectroscopy. *Nat Commun* **2020**, *11* (1).

10. Paraskevaidi, M.; Morais, C. L. M.; Ashton, K. M.; Stringfellow, H. F.; McVey, R. J.; Ryan, N. A. J.; O'flynn, H.; Sivalingam, V. N.; Kitson, S. J.; Mackintosh, M. L.; Derbyshire, A. E.; Pow, C.; Raglan, O.; Lima, K. M. G.; Kyrgiou, M.; Martin-

Hirsch, P. L.; Martin, F. L.; Crosbie, E. J. Detecting Endometrial Cancer by Blood Spectroscopy: A Diagnostic Cross-Sectional Study. *Cancers (Basel)* **2020**, *12* (5).

11. Tiernan, H.; Byrne, B.; Kazarian, S. G. ATR-FTIR Spectroscopy and Spectroscopic Imaging for the Analysis of Biopharmaceuticals. *Spectrochimica Acta - Part A: Molecular and Biomolecular Spectroscopy*. Elsevier B.V. November 5, **2020**.

12. Stani, C.; Vaccari, L.; Mitri, E.; Birarda, G. FTIR Investigation of the Secondary Structure of Type I Collagen: New Insight into the Amide III Band. *Spectrochim Acta A Mol Biomol Spectrosc* **2020**, *229*.

13. Das, R. S.; Agrawal, Y. K. Raman Spectroscopy: Recent Advancements, Techniques and Applications. *Vib Spectrosc* **2011**, *57* (2), 163–176.

14. Baker, M.; Hollywood, K. A.; Hughes, C. Raman Spectroscopy. In *Biophotonics: Vibrational Spectroscopic Diagnostics*; Morgan & Claypool Publishers, **2016**; pp 1–13.

15. Xu, J.; Yu, T.; Zois, C. E.; Cheng, J. X.; Tang, Y.; Harris, A. L.; Huang, W. E. Unveiling Cancer Metabolism through Spontaneous and Coherent Raman Spectroscopy and Stable Isotope Probing. *Cancers*. MDPI AG April 1, **2021**.

16. Wiercigroch, E.; Szafraniec, E.; Czamara, K.; Pacia, M. Z.; Majzner, K.; Kochan, K.; Kaczor, A.; Baranska, M.; Malek, K. Raman and Infrared Spectroscopy of Carbohydrates: A Review. *Spectrochimica Acta - Part A: Molecular and Biomolecular Spectroscopy*. Elsevier B.V. October 5, **2017**, pp 317–335.

17. Krafft, C.; Knetschke, T.; Siegner, A.; Funk, R. H. W.; Salzer, R. Mapping of Single Cells by near Infrared Raman Microspectroscopy. In *Vibrational Spectroscopy*; Elsevier, **2003**; Vol. 32, pp 75–83.

18. Taleb, A.; Diamond, J.; McGarvey, J. J.; Beattie, J. R.; Toland, C.; Hamilton, P. W. Raman Microscopy for the Chemometric Analysis of Tumor Cells. *Journal of Physical Chemistry B* **2006**, *110* (39), 19625–19631.

19. Chan, J. W.; Taylor, D. S.; Zwerdling, T.; Lane, S. M.; Ihara, K.; Huser, T. Micro-Raman Spectroscopy Detects Individual Neoplastic and Normal Hematopoietic Cells. *Biophys J* **2006**, *90* (2), 648–656.

20. Konorov, S. O.; Schulze, H. G.; Piret, J. M.; Blades, M. W.; Turner, R. F. B. Label-Free Determination of the Cell Cycle Phase in Human Embryonic Stem Cells by Raman Microspectroscopy. *Anal Chem* **2013**, *85* (19), 8996–9002.

21. Schie, I. W.; Huser, T. Methods and Applications of Raman Microspectroscopy to Single-Cell Analysis. In *Applied Spectroscopy*; **2013**; Vol. 67, pp 813–828.

22. Wen, J.; Tang, T.; Kanwal, S.; Lu, Y.; Tao, C.; Zheng, L.; Zhang, D.; Gu, Z. Detection and Classification of Multi-Type Cells by Using Confocal Raman Spectroscopy. *Front Chem* **2021**, *9*.

23. Pezzotti, G. Raman Spectroscopy in Cell Biology and Microbiology. *Journal of Raman Spectroscopy*. John Wiley and Sons Ltd December 1, **2021**, pp 2348–2443.

24. Johnson, D. G.; Walker, C. L. *Cyclins and Cell Cycle Checkpoints*; **1999**; Vol. 39.

25. Suski, J. M.; Braun, M.; Strmiska, V.; Sicinski, P. Targeting Cell-Cycle Machinery in Cancer. *Cancer Cell*. Cell Press June 14, **2021**, pp 759–778.

26. Williams, G. H.; Stoeber, K. The Cell Cycle and Cancer. *Journal of Pathology*. January **2012**, pp 352–364.

27. Schafer, K. A. The Cell Cycle: A Review. *Vet Pathol* **1998**, *35*, 461–478.

28. Kastan, M. B.; Bartek, J. Cell-Cycle Checkpoints and Cancer. *Nature* **2004**, *432*, 316–322.

29. Malumbres, M.; Barbacid, M. Cell Cycle, CDKs and Cancer: A Changing Paradigm. *Nature Reviews Cancer*. March **2009**, pp 153–166.

30. Matthews, H. K.; Bertoli, C.; de Bruin, R. A. M. Cell Cycle Control in Cancer. *Nature Reviews Molecular Cell Biology*. Nature Research January 1, **2022**, pp 74–88.

31. Barnum, K. J.; O'Connell, M. J. Cell Cycle Regulation by Checkpoints. *Methods in Molecular Biology* **2014**, *1170*, 29–40.

32. Guo, W.; Lasky, J. L.; Wu, H. Cancer Stem Cells. *Pediatric Research*. April **2006**.

33. Walcher, L.; Kistenmacher, A. K.; Suo, H.; Kitte, R.; Dluczek, S.; Strauß, A.; Blaudszun, A. R.; Yevsa, T.; Fricke, S.; Kossatz-Boehlert, U. Cancer Stem Cells—Origins and Biomarkers: Perspectives for Targeted Personalized Therapies. *Frontiers in Immunology*. Frontiers Media S.A. August 7, **2020**.

34. Clarke, M. F.; Dick, J. E.; Dirks, P. B.; Eaves, C. J.; Jamieson, C. H. M.; Jones, D. L.; Visvader, J.; Weissman, I. L.; Wahl, G. M. Cancer Stem Cells - Perspectives on Current Status and Future Directions: AACR Workshop on Cancer Stem Cells. In *Cancer Research*; **2006**; Vol. 66, pp 9339–9344.

35. Yu, Z.; Pestell, T. G.; Lisanti, M. P.; Pestell, R. G. Cancer Stem Cells. *International Journal of Biochemistry and Cell Biology*. Elsevier Ltd **2012**, pp 2144–2151.

36. Batlle, E.; Clevers, H. Cancer Stem Cells Revisited. *Nature Medicine*. Nature Publishing Group October 6, **2017**, pp 1124–1134.

37. O'Brien, C. A.; Kreso, A.; Jamieson, C. H. M. Cancer Stem Cells and Self-Renewal. *Clinical Cancer Research*. June 15, **2010**, pp 3113–3120.

38. Reya, T.; Morrison, S.; Clarke, M.; Weissman, I. L. Stem Cells, Cancer, and Cancer Stem Cells. *Nature* **2001**, *414*, 105–111.

39. Lobo, N. A.; Shimono, Y.; Qian, D.; Clarke, M. F. The Biology of Cancer Stem Cells. *Annual Review of Cell and Developmental Biology*. **2007**, pp 675–699.

40. Dalerba, P.; Cho, R. W.; Clarke, M. F. Cancer Stem Cells: Models and Concepts. *Annual Review of Medicine*. **2007**, pp 267–284.

41. Jordan, C. T.; Guzman, M. L.; Noble, M. Cancer Stem Cells. *N Engl J Med* **2006**, *355* (12), 1253–1259.

42. Aponte, P. M.; Caicedo, A. Stemness in Cancer: Stem Cells, Cancer Stem Cells, and Their Microenvironment. *Stem Cells International*. Hindawi Limited **2017**.

43. Iwasaki, H.; Suda, T. Cancer Stem Cells and Their Niche. *Cancer Science*. **2009**, pp 1166–1172.

44. Lens, M. B.; Dawes, M. Global Perspectives of Contemporary Epidemiological Trends of Cutaneous Malignant Melanoma. *British Journal of Dermatology* **2004**, *150*, 179–185.

45. Cummins, D. L.; Cummins, J. M.; Pantle, H.; Silverman, M. A.; Leonard, A. L.; Chanmugam, A. Cutaneous Malignant Melanoma. *Mayo Clinic Proceedings*. Elsevier Ltd **2006**, pp 500–507.

46. Bandarchi, B.; Ma, L.; Navab, R.; Seth, A.; Rasty, G. From Melanocyte to Metastatic Malignant Melanoma. *Dermatology Research and Practice*. Hindawi Publishing Corporation **2010**.

47. Davey, M. G.; Miller, N.; McInerney, N. M. A Review of Epidemiology and Cancer Biology of Malignant Melanoma. *Cureus* **2021**.

48. Mccourt, C.; Dolan, O.; Gormley, G. Malignant Melanoma: A Pictorial Review. *Ulster Med J* **2014**, *83* (2), 103–110.

49. Perera, E.; Gnaneswaran, N.; Jennens, R.; Sinclair, R. Malignant Melanoma. *Healthcare (Switzerland)*. MDPI March 1, **2014**.

50. Liu, Y.; Saeed Sheikh, M. Melanoma: Molecular Pathogenesis and Therapeutic Management. *Mol Cell Pharmacol.* **2015**, *6* (3), 228-.

51. Dvořánková, B.; Szabo, P.; Kodet, O.; Strnad, H.; Kolář, M.; Lacina, L.; Krejčí, E.; Naňka, O.; Šedo, A.; Smetana, K. Intercellular Crosstalk in Human Malignant Melanoma. *Protoplasma*. Springer-Verlag Wien May 1, **2017**, pp 1143–1150.

52. Gosman, L. M.; Ţăpoi, D. A.; Costache, M. Cutaneous Melanoma: A Review of Multifactorial Pathogenesis, Immunohistochemistry, and Emerging Biomarkers for Early Detection and Management. *International Journal of Molecular Sciences*. Multidisciplinary Digital Publishing Institute (MDPI) November 1, **2023**.

53. Clarke, M. F.; Dick, J. E.; Dirks, P. B.; Eaves, C. J.; Jamieson, C. H. M.; Jones, D. L.; Visvader, J.; Weissman, I. L.; Wahl, G. M. Cancer Stem Cells - Perspectives on Current Status and Future Directions: AACR Workshop on Cancer Stem Cells. In *Cancer Research*; **2006**; Vol. 66, pp 9339–9344.

54. Guo, W.; Lasky, J. L.; Wu, H. Cancer Stem Cells. *Pediatric Research*. April **2006**.

55. Walcher, L.; Kistenmacher, A. K.; Suo, H.; Kitte, R.; Dluczek, S.; Strauß, A.; Blaudszun, A. R.; Yevsa, T.; Fricke, S.; Kossatz-Boehlert, U. Cancer Stem Cells—Origins and Biomarkers: Perspectives for Targeted Personalized Therapies. *Frontiers in Immunology*. Frontiers Media S.A. August 7, **2020**.

56. Güler, G.; Acikgoz, E.; Karabay Yavasoglu, N. Ü.; Bakan, B.; Goormaghtigh, E.; Aktug, H. Deciphering the Biochemical Similarities and Differences among Mouse Embryonic Stem Cells, Somatic and Cancer Cells Using ATR-FTIR Spectroscopy. *Analyst* **2018**, *143* (7), 1624–1634.

57. Güler, G.; Acikgoz, E.; Mukhtarova, G.; Oktem, G. Biomolecular Fingerprints of the Effect of Zoledronic Acid on Prostate Cancer Stem Cells: Comparison of 2D and 3D Cell Culture Models. *Arch Biochem Biophys* **2024**, *753*.

58. Ozdil, B.; Güler, G.; Acikgoz, E.; Kocaturk, D. C.; Aktug, H. The Effect of Extracellular Matrix on the Differentiation of Mouse Embryonic Stem Cells. *J Cell Biochem* **2020**, *121* (1), 269–283.

59. Güler, G.; Guven, U.; Oktem, G. Characterization of CD133+/CD44+ Human Prostate Cancer Stem Cells with ATR-FTIR Spectroscopy. *Analyst* **2019**, *144* (6), 2138–2149.

60. Mishra, P.; Singh, U.; Pandey, C. M.; Mishra, P.; Pandey, G. Application of Student's t-Test, Analysis of Variance, and Covariance. *Ann Card Anaesth* **2019**, *22* (4), 407–411.

61. Albers, C. A Note on the Alpha-Level. **2022**.

62. Pirhadi, S.; Shiri, F.; Ghasemi, J. B. Multivariate Statistical Analysis Methods in QSAR. *RSC Advances*. Royal Society of Chemistry **2015**, pp 104635–104665.

63. Carey, D. M. *Measurement of the Raman Spectrum of Liquid Water*; **1996**.

64. Lasch, P.; Boese, M.; Pacifico, A.; Diem, M. *FT-IR Spectroscopic Investigations of Single Cells on the Subcellular Level*; **2002**.

65. Movasaghi, Z.; Rehman, S.; Rehman, I. U. Fourier Transform Infrared (FTIR) Spectroscopy of Biological Tissues. *Applied Spectroscopy Reviews*. **2008**, pp 134–179.

66. Barth, A. *The Infrared Absorption of Amino Acid Side Chains*; **2000**; Vol. 74.

67. Bellisola, G.; Sorio, C. Infrared Spectroscopy and Microscopy in Cancer Research and Diagnosis. *Am J Cancer Res* **2012**, *2* (1), 1–21.

68. Hong Ong, Y.; Lim, M.; Liu, Q. *Comparison of Principal Component Analysis and Biochemical Component Analysis in Raman Spectroscopy for the Discrimination of Apoptosis and Necrosis in K562 Leukemia Cells*; **2012**.

69. Wen, J.; Tang, T.; Kanwal, S.; Lu, Y.; Tao, C.; Zheng, L.; Zhang, D.; Gu, Z. Detection and Classification of Multi-Type Cells by Using Confocal Raman Spectroscopy. *Front Chem* **2021**, *9*.